

# **PERFORMANCE EVALUATION OF VERTICAL POROUS SCREEN IN A SLOSHING TANK BY ANALYTICAL AND EXPERIMENTAL INVESTIGATION**

**Thesis**

**Submitted in partial fulfilment of the requirements for the degree of  
DOCTOR OF PHILOSOPHY**

by

**MALLIKARJUN S BHANDIWAD**



**DEPARTMENT OF WATER RESOURCES AND OCEAN ENGINEERING  
NATIONAL INSTITUTE OF TECHNOLOGY KARNATAKA,  
SURATHKAL, MANGALURU - 575 025**

**July 2023**



# **PERFORMANCE EVALUATION OF VERTICAL POROUS SCREEN IN A SLOSHING TANK BY ANALYTICAL AND EXPERIMENTAL INVESTIGATION**

**Thesis**

**Submitted in partial fulfilment of the requirements for the degree of  
DOCTOR OF PHILOSOPHY**

by

**MALLIKARJUN S BHANDIWAD**



**DEPARTMENT OF WATER RESOURCES AND OCEAN ENGINEERING  
NATIONAL INSTITUTE OF TECHNOLOGY KARNATAKA,  
SURATHKAL, MANGALURU - 575 025**

**July 2023**



# DECLARATION

*By the Ph.D. Research Scholar*

I hereby *declare* that the Research Thesis entitled “**Performance Evaluation of Vertical Porous Screen in a Sloshing Tank by Analytical and Experimental Investigation**” which is being submitted to the **National Institute of Technology Karnataka, Surathkal** in partial fulfilment of the requirements for the award of the Degree of **Doctor of Philosophy in Department of Water Resources and Ocean Engineering** is a *bonafide report of the research work* carried out by me. The material contained in this Research Thesis has not been submitted to any University or Institution for the award of any degree.



177112AM006, MALLIKARJUN S BHANDIWAD.

(Register Number, Name & Signature of the Research Scholar)


Department of Water Resources and Ocean Engineering

Place: NITK-Surathkal

Date: 10-07-2023

## CERTIFICATE

This is to *certify* that the Research Thesis entitled “**Performance Evaluation of Vertical Porous Screen in a Sloshing Tank by Analytical and Experimental Investigation**” submitted by **Mallikarjun S Bhandiwad** (Register Number: 177112AM006) as the record of the research work carried out by him, is *accepted as the Research Thesis submission* in partial fulfilment of the requirements for the award of degree of **Doctor of Philosophy**.

  
**Prof. B M Dodamani**  
(Research Guide)

  
For **Dr. Varija K**  
(Chairman - DRPC)

**DEPARTMENT OF WATER RESOURCES AND OCEAN ENGINEERING**  
**NATIONAL INSTITUTE OF TECHNOLOGY KARNATAKA,**  
**SURATHKAL, MANGALURU - 575 025**

## **ACKNOWLEDGMENT**

With a deep sense of gratitude, I express my heartfelt thanks to Prof. B M Dodamani, Research Guide, Department of Water Resources and Ocean Engineering, NITK, Surathkal. His support and suggestions have been very valuable and encouraging during this research. I acknowledge, the time spent in the discussions with my supervisor regarding the completion of this research work. His moral support and guidance have been priceless and have given me a technical suggestion to publish my research work in international journals and conferences.

I express my heartfelt gratitude to my Research Progress Assessment Committee (RPAC) members, Prof. P. Jeyaraj and Dr. Manu, for their valuable suggestions for the betterment of this research work. I am thankful to Prof. Amai Mahesha and Prof. Amba Shetty, former Head of the Department, for permitting me to utilize the laboratory and departmental facilities for the completion of this work. I thank all the faculty members of the Department of Water Resources and Ocean Engineering for their support.

I would like to express my gratitude to Prof. Prasad Krishna, Director (Additional-charge), Prof. Udaykumar R. Yaragatti, former Director (In-charge), and Prof. Karanam Uma Maheshwar Rao, former Director of NITK Surathkal for permitting me to use the institutional infrastructure facilities.

I am greatly indebted to Dr. Raviraj H.M, Prof. Lakshman Nandagiri, Dr. Varija K, Dr. Ramesh H, Dr. Manu, Dr. Subrahmanya K, Dr. Pruthviraj U, Dr. Debabrata Karmakar for their encouragement during my research works.

Nothing great was ever accomplished alone. I would like to thank Shwetha shri, Sreenivasulu, Pavan Kumar, and Keshav for their valuable support during the experimental investigation and encouragement.

I sincerely acknowledge the help and support rendered by the department staff Mr. Seetharam, Mr. Anil Kumar, Mr. Ananda Devadiga, Mr. Gopalakrishna, and all the staff

of the Department for their encouragement and support during the experimental work. I also thank Mr. Balakrishna and Ms. Sweekritha for their support in academic documentation.

I also sincerely thank the present and former Principal, HOD, and all staff members of the Civil Engineering Department of SDM College of Engineering and Technology, Dharwad for their cooperation.

Finally, I wish to express gratitude, love, and affection to my beloved family member and all my friends and relatives for their encouragement, moral support, and all their big and small sacrifices during this research. I also bow down to the Almighty in making this thesis a reality.



## ABSTRACT

Liquid participation in the vessels or tanks is called as sloshing. The sloshing dynamics in the tank is a complicated phenomenon. Dynamics of sloshing mainly include transient motion of liquid, resonant condition, linear and nonlinear motion, frequency shift phenomenon etc. Therefore, it attracts many researcher and scantiest to study the dynamics of liquid motion in the tanks. Due to its complex and significant phenomenon that has many engineering applications. Stability of sloshing tank and stability of moving vehicles or/and structures coupled with sloshing tank are most concern. In view of fact of sloshing in the tank for many engineering application, it is important to control and/or reduce the liquid participation in the sloshing tank and achieve a required level damping. The damping in tank include viscous effect of liquid in the tank, wave- tank interaction, and wave motion in the baffled tank. For this purpose, one such system is the liquid (water) tank with flow damping device. Many researchers have investigated the sloshing dynamics in the tank with solid and porous baffles in order to control and/or reduce the wave elevations in the sloshing tank. The varying types solid baffles in the sloshing tanks are used to reduce the hydrodynamic action (force and pressure) on tank walls and reduce the weight penalty and cost. Similar to the solid baffles, the porous baffles with varying porosities are also being used in the sloshing tank not only to control hydrodynamics action but also used to enhance the required level damping in the tank. The perforation in the baffles generally include slat type configuration with horizontal and vertical arrangement with respect flow direction. In the porous baffled tank, the dynamic of sloshing includes wave-baffle interaction associated with linear and nonlinear phenomenon. The wave- structures (baffles) interaction is dependent in tank geometry, liquid fill level, type of excitation, flow through baffles, and most importantly drag, loss, and inertia coefficients. The tank with varying porous baffled with optimum liquid fill level in the tank are mainly designed as a Tuned Liquid Damper (TLD) to reduce the structural vibrations. In this regard, many researchers have been working on sloshing dynamics in the tanks to construct the damping in the tank with porous baffles and appropriate liquid fill level. And, the screen drag coefficient is an important parameter to consider to study the dynamic of liquid sloshing the porous baffled tank,

The liquid free surface is most important, where the wave energy is concentrated during liquid motion and first resonant mode of sloshing in the tank is an important factor for structure-TLD interaction problems. On this basis, using fully extended porous baffles from tank bottom may result in increased wave baffles interaction inducing larger sloshing attenuation near the resonant modes. Hence, the concept of using circular hole perforation in the baffle is comprehended for the advancement of porous baffles in the sloshing tank. In the present study, free surface elevations, sloshing force, and energy dissipation of the porous baffle in the rectangular sloshing tank are examined by both analytical and experimental program. The three varying porosity is adopted for porous baffles in the sloshing study. To concerns of first resonant mode in the sloshing tank, the porosity of 4.4%, 6.8%, and 9.2% are adopted for the baffles.

Initially, the gravitational flow test is planned and conducted to study the flow phenomena through porous baffles, and documented the drag coefficient variation for all porous baffles based on the Reynold numbers. Secondly, the linear second-order ordinary differential equations for sloshing dynamics in the rectangular tank were solved using Newmark's beta method and obtained the analytical solutions for liquid sloshing with and without baffles in the tank following the procedure similar to Warnitchai and Pinkaew (1998) and Tait (2008). The porous baffle loss coefficient is an important parameter to study the baffle's performance in the tanks. Hence, the two analytical models based on porous baffle loss coefficients were formulated for rectangular sloshing tanks with porous baffles. The analytical model-1 includes both Reynold's number and porosity dependent loss coefficient, whereas model-2 includes porosity dependent and independent of Reynold's number. The model's test results were validated with a series of shake table experiments under sway motion at different excitation frequencies which cover up to the first four sloshing resonant modes.

In the third stage, experiment shake table tests are performed to validate analytical model results. Initially the test includes rectangular clean tank with varying liquid fill level to study the effect of liquid fill level in the sloshing tank. Considered small, medium, high, and liquid fill in the tank based on tank height ( $H$ ) which include

aspect ratio (ratio of static liquid depth to tank length) of 0.163, 0.325, and 0.488 respectively. In the experiment test series, the sloshing with varying fill level subjected to seventeen different excitation frequencies which include first five resonant mode of liquid sloshing in the tank and the tank driven by sway amplitude ( $A/L$ ) of 0.0075. Further, the shake table tests are performed for porous baffled tank. In the test series, initially the tank with two baffle condition were considered. In the tank the two baffles are positioned at 0.33 distance of tank length from both end walls. And tank with single baffle case, the baffle positioned at centre of the tank length.

The response of free surface elevation and sloshing force variations in the tank analytical models were compared with the experiment's test results. In the two porous baffled sloshing tank under the range of sway excitations, the response of wave motion and sloshing force by both analytical and experimental tests results exhibit the resonant frequency shift phenomenon which is provoked by the low-level porosity of screens (4.4% and 6.8%) in all three fill levels. As porosity of baffle increases (9.2%), the secondary peak start appearing near the first resonant mode along with secondary peak at third resonant mode of sloshing tank. The analytical results matched with shake table test results with a quantitative difference near the first resonant frequency. It is found that Reynolds number dependent porous baffles in the sloshing tank significantly reduce the sloshing elevations in the tank compared to Reynolds number independent one. As a result, Reynold's number and porosity dependent loss coefficient for porous baffles was found to be more effective. In the case of tank with single porous baffle condition, the analytical model fails to exhibits the exact resonant phenomenon near the secondary resonant excitation mode. but, experiment rest results show the exact resonant frequency shift phenomenon in the tank with centrally positioned porous baffle.

**Keywords:** Analytical and experimental investigation; Loss and Drag coefficient; Reynolds number; Porous baffles; Sloshing motion; Resonant frequency; Sloshing force; Energy dissipation.

# CONTENTS

<b>ABSTRACT</b>	<b>i</b>
<b>CONTENTS</b>	<b>iv</b>
<b>LIST OF FIGURES</b>	<b>ix</b>
<b>LIST OF TABLES</b>	<b>xv</b>
<b>NOMENCLATURE</b>	<b>xvii</b>
<b>CHAPTER 1</b>	
<b>INTRODUCTION.....</b>	<b>1</b>
1.1 GENERAL	1
1.2 RESONANT SLOSHING	3
1.3 SLOSHING IN REAL-LIFE CIRCUMSTANCES	3
1.4 SLOSHING IN A RECTANGULAR TANK	9
1.5 DRAG COEFFICIENT	11
1.6 STRUCTURE-TLD INTERACTION	12
1.6.1 Tuned Mass Damper (TMD) .....	12
1.6.2 Tuned Liquid Damper (TLD) .....	14
1.7 MOTIVATION FOR THE PRESENT STUDY	14
1.8 ORGANIZATION OF THE THESIS	16
<b>CHAPTER 2</b>	
<b>BACKGROUND AND LITERATURE REVIEW .....</b>	<b>19</b>
2.1 INTRODUCTION	19
2.2 EXPERIMENTAL LOSS COEFFICIENT / DRAG COEFFICIENT FOR POROUS BAFFLES	19
2.3 SLOSHING DYNAMICS IN THE TANKS	23
2.3.1 Experimental investigation .....	23
2.3.2 Analytical and numerical investigation .....	26
2.4 TUNED LIQUID DAMPER	29
2.5 SUMMARY OF LITERATURE REVIEW	37

2.6	KNOWLEDGE GAP	38
2.7	OBJECTIVE OF THE PRESENT STUDY	38
<b>CHAPTER 3</b>		
<b>EXPERIMENTAL SET-UP AND INVESTIGATIONS .....</b>		<b>39</b>
3.1	INTRODUCTION	39
3.2	RECTANGULAR TANK	39
3.3	INSTRUMENTATION AND CALIBRATION OF INSTRUMENTS	41
3.3.1	General .....	41
3.3.2	Wave Probes .....	42
3.3.3	Load Cell .....	44
3.3.4	Linear Variable Differential Transformer (LVDT) .....	45
3.3.5	Shake Table .....	46
3.3.6	Data Acquisition System (DAQ) .....	50
3.3.7	Porous baffles .....	51
3.4	GRAVITATIONAL FLOW TEST	52
3.4.1	Model details .....	52
3.5	EXPERIMENTAL PLAN	53
3.6	EXPERIMENTAL PROCEDURE	55
3.6.1	The drag coefficient for the porous screens in a non- oscillating flow.....	55
3.6.2	Sloshing test in the tank.....	57
3.6.3	Wave surface elevations .....	59
3.6.4	Sloshing force .....	59
3.6.5	Energy dissipation .....	60
3.7	ANLYTICAL MODEL FOR LIQUID SLOSHING IN A TANK	60
3.7.1	Tank with no screen (clean tank).....	63
3.7.2	Tank with screens .....	64
3.8	STRUCTURE-TLD WITH POROUS SCREEN INTERACTION MODEL	65
<b>CHAPTER 4</b>		
<b>RESULTS AND DISCUSSIONS .....</b>		<b>69</b>
4.1	GRAVITY FLOW TEST FOR DRAG COEFFICIENT FOR POROUS SCREENS	69

4.2	SLOSHING DYANAMIC IN THE RECTANGUALR clean TANK	73
4.2.1	Analytical model validation.....	74
4.2.2	Maximum free surface motion .....	77
4.2.3	Maximum sloshing force .....	81
4.2.4	Energy dissipation .....	83
4.3	SLOSHING DYANAMIC IN THE RECTANGUALR TANK WITH TWO POROUS BAFFLES	86
4.3.1	Max free surface elevation in a 25% FL tank with two porous baffles .....	86
4.3.2	Max free surface elevation in a 50% FL tank with two porous baffles .....	89
4.3.3	Max free surface elevation in a 75% FL tank with two porous baffles .....	91
4.3.4	Max sloshing force variations in a 25% FL tank with two porous baffles .....	94
4.3.5	Max sloshing force variations in a 50% FL tank with two porous baffles .....	96
4.3.6	Max sloshing force variations in a 75% FL tank with two porous baffles .....	98
4.3.7	Energy dissipation variations in a 25% FL tank with two porous baffles .....	101
4.3.8	Energy dissipation variations in a 50% FL tank with two porous baffles .....	102
4.3.9	Energy dissipation variations in a 75% FL tank with two porous baffles .....	103
4.3.10	Free surface elevation time series.....	105
4.4	SLOSHING DYANAMIC IN THE RECTANGUALR TANK WITH SINGLE POROUS BAFFLES	106
4.4.1	Max free surface elevation in a 25% FL tank with single porous baffles .....	106
4.4.2	Max free surface elevation in a 50% FL tank with single porous baffles .....	108
4.4.3	Max free surface elevation in a 75% FL tank with single porous baffles .....	110
4.4.4	Max sloshing force variations in a 25% FL tank with Single porous baffles .....	111
4.4.5	Max sloshing force variations in a 50% FL tank with Single porous baffles .....	113
4.4.6	Max sloshing force variations in a 75% FL tank with Single porous baffles .....	115
4.4.7	Energy dissipation variations in a 25% FL tank with single porous baffles.....	117
4.4.8	Energy dissipation variations in a 50% FL tank with single porous baffles.....	118
4.4.9	Energy dissipation variations in a 75% FL tank with single porous baffles.....	119
4.5	POROUS BAFFLES PERFORMANCE IN A SLOSHING FOR STRUCTURE-TLD INTERACTION	119
4.5.1	Model validation .....	119
4.5.2	Performance of porous baffles in the TLD .....	122

## **CHAPTER 5**

<b>SUMMARY AND CONCLUSIONS .....</b>	<b>127</b>
5.1 GENERAL CONCLUSIONS	127
5.2 SCREEN DRAG COEFFICIENT	127
5.3 TANK WITHOUT BAFFLES (CLEAN TANK) and with porous baffle.	128
5.4 SCOPE FOR FURTHER RESEARCH	130
<b>REFERENCES</b>	<b>131</b>
<b>PUBLICATIONS</b>	<b>139</b>
<b>RESUME</b>	<b>141</b>





## LIST OF FIGURES

Fig. No.	Title	Page No
Figure 1.1	FPSO Ship and shuttle tanker (source: MODEC, Inc.) .....	6
Figure 1.2	Pure Car and Truck Carriers (source: MODEC, Inc.) .....	6
Figure 1.3	Moss-type LNG carrier (source: MODEC, Inc.) .....	6
Figure 1.4	Rectangular tank with static liquid depth ' $h$ ' .....	9
Figure 1.5	Resonant sloshing modes in a tank .....	10
Figure 1.6	Mechanical Representation of Structure-TMD System .....	13
Figure 1.7	(a) Frame structure, (b) Liquid damper on a frame structure .....	15
Figure 1.8	Structure-TLD model: (a) Structure -TLD system and, (b)Equivalent mechanical linearized structure-TLD system .....	16
Figure 3.1	View of rectangular sloshing tank .....	40
Figure 3.2	A view of Runup probe at near the tank wall .....	41
Figure 3.3	View of the Runup Probe .....	42
Figure 3.4	Calibration chart for the Probes .....	43
Figure 3.5	View of the S-type Load cell .....	44
Figure 3.6	Calibration chart for the Load cells .....	45
Figure 3.7	View of LVDT connected with edge of the shake table larger plate .....	46
Figure 3.8	Calibration chart for the LVDT .....	47
Figure 3.9	Schematic diagram of the experimental shake table setup .....	48
Figure 3.10	view of experimental shake table setup .....	48
Figure 3.11	View of the Position Controller .....	49
Figure 3.12	View of the Wave generator .....	49
Figure 3.13	view of porous baffles with hole arrangements .....	51
Figure 3.14	Hole arrangements in the porous baffles .....	52
Figure 3.15	Nomenclature diagram for measurement of screen drag coefficient .....	53
Figure 3.16	view gravity flow setup .....	54
Figure 3.17	view of porous screens of six varying porosities .....	54
Figure 3.18	Experimental setup, water is stored in one tank with a known head .....	56

Figure 3.19 Experimental setup, water in the equilibrium state .....	56
Figure 3.20 Sloshing tank with porous baffles .....	60
Figure 4.1 Head against strain rate .....	69
Figure 4.2 Variation of $C_d$ with $R_e$ for different porosity of screens: (a) 4.4%, (b) 6.8%, (c) 9.2%, (d) 15%, (e) 20% and, (f) 25% .....	71
Figure 4.3 Error bar chart for screens of porosity: (a) 4.4% and, (b) 25% .....	75
Figure 4.4 Variation of damping ratio of porous screens with filling ratio .....	76
Figure 4.5 (a) The liquid free surface motion variation with the numerical results of (Frandsen, 2004). (b) The frequency response curve with the experimental results of Jin et al., 2014. (c) Maximum wave elevations with experimental results of (Faltinsen et al., 2011) [ $h/L = 0.5$ , $A = 0.005h$ , $P = 0.0672$ & $\omega = 0.7\omega_1$ ] .....	77
Figure 4.6 Maximum free surface elevation ( $\eta_{max}/A$ ) variations in a no-screen tank with 25% FL .....	78
Figure 4.7 Maximum free surface elevation ( $\eta_{max}/A$ ) variations in a no-screen tank with 50% FL .....	79
Figure 4.8 Maximum free surface elevation ( $\eta_{max}/A$ ) variations in a no-screen tank with 75% FL .....	80
Figure 4.9 Time history of free surface elevation in a tank with no screen for 25%, 50%, and 75% fill levels at $\omega = \omega_1$ , $\omega_3$ , and $\omega_5$ . .....	80
Figure 4.10 Maximum sloshing force variations in a no-screen tank with 25% FL....	81
Figure 4.11 Maximum sloshing force variations in a no-screen tank with 50% FL....	82
Figure 4.12 Maximum sloshing force variations in a no-screen tank with 75% FL....	82
Figure 4.13 Energy dissipation variations in a no-screen tank with 25% FL .....	83
Figure 4.14 Energy dissipation variations in a no-screen tank with 50% FL .....	84
Figure 4.15 Energy dissipation variations in a no-screen tank with 75% FL .....	84
Figure 4.16 Tank with two porous baffle of 4.4% porosity.....	86
Figure 4.17 Tank with two porous baffle of 6.8% porosity.....	87
Figure 4.18 Tank with two porous baffle of 9.2% porosity.....	87
Figure 4.19 Tank with two porous baffle of 4.4% porosity.....	89
Figure 4.20 Tank with two porous baffle of 6.8% porosity.....	89

Figure 4.21 Tank with two porous baffle of 9.2% porosity .....	90
Figure 4.22 Tank with two porous baffle of 4.4% porosity .....	91
Figure 4.23 Tank with two porous baffle of 6.8% porosity .....	91
Figure 4.24 Tank with two porous baffle of 9.2% porosity .....	92
Figure 4.25 Time history of free surface elevation for the tank with baffles at $\omega = \omega_3$ . .....	93
Figure 4.26 Tank with two porous baffle of 4.4% porosity .....	94
Figure 4.27 Tank with two porous baffle of 6.8% porosity .....	95
Figure 4.28 Tank with two porous baffle of 9.2% porosity .....	95
Figure 4.29 Tank with two porous baffle of 4.4% porosity .....	96
Figure 4.30 Tank with two porous baffle of 6.8% porosity .....	97
Figure 4.31 Tank with two porous baffle of 9.2% porosity .....	98
Figure 4.32 Tank with two porous baffle of 4.4% porosity .....	98
Figure 4.33 Tank with two porous baffle of 6.8% porosity .....	99
Figure 4.34 Tank with two porous baffle of 9.2% porosity .....	99
Figure 4.35 Tank with two porous baffles of (a) 4.4%, (b) 6.8%, and (c) 9.2% porosity .....	101
Figure 4.36 Tank with two porous baffles of (a) 4.4%, (b) 6.8%, and (c) 9.2% porosity .....	102
Figure 4.37 Tank with two porous baffles of (a) 4.4%, (b) 6.8%, and (c) 9.2% porosity .....	103
Figure 4.38 Time history of free surface elevation in a sloshing tank.....	104
Figure 4.39 Tank with single porous baffle of 4.4% porosity .....	106
Figure 4.40 Tank with single porous baffle of 6.8% porosity .....	107
Figure 4.41 Tank with single porous baffle of 9.2% porosity .....	107
Figure 4.42 Tank with single porous baffle of 4.4% porosity .....	108
Figure 4.43 Tank with single porous baffle of 6.8% porosity .....	109
Figure 4.44 Tank with single porous baffle of 9.2% porosity .....	109
Figure 4.45 Tank with single porous baffle of 4.4% porosity .....	110
Figure 4.46 Tank with single porous baffle of 6.8% porosity .....	110

Figure 4.47 Tank with single porous baffle of 9.2% porosity .....	111
Figure 4.48 Tank with single porous baffle of 4.4% porosity .....	111
Figure 4.49 Tank with single porous baffle of 6.8% porosity .....	112
Figure 4.50 Tank with single porous baffle of 9.2% porosity .....	112
Figure 4.51 Tank with single porous baffle of 4.4% porosity .....	113
Figure 4.52 Tank with single porous baffle of 6.8% porosity .....	114
Figure 4.53 Tank with single porous baffle of 9.2% porosity .....	114
Figure 4.54 Tank with single porous baffle of 4.4% porosity .....	115
Figure 4.55 Tank with single porous baffle of 6.8% porosity .....	115
Figure 4.56 Tank with single porous baffle of 9.2% porosity .....	116
Figure 4.57 Tank with single porous baffles of (a) 4.4%, (b) 6.8%, and (c) 9.2% porosity .....	117
Figure 4.58 Tank with single porous baffles of (a) 4.4%, (b) 6.8%, and (c) 9.2% porosity .....	118
Figure 4.59 Tank with single porous baffles of (a) 4.4%, (b) 6.8%, and (c) 9.2% porosity .....	119
Figure 4.60 Displacement time history of the first mass .....	120
Figure 4.61 Normalized linearized equivalent damping ratio .....	121
Figure 4.62 Frequency response curve for the structure-TLD system model.....	122
Figure 4.63 TLD with 4.4% porosity baffle .....	123
Figure 4.64 TLD with 6.8% porosity baffle .....	124
Figure 4.65 TLD with 9.2% porosity baffle .....	125
Figure 4.66 TLD with 58%% porosity baffle .....	125

## LIST OF TABLES

<b>Table No.</b>	<b>Title</b>	<b>Page No.</b>
Table 1	Frequency range for shake table experiments.....	58
Table 2	Details of empirical relation .....	70
Table 3	Experimental data .....	72
Table 4	Natural frequencies of clean tank sloshing.....	74
Table 5	Building Properties .....	121
Table 6	TLD Properties (Soliman et al. (2015)).....	121



## NOMENCLATURE

$A$	Excitation amplitude	$\beta$	Forcing frequency ratio
$b$	Tank width	$\gamma$	Excitation factor
$C_d$	Screen drag coefficient	$\Delta$ & $\Xi$	Screen parameters
$C_l$	Screen loss coefficient	$\eta$	Free surface oscillation in a tank
$c$	Generalized damping coefficient	$\rho$	Density of water
$f$	Sloshing frequency		
$g$	Acceleration due to gravity		
$H$	Height of sloshing tank		
$h$	Depth of water in the tank		
$k$	Generalized stiffness		
$L$	Length of tank		
$l$	Length of compartment tank		
$m$	Generalized mass of liquid		
$n$	Sloshing modes		
$P$	Porosity of screen		
$q$	Free surface sloshing amplitude		
$S$	Solidity ratio		
$FL$	Fill level		
$TLD$	Tuned Liquid Damper		

# CHAPTER 1

## INTRODUCTION

---

### 1.1 GENERAL

Sloshing is the participation or wave motion of fluid in a partially filled moving tank/vessel. Sloshing can happen as a result of the tank liquid's resonant excitation and should be taken into account for practically any moving structures or vehicles that contains a liquid with an open surface. Sloshing may also result from transient motion. These motions produce severe hydrodynamic forces and pressure, which can adversely impact the sloshing tanks, and structure/vehicles which are coupled with the sloshing tank. Excitation at frequencies close to the fundamental natural frequencies of liquid movement is of basic functional importance. Sloshing is a complex and significant phenomenon that has many engineering applications. For example, it has been studied in the area of Chemical engineering as a reactor, nuclear vessels and reactors in nuclear engineering. Tower stations and tall buildings with Tuned Liquid Damper (TLD) in Civil engineering, Liquefied Natural Gas (LNG), Bulk carriers-SOLAS (Safety of Life at Sea), Re-Gasification Units (FSRU), Liquefied petroleum gas (LPG), Production Storage and Offloading (FPSO)/Floating Storage in Marine engineering. Bulk cargo carriers in Highway engineering, and rockets and space vehicles in Space engineering.

Sloshing is extremely useful for both onshore and offshore-based applications. Extensive research has been conducted on amplification free-surface liquid movement in container in aircraft, missiles, and rockets. Sloshing has a significant impact on the dynamic stability of these vehicles. The possibility is that sloshing could have a significant impact on the dynamics of the carrying bodies. The effectiveness of oil-gas separators is impacted by liquid movement on floating platforms of oil and gas generation. A special emphasis on the sloshing phenomenon in a tank can be taken into consideration during the assessment of floating stability ships, where tank motion frequencies are lower than natural sloshing frequencies. When the ship is moving with energy close to the fundamental natural period of the liquid fill level of the ship tank,



Violent liquid motion could occur in a ship tank which is simply partially filled, resulting in a high-impact liquid tank interaction.

The land-based structures are exposed to sloshing under earthquake and wind actions. The sloshing effects are one of the essential parameters in the design and analysis of structures coupled with sloshing tanks. Unbalanced liquid movement in a tanks can be used to suppress the accelerations caused by wind or earthquake on all land based structures. In the field of civil and/or construction engineering, the concept of a TLD is well-known. A landslide or earthquake could create massive sloshing in a lake with steep sides. This kind of situations should be considered and analysed with suitable guidelines during dam construction. A massive liquid sloshing effects also experience in rivers and harbours environment. In moving containers like tank vehicles on highways, transport safety issues are caused by liquid motion in the containers.

The dynamics of liquid in the partially filled containers/tanks is a complicated event in the engineering field. Its comprehension necessitates the use of sloshing theories, experimental studies, analytical/theoretical, numerical, computational fluid dynamics (CFD), and combinations of different approaches with experimental investigations. Over the last ten decades, researchers have studied sloshing using various approaches, which have been reviewed in the literature chapter.

The research on liquid motion in the tanks/vessels involves estimating the hydrodynamic characteristics of sloshing under various types of excitations. The preliminary study involves the size and shape of the sloshing tank, liquid depth, excitation type, natural frequencies and modes of liquid oscillation, and other factors that affect liquid movement. The characteristics of liquid motion include frequency/period and mode of oscillation. This approach is used to evaluate a tank's natural periods and corresponding modes. with varying tank dimensions and liquid levels (Ibrahim, 2005). Experiments are frequently used in tank design and to study the dynamics of wave-tank interaction problems. The inclusion of hydrodynamics and structural mechanics is critical in tank design. The flow-damping devices (solid/porous baffles) are being used in the liquid containers to reduce/ handle the sloshing loads on tank walls and increase the stability of liquid-carrying vehicles. Tanks with baffles are

also used in structure-TLD interaction problems to mitigate structural vibrations. However, many researchers are working and studies are being conducted to investigate the sloshing dynamics from scale model to full-scale.

## **1.2 RESONANT SLOSHING**

The lowest natural frequencies are crucial for determining how violent sloshing is. The tank's geometry, the liquid's depth, and the tank's length are main parameters to determine the natural sloshing periods and/or frequencies and related sloshing modes in the tanks. The liquid fill level in the tank is an important parameter to have a major impact on the sloshing frequency with tank length. The liquid fill level is classified as shallow, intermediate, or shallow based on the liquid motion in the tank. The resonance will exist regardless of the liquid fill level in the tank when the excitation frequencies are nearly in phase with the liquid's natural frequencies in the tank. The resonant conditions in a clean sloshing tank are dependent on liquid fill level, i.e., amplification may vary with shallow, intermediate, and finite liquid-depth conditions. Clean tank refers that, the liquid participation in the tank without any flow-damping devices such as baffles (devices in the tank that do not influence the fluid flow) and negligible viscous damping effect. The linear sloshing theory of an incompressible fluid can accurately characterise liquid motion in the containers in many practical and real-world situations. There are an infinite number of eigenfrequencies and eigenmodes in which there are solutions meeting the Laplace equation. The analytically based multimodal method is built on these eigensolutions, which helps to describe nonlinear forced sloshing.

## **1.3 SLOSHING IN REAL-LIFE CIRCUMSTANCES**

Liquid sloshing dynamics investigation aims to attract a significant amount of attention with regard to its relevance in a wide range of applications: The application mainly includes

- Sloshing in ship tanks: Liquefied gas carriers (LPG and LNG)
- Liquid sloshing in FPSO ships and oil / Shuttle tankers
- Sloshing in holds in the Bulk carriers

- Sloshing in liquid dampers
- Sloshing in ballast tanks and oil-gas separators of offshore platforms
- Liquid participation in the fabric structures
- Sloshing in coastal engineering
- Liquid-fuel motion in space vehicles
- Liquid motion inland transportation
- Sloshing in onshore tanks (Oil storage and elevated water tanks)

In a marine environment, the ship's tank experiences a sloshing effect. Ship tanks are primarily classified based on tank geometry for different engineering conditions and applications. Liquid participation in the many ship containers mainly influence by the size and shape of the tank, which includes tank breadth and liquid fill level in the tank. The ship tank shapes mainly include rectangular, prismatic, spherical, etc. the ship's tanks with partially filled liquid could be water, petroleum and its by-products, gas, etc. A ship's length is an important parameter for ship motion. Wave-induced ship motions are the main source of excitation for sloshing in ship tanks. Sloshing in the tank is also experienced due to interaction of two ships or impact between ship and ice structures. Angular ship movements cause liquid motion relative to tank movement even when a tank is completely filled with liquid. The sloshing dynamics in the ship tanks under wave actions include types of excitations such as surge, sway, heave, roll, pitch, and yaw of a ship. In the frequency range of interest, according to linear theory, tank lateral excitation causes more liquid participation than vertical tank motions. The ship tank experienced hydrodynamic loading inside the sloshing tank due to action of sea wave action. The assessment of tank response under sloshing loads is important for both the ultimate limit state (collapse caused by the highest load at the time) and the fatigue limit state (repetitive load which causes fatigue). The transverse webs and horizontal stringers are being used as internal structures to have a damping effect on sloshing in the ship tanks.

In the case of oil tankers, the tank owner avoids having extra structural elements in cargo tanks for business circumstances, and there are no restrictions on specific fill levels in the tanks. As a result, a tank with no internal structure and varying fill levels

will likely have more sloshing. The tank with optimum fill level and/or use swash bulkhead of different porosities is a more important criterion for controlling the sloshing impact. The concept of dampening structural motions with liquid-filled tanks first appeared in the late 1800s (Winden 2009). Later in 1862, William Froude proposed that if the frequency and phase of the oscillating water in the tank were properly tuned, a tank partially filled with liquid could minimise a ship's rolling motions in the marine environment. In the 1960s (Miles 1963) partially filled tank with optimum/tuned fill level concept was used to control the wobbling movement of in space structure. And, resonant sloshing will be reduced by perforated swash bulkheads by flow separation caused by flow through the holes (Crowley and Porter (2012a, 2012b); Bellezi et al., 2019). Dodge (2000) explored the concept of liquid sloshing in tank compartments, namely the tank with porous baffle of porosity equal to or less than 10%, the full tank acting as two smaller tanks without baffle condition, the liquid will slosh between the compartments, and the natural sloshing frequency will approach the value of a tank without baffle condition. The tanks with the low level of porosities of bulkheads may effective to reduced amplification where the fundamental natural frequency is an important parameter. Because of ship tanks' importance in a variety of applications, research into liquid sloshing dynamics continues to solicit significant attention. The applications include floating production storage and offloading (FPSO) and shuttle tankers (Figure 1.1), Floating Storage & Regasification Units (FSRU), Pure Car and Truck Carriers (Figure 1.2), LNG carriers (freestanding and nonfreestanding) shown in Figure 1.3, Bulk carriers, Liquefied gas carriers, LPG carriers, Chemical tankers, Fish transportation, Cruise vessels, and antirolling tanks. Sloshing in ship tanks can result in higher pressures/forces that can cause significantly damage the walls and roof of the tank. In order to build liquid tank structures and assure safe operations, it is crucial to investigate the sloshing phenomenon.

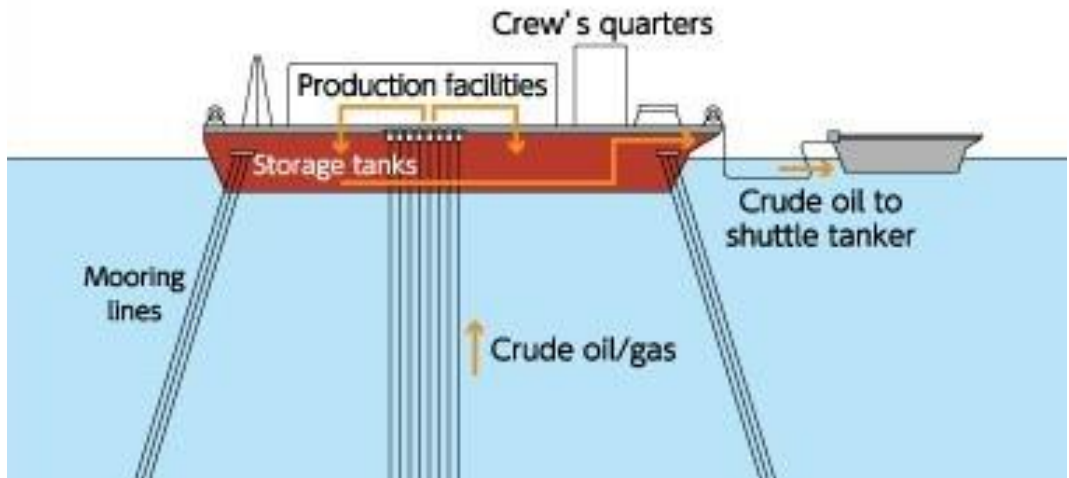


Figure 1.1 FPSO Ship and shuttle tanker (source: MODEC, Inc.)

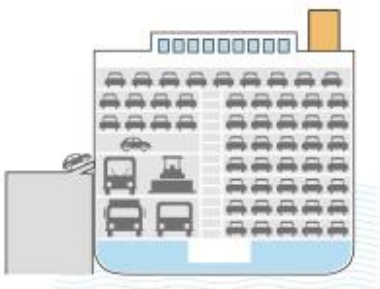


Figure 1.2 Pure Car and Truck Carriers (source: MODEC, Inc.)

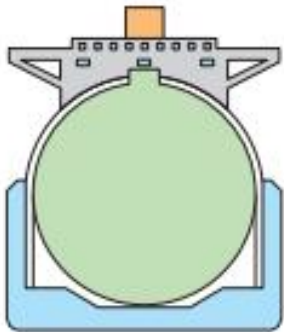


Figure 1.3 Moss-type LNG carrier (source: MODEC, Inc.)

The sloshing technology for space applications primarily includes resonant sloshing periods and entire loads to manage structures needful. and, with less emphasis on the impact of slosh pressure on structural requirements. When compared to other applications, the excitation amplitudes considered for spacecraft are too small. A greater percentage of a space vehicle is fuel to boost or launch vehicles. The fact that spacecraft in orbit around the Earth is close to weightless has a significant impact on sloshing in fuel tanks. Therefore, dominant fuel-slosh frequencies are of more concern for researchers and scientists to increase stability. The monitoring system frequencies and/or the frequencies at which elastic bodies bend are not far from the dominating fuel-slosh frequencies, which is cause for concern. The dynamic non control system and higher order amplitude response of space structures may occur as a result of fuel-slosh frequencies that are not associated with flexible body bending frequencies and system control harmonics. Therefore, the flow-damping devices in the sloshing tank may lead an important role to increase stability.

Earthquakes, wind, and wave action are among the most destructive natural disasters, causing significant loss of life and livelihood. The response of a structure during these actions is mainly governed by the load characteristics and the structure itself. The land, ocean, and space structures are often susceptible to seismic, wave, and wind-induced vibrations due to low levels of inherent damping. The use of Dynamic Vibration Absorbers (DVAs) to reduce exorbitant vibrations caused by various types of dynamic actions has grown in the last few decades. Tuned Liquid Dampers (TLDs) is one technique for reducing excessive vibrations. A DVA improves damping by dissipating some of the energy generated when a structure moves under both regular and irregular excitations. As a result, the displacement of primary structures coupled with the liquid tank (DVAs) is reduced, and the structures become more stable. Various systems are proposed to mitigate the structural vibration against loads. Based on structural conditions, configuration, and applications, different categories of protection systems have been implemented in the last few decades, in which the sloshing tank was found to be more effective.

For land-based structures and/or buildings, water storage tanks are used as liquid sloshing tanks so-called tuned liquid dampers (TLD). The TLDs are a type of passive

mechanical damper and are designed as a sloshing tank. These partially filled rigid tanks are located in the structure at or near the location of maximum modal displacement for suppressing structural vibrations. In the 1960s this concept was implemented to reduce the wobbling movement of satellites in space. The dynamics of sloshing in the tank provide an effective and easy technique to enhance the damping of a system and relies on liquid sloshing inside the tank to dissipate energy from the viscous action and wave breaking. The sloshing in the tank functions similarly to a tuned mass damper, with the main difference being that the liquid tank relies on the sloshing fluid's inertial force to reduce the vibratory motion. The efficiency of sloshing in the tank mainly depends on the fluid height in the tank, the tank length, and the type of structure that couples with the sloshing tank. A tall storey hotel called “Shin Yokohama Prince” located at Japan was first introduced to understand the performance of TLD as response control of tall storey buildings. A liquid damper with shallow liquid depths are more efficient energy dissipators than those of tank with large liquid depths (Marsh et al. 2010). According to preliminary research on the structure-TLD interaction, using highly viscous fluids or extremely shallow water depths to achieve higher damping is practically more expensive. Given these limitations, the use of baffles seems to be more practical (Warnitchai and Pinkaew,1998).

TLDs are classified into two types: tuned sloshing dampers (TSDs) and tuned liquid column dampers (TLCDs). A U-tube sloshing damping device with a flow type opening in the centre is the basic structure with liquid type tuned column dampers. The TLCD dissipates the structural vibration energy through actions of sloshing including liquid mass movement within the container, gravity's restoring force on the liquid, and other factors. The damping screens in the TLCDs are found to be more effective for sloshing damping elements.

Sloshing in liquid-carrying tanks of vehicles affects the carrying vehicle's stability and causes road accidents. The sloshing mainly occurs due to sudden stops and vehicles rapidly changing lanes on a highway. When the vehicle comes to a sudden stop, shallow liquid type waves form, causing longitudinal sloshing in the tank. When the waves hit the tank's end, the waves forced the vehicle along the direction of the wave propagation. This is extremely crucial if the tank has not been baffled. As a result, adding baffles is

a good way to improve the vehicle's stability. During changing lanes, the tanker vehicle experiences oscillating transverse force and roll moment due to the sloshing, which could lead to vehicle rollover. The tank geometry and liquid fill levels may affect the highest natural period.

#### 1.4 SLOSHING IN A RECTANGULAR TANK

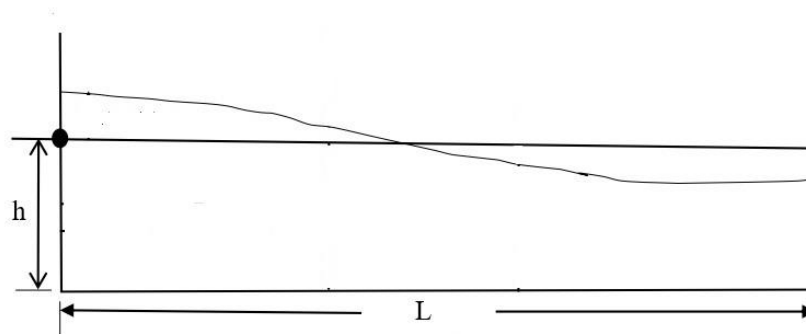
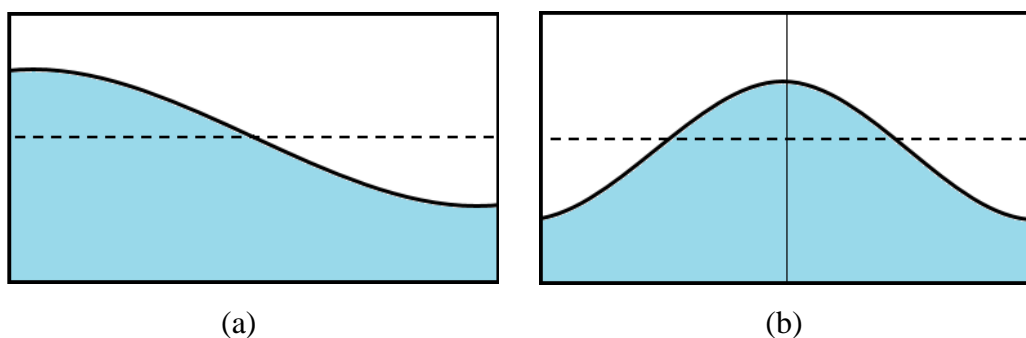


Figure 1.4 Rectangular tank with static liquid depth ' $h$ '

The natural period and frequency in the varying size of the rectangular tanks depend on tank length ( $L$ ) and depth of liquid fill level ( $h$ ) in the tank. For two-dimensional rectangular tanks (Figure 1.4), to determine the natural frequency and other possible solutions reported by Fox and Kuttler (1983) and Ibrahim (2005). The linear and nonlinear behavior in the tank depends on the tank aspect ratio (liquid depth to tank larger dimension). The aspect ratio of the tank appears in the hyperbolic tangent form for natural periods and frequencies. The  $\tanh(i\pi h/L)$  term behaves in different ways for varying aspect ratios. Based on this behavior, shallow liquid, intermediate liquid, finite liquid, and deep liquid approximations can be deduced.





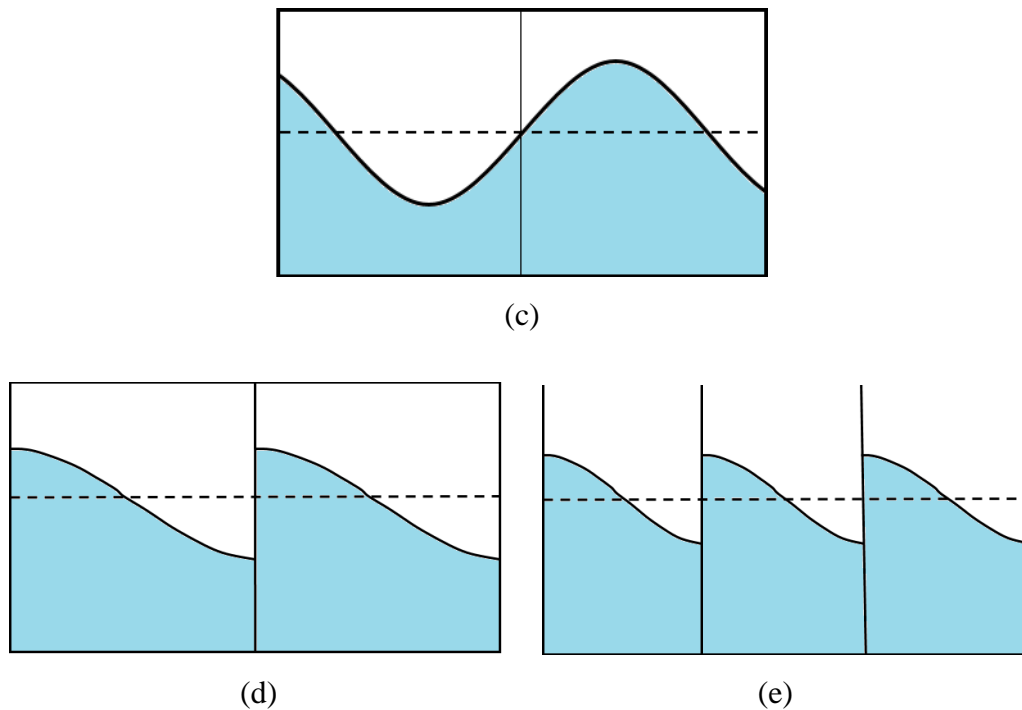


Figure 1.5 Resonant sloshing modes in a tank

Figure 1.5 depicts three resonance situations (mode shapes) for sloshing in tanks with and without porous baffles. These modes are essential for comprehending the various flow patterns in a sloshing tank. The odd modes are anti-symmetric, whereas the even modes are symmetric. The linear superposition of these natural modes can represent any arbitrary motion of a free surface. Figure 1.5a represents the rectangular tank's first resonant sloshing mode ( $n_1$ ), which consists of a standing wave with a wavelength of  $2L$ . The first sloshing mode is also known as the first antisymmetric mode of the tank without baffle (non-compartment tank). The compartment tank refers to the tank with non-perforated baffles. In the tank, the one baffle at the center of the tank, the whole tank ( $L$ ) is divided into two clean tanks of each length ( $L/2$ ). Similarly, when two porous baffles are impermeable or watertight, the rectangular tank functions as three independent/separate tanks with no screen case. The three separate smaller tanks of each length ( $L/3$ ) are defined as compartment tanks (Figure 1.5e). The second sloshing mode in the tank,  $n_2$  (Figure 1.5b), is referred to as fundamental symmetric mode in non-compartment tank and the fundamental antisymmetric mode for the

compartmented tank (Figure 1.5d), which consists of a standing wave with a wavelength of  $L$ . Figure 1.5c represents the third sloshing mode ( $n=3$ ) in the tank, which is the second antisymmetric mode of the clean tank and consists of a standing wave with a wavelength of  $0.67L$ .

## 1.5 DRAG COEFFICIENT

The fluid flow through or flow around bodies problem and their solutions are more of interest in fluid mechanics. The vehicle of a liquid-fuelled rocket in space, the liquid tank of cargo ships in an offshore environment, elevated tanks and buildings with overhead tanks onshore, etc. are usually oscillating or slosh due to the motion of parent structures. Damping of the fluid inside the sloshing tank is an important part of the design. The hydrodynamic damping may perfectly be achieved by the use of baffle and porous bodies/structures with optimum porosity inside the sloshing tank and in wave structure, respectively. The study of forces on piles due to the wave action (Morison et al. 1950) has given a useful approximation. The forces are divided into two parts, one due to the drag and the other due to inertia. This concept necessitates the introduction of a drag coefficient ( $C_d$ ). The hydrodynamic drag and inertial forces on cylinders and plates in an oscillating fluid were studied by conducting an experimental program (Keulegan 1958). Different authors have given definitions for Reynold's number based on viscous flow regimes by conducting a range of tests. The steady flow drag mechanism shows viscous nature for  $Re < 100$  whereas, the drag mechanism is primarily turbulent for  $Re > 100$ . It was suspected, the viscous flow portion in an oscillatory flow might contribute a substantial drag force to cause the overall drag coefficient if the Reynolds number is used based on the peak velocity. The equation for the drag coefficient of the screen is derived over a wide range of flow velocity based on the total area of the screen by conducting simple tests on the gravitational flow between two tanks (Warnitchai and Pinkaew 1998). The drag coefficient was found to be a function of the Reynolds number and the screen-induced damping is estimated by the energy-ratio procedure. "Keulegan (1968) prepared design of filters and wave absorber as a part of the wave-structure investigation." The analytical and experimental works on-screen filters have been conducted for the estimation of damping. The screens of given mesh size and wire diameter were selected, and these are constructed in two

ways, interlaced screen filters, and plane screen filters. The lab test shows that the wave oscillation characteristic was found to be simple in the case of plane screen filters, whereas, difficult to generalize the information due to the absence of suitable analytical treatment in the case of interlace screen filters. The experiment test with assemblies of screens of wire under a steady current was carried out to examine the energy loss phenomena. The resistance of the screen was found to be greater than the computed values based on the law for single wires. For the low value of the Reynolds number, the loss coefficient of a single screen is inversely proportional to the Reynolds number, whereas, proportions are changed for moderately high values of the Reynolds number. To assess the damping nature of the screen with wire mesh authors have conducted a test on the flow between two reservoirs with a range of Reynolds number, and it was observed that the computed resistance is about seven times smaller than the observed resistance. The damping can be predicted by a suitable theory; however, the behavior of screens cannot be judged by theory alone. Therefore, it is necessary to conduct experiments to establish the values of the empirical constants. The studies conclude that the experimental procedures are preferred due to the difficulties of reproducing the physical phenomena involved in fluid-structure interaction problems even though the theoretical and numerical models had a good agreement.

In the area of sloshing dynamics, an oscillation of liquid in a tank with baffles/screen arrangement, it is necessary to calculate the additional damping effect developed through damping screen. The ratio of a system's total energy to its rate of energy dissipation in time steps could be used to define the damping ratio. By considering the importance of damping in fluid-structure interaction problems, the drag coefficient for porous screens plays an important role.

## **1.6 STRUCTURE-TLD INTERACTION**

### **1.6.1 Tuned Mass Damper (TMD)**

Passive control systems have been widely used in engineering practice to mitigate the vibration of the structure caused by wind and earthquakes. A supplementary/additional mass (TMD) concept is used to mitigate the displacement in the primary structure. The easy technique for controlling structural vibration is due to the force which exerted due

to inertia effect by the TMD on the primary structure, which can be anti-phase to the excitation force. A TMD system includes the mass ( $m$ ), a spring system which refers the TMD stiffness ( $k$ ), and a dashpot arrangement refers the system damping ( $c$ ) as designed in Figure 1.6. In the same context, the main structure is represented by a generalized mass -  $M_s$ , generalized stiffness -  $K_s$ , and generalized damping -  $C_s$ .

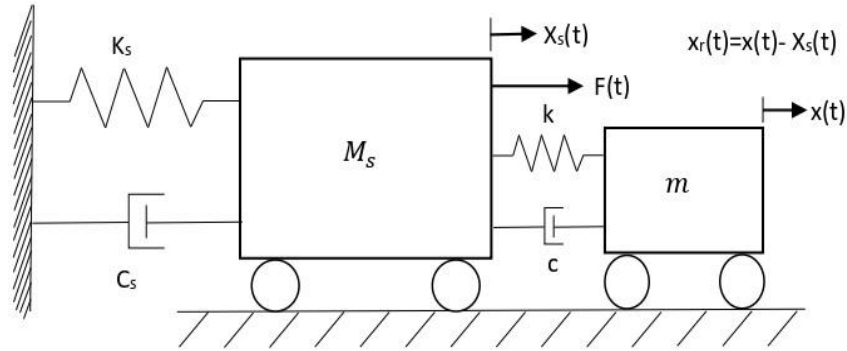


Figure 1.6 Mechanical Representation of Structure-TMD System

In a Structure-TMD system, the response behavior of the secondary system mass is related with the response of the primary structure. The governing equations of motion the main mass (Equation 1) and the secondary mass (Equation 2) are given as follows

$$M_s \ddot{X}_s(t) + C_s \dot{X}_s(t) + K_s X_s(t) = F(t) + c(\dot{x}_s(t) - \dot{X}_s(t)) + k(x_s(t) - X_s(t)) \quad (1)$$

$$m(\ddot{x}_s(t) - \ddot{X}_s(t)) + c(\dot{x}_s(t) - \dot{X}_s(t)) + k(x_s(t) - X_s(t)) = -m\ddot{X}_s(t) \quad (2)$$

Summation of the above two equations leads to the equation of motion of the main system coupled with secondary mass is given as

$$(M_s + m) \ddot{X}_s(t) + C_s \dot{X}_s(t) + K_s X_s(t) = F(t) - m(\ddot{x}_s(t) - \ddot{X}_s(t))$$

The addition of a secondary mass to the main system, the change in the natural frequency can be noticed due to TMD mass as well inertial force term ( $m(\ddot{x}_s(t) - \ddot{X}_s(t))$ ). In the structure-TMD interaction, the mass ratio, frequency ratio or tuning ratio, and

damping ratio contribute a unique role to mitigate the resonant response of main/primary structures.

### **1.6.2 Tuned Liquid Damper (TLD)**

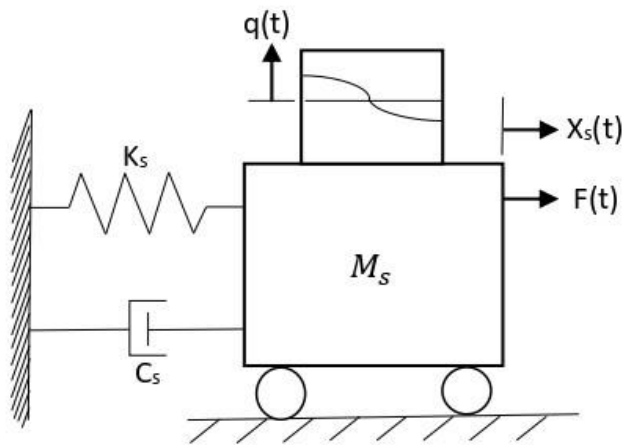
A partially filled rigid liquid tank used to mitigate the structural vibration under large excitation condition is called as a tuned liquid damper. It is a type of passive control system and is installed in a structure at or near (Figure 1.7b) the maximum modal displacement to suppress structural vibrations. The Tuned Liquid Dampers (TLD) concept is an effective and easiest technique for increasing structural damping that relies on liquid sloshing inside the tank to dissipate energy. The TLD works similarly to TMD, the main difference is that the TLD works on the inertial force due to the liquid participation inside the tank to mitigate the resonant motion of the main structure. Figures 1.8a and b show a mechanical representation of the SDOF system with a Tuned Liquid Damper and Equivalent mechanical linearized structure-TLD model based on the TMD analogy (Tait 2008).

## **1.7 MOTIVATION FOR THE PRESENT STUDY**

To achieve better performance of on-shore, off-shore, and space structures connected with a liquid tank under different types of actions, the damping effects for liquid sloshing due to porous baffle in a sloshing tank have been studied rigorously and are widely used. The tank with porous baffle modifies the liquid motion in the rigid tank which reduces the sloshing oscillations, reduces the hydrodynamic force on end walls, and increases the damping in it by energy dissipation. And, determination of the drag coefficient is an important element to evaluate the damping effect due to porous screen in the sloshing tank. In this connection, the present work is intended to fill the knowledge gap by investigating the proposed sloshing characteristics in the tank with porous screens of varying porosities, different filling levels, and loss characteristics of porous screens with new drag-coefficient in the tank.



Figure 1.7 (a) Frame structure, (b) Liquid damper on a frame structure



(a)

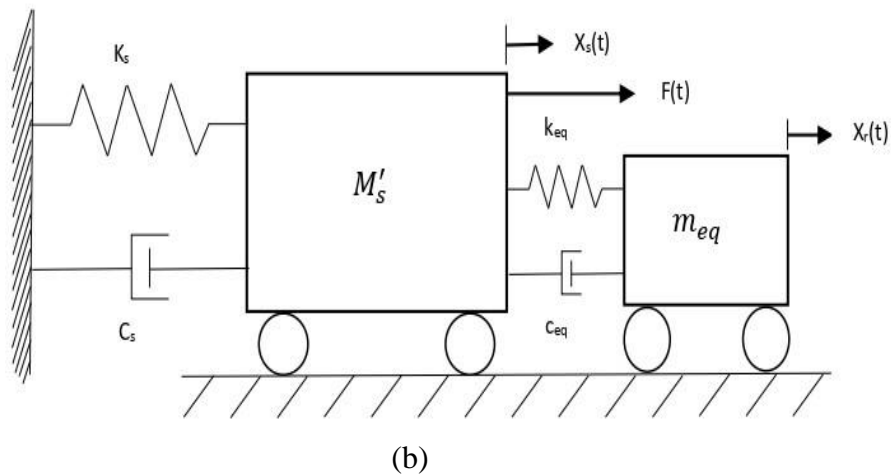


Figure 1.8 Structure-TLD model: (a) Structure -TLD system and, (b)Equivalent mechanical linearized structure-TLD system

## 1.8 ORGANIZATION OF THE THESIS

Chapter 1, provides an overview of liquid sloshing in tanks, its consequences, and its application. The physics of sloshing in the tank and the theory used in the current investigation are also discussed, together with the relevant approach and mathematical background.

Chapter 2, is concerned with the available literature review studies on the topic of sloshing and screen drag coefficient. The literature has been focused on the drag coefficient for porous baffles in an oscillating and non-oscillating flow condition, liquid sloshing models with perforated baffles, experimental shake table tests involving the details of hydrodynamic action in the rectangular sloshing tanks

Chapter 3, describes the problem formulation and the details of the experiment's setup and instrumentation, including working principles and procedures, and instrument calibration details. Formulation of liquid sloshing in the tank and structure -TLD model details.

Chapter 4, details of analytical model performance in the baffled and clean sloshing tanks. Liquid motion response with wave elevation, sloshing force, and energy dissipation characteristics are validated with an experimental sloshing test. Porous baffles performance in a TLD for SDOF system.

Chapter 5, gives a summary of the work and conclusions drawn from the current study, as well as the scope of future work in the continuation of work on the topic of sloshing.





### BACKGROUND AND LITERATURE REVIEW

---

#### 2.1 INTRODUCTION

Over the past few decades, there has been extensive research into the dynamics of liquid participation in various geometry of tanks, tanks with flow-damping devices (baffles), and their applications. Controlling the liquid sloshing in the tanks is important for safety and operation in many engineering fields. Several studies have been carried out in order to generate hypotheses in the form of experimental, analytical, and numerical models. As a result of narrowing our focus to the objectives of the current study, a limited number of research studies relevant to the current investigation are reviewed and included in this section. Based on the study objectives the review is divided into the following sections.

- Loss coefficient / Drag coefficient for porous baffles
- Sloshing dynamics in rectangular tanks with and without baffles
- Rectangular TLDs with baffles for structural response control

#### 2.2 EXPERIMENTAL LOSS COEFFICIENT / DRAG COEFFICIENT FOR POROUS BAFFLES

Damping of the fluid inside the sloshing tank is an important part of the design. The hydrodynamic damping may perfectly be achieved by the use of baffle and porous bodies/structures with optimum porosity inside the sloshing tank and in wave structure, respectively. The study of forces on piles due to the wave action has given a useful approximation (Morison et al., 1950). The forces are divided into two parts, one due to the drag and the other due to inertia. This concept necessitates the introduction of a drag coefficient ( $C_d$ ) / loss coefficient ( $C_l$ ).

*Keulegan and Carpenter (1958)* investigated forces on cylinders and plates under normal harmonic currents. Based on experimental results an empirical equation for the drag coefficient was developed through the Fourier analysis. The coefficient was

examined under varying flow velocities with time period (Keulegan-Carpenter number). The coefficient of drag variation under range of harmonic currents were observed to be function of period parameter than the Reynold number.

*Keulegan (1968)* prepared the design of filters and wave absorbers as a part of the wave-structure investigation.” The analytical and experimental works on screen filters have been conducted for the estimation of damping. The screens of given mesh size and wire diameter were selected, and these are constructed in two ways, interlaced screen filters, and plane screen filters. The lab test shows that the wave oscillation characteristic was found to be simple in the case of plane screen filters, whereas, difficult to generalize the information due to the absence of suitable analytical treatment in the case of interlace screen filters. The experiment test with assemblies of screens of wire under a steady current was carried out to examine the energy loss phenomena. The resistance of the screen was found to be greater than the computed values based on the law for single wires. For the low value of the Reynolds number, the loss coefficient of a single screen is inversely proportional to the Reynolds number, whereas, proportions are changed for moderately high values of the Reynolds number. To assess the damping nature of the screen with wire mesh authors have conducted a test on the flow between two reservoirs with a range of Reynolds number, and it was observed that the computed resistance is about seven times smaller than the observed resistance. The damping can be predicted by a suitable theory; however, the behavior of screens cannot be judged by theory alone. Therefore, it is necessary to conduct experiments to establish the values of the empirical constants. The studies conclude that the experimental procedures are preferred due to the difficulties of reproducing the physical phenomena involved in fluid-structure interaction problems even though the theoretical and numerical models had a good agreement.

*Shih et al. (1971)* analysed the fluid flow around oscillating flat plates using an experimental study, and identified the types of forces exerted on the plates at low Reynolds numbers (1.01 to 1057). When the Reynolds number exceeded 250 during the test series, the drag coefficient's dependence on the value reduced. In addition, a mathematical expression was established to relate the Drag coefficient, KC number, and Reynolds number.

**Baines and Peterson (1951)** described both theoretical and experimental flow through screen investigations. The investigation includes pressure drop, velocity distribution, and turbulence characteristics from various screen types and porosities. The authors suggested an empirical relation to evaluate the screen loss coefficient based on the screen contraction coefficient and varying porosity.

**Fediw et al. (1995)** conducted experimental and theoretical investigations on damping screens performance in the sloshing tank for TLD. Loss coefficients based on water velocity through the screens were considered to account for the additional damping by the screen. In the test series, the authors presented the coefficient of drag for screens in the test series is a depends on the Keulegan–Carpenter number.

**Warnitchai and Pinkaew (1998)** carried out experimental gravity flow tests between two tanks to evaluate the screen drag coefficient. An empirical equation was derived to calculate the screen drag coefficient based on perforation variation in the screen and the Reynolds number. Further, the energy-ratio procedure was used to estimate additional screen induced damping.

**Isaacson et al. (2001)** studied the effectiveness of horizontal and vertical baffles in the liquid sloshing tank. The drag coefficient was found to be a function of hydrodynamic behavior of liquid sloshing in tank with varying position of baffles. The drag coefficients were considered using test results of wall-bounded plates, as suggested by Sarpkaya and O’Keefe (1996).

**Tait et al. (2005)** explained an iterative procedure by assuming velocity and loss coefficient in the sloshing tank. Further, the authors conducted an experimental investigation on sloshing tanks with slotted screens under known excitation amplitude and frequency near resonance to determine the drag coefficient based Keulegan-Carpenter ( $KC$ ) number. The test results of the  $KC$  number are well matched with results for the non-oscillating flow condition (Baines and Peterson (1951)).

**Tait (2008)** described total forces acting on screens based on the Morison equation and provided values for theoretical equations used to calculate both inertia and drag forces on screens using appropriate inertia, drag, and loss coefficients.

*Crowley and Porter (2012a, 2012b)* studied the transmission of waves through thin vertical porous screens, and the effects of both inertial and dominant quadratic drag were included in a proposed linearized model. Both inertial and drag coefficients are determined empirically from idealized mathematical models (boundary-value problem). The same procedure was used to analyze screen arrangements in a TLD.

*Goudarzi and Yazdi (2012)* obtained an solution for the damping ratio through analytical an model provided by both horizontal and vertical baffles in the sloshing tank by the energy ratio formula. The drag force and drag coefficient for the damping ratio was expressed based on the equation and parameter suggested by Stricklin and Baird (1966); Keulegan and Carpenter (1958); and Sarpkaya and O’Keefe (1996).

*Hamelin et al. (2013)* carried out a series of shake table tests for slotted baffle screen performance in the TLD with Keulegan-Carpenter (*KC*)- number dependent drag coefficient. Expected performance was observed by screen in the tank. A relationship was established to explore the drag coefficient value under range of flow velocities through screen is dependent on *KC* number. Further, the best curve fit on the experimental data was performed to express the relationship between the parameters for specific TLD models.

*Molin and Remy (2013)* considered the drag coefficient for the vertical perforated screen in the sloshing tank using a discharge equation based on linearized hydrodynamics pressure and Lorentz linearization, similar to Crowley and Porter (2012a, 2012b) work. The main difference between Crowley and Porter (2012a, 2012b) and Molin and Remy (2013) is that the drag coefficient in Crowley and Porter (2012a, 2012b) is averaged over depth, whereas in Molin and Remy (2013) it is depth-dependent.

*Cho and Kim (2016)* used two porous baffles of three different porosities and varying submerged depths of baffles in the rectangular sloshing tank. The dynamics of sloshing include both inertial and quadratic-drag terms. The drag coefficient for porous baffles was obtained using the relation suggested by Mei (1989); Tait et al (2005), which represents the energy dissipation across the porous baffle.

## **2.3 SLOSHING DYNAMICS IN THE TANKS**

Dynamics of sloshing in the tanks are mainly classified based on nonlinear and linear phenomena, and these include tank geometry, liquid fill level in the tank, state of excitation, particle velocity, free surface amplitude, wave breaking, amplitude dispersion, wave run-up, resonant frequency shift phenomenon, wave-tank interaction, air-water interaction, jump phenomenon, beating phenomenon, the sum of sloshing modes, and so on.

Faltinsen and Timokha (2009) presented a book on the dynamics of sloshing with both offshore and onshore applications. In the book, the authors discussed primarily the multimodal method and preliminary discussion on computational fluid dynamics. They also highlight various experimental findings, which cover the linear and nonlinear sloshing dynamics, damping characteristics, and wave actions in the sloshing tanks with illustrations and examples.

Even if there are documents, books, and a few review articles on sloshing dynamics, they fall short in terms of in-depth explanation. Hence, a detailed assessment of the sloshing in the rectangular tanks is given in this section.

### **2.3.1 Experimental investigation**

Many organizations, institutes, scientists, and researchers carried out a range of experimental investigation to study the physical sloshing phenomenon. Several experimental sloshing studies were carried out using shake table tests, with a few conducted in a wave flume and a tank attached to a wall by spring-damper system arrangements.

Experimental and theoretical aspects of the sloshing phenomenon and characteristics for spacecraft application have been carried out by Abramson (1966) and Feschenko et al. (1969). The investigation includes both linear and nonlinear sloshing phenomena, and slosh-suppressing devices in the sloshing tank were introduced to model sloshing in the tank using linear theories. A nonlinear sloshing investigation was also attempted.

*Isaacson and Premasiri (2001)* presented a theoretical model that predicted the effects of vertical and bottom-mounted baffles in a sloshing tank under horizontal motion. To validate the model, experimental tests were conducted on the impacts of various baffle arrangements. The results showed that the damping coefficient of vertical and horizontal baffles varies with tank length and depth. Researchers revealed that vertical and horizontal baffles are more effective at dampening liquid motions in elevated tanks. Both types of baffles are recommended for application in near-resonance situations.

*Akyildiz and Ünal (2005)* studied liquid sloshing dynamics in a rectangular tank by experiments investigation, allowing for 3D liquid motion. The investigation includes both unbaffled and baffled conditions with varying fill levels in the sloshing tank. The test findings exhibit variations of sloshing load, sloshing pressure, and sloshing elevations under the effect of fluid viscosity, range of excitations, and amplitude of 4 and 8 degrees. The pressure variation in the tank increases as the fill level and amplitude increase both in the baffled and unbaffled tank.

*Akyildiz and Unal (2006)* carried out a series of experiments to investigate the performance of various baffle arrangements in a partially filled liquid tank with varying excitation amplitudes. The dynamics of liquid motion in the sloshing tank were studied using numerical model simulation. The authors observed the nonlinear phenomena in the tank by increasing the excitation amplitude in the test series.

*Panigrahy et al. (2009)* developed an experimental shake table setup for liquid sloshing in the square tank. Initially, the experimental test was carried out for a tank without baffle conditions with varying liquid depth (10 cm to 40 cm). The pressure variation and wave elevation were measured in the test series under a range of excitation frequencies (0.25 to 0.42 cycles/sec). Further, the authors used varying baffles (horizontal, vertical, and ring baffles) in the tank to control sloshing behavior. It was observed that, the participation of liquid decreases as the liquid filling level increases in the tank. The baffles in the sloshing tank were found to be effective in reducing pressure on the tank wall as well as wave elevation. In the tank with varying baffle configurations, the ring baffle was found to be more effective than both horizontal and vertical baffles.

*Saghi and Ketabdari (2012)* constructed a finite element and boundary element numerical model to investigate the dynamics of liquid movement in a partially filled rectangular tank. The hydrodynamic action in terms of pressure on tank walls was investigated with varied tank fill levels. The author suggested an optimal fill level in the tank to reduce pressure.

*Xue et al. (2013)* performed a numerical simulation in a rectangular tank with both horizontal and vertical baffles. Using Fourier transformation, the resonant conditions in a time series signal of wave amplitude were identified. Vertical baffles have been found to be more effective at mitigating sloshing amplitudes, particularly at lower excitation amplitudes.

*Jin et al. (2014)* designed a rectangular sloshing tank for a horizontal submerged slotted baffle to conduct shake table tests. Three different porosities of 10%, 30%, and 50% were considered for the baffle, and the baffle was fixed and arranged in the tank so that the position of the baffle can be changed. The study aims to reduce the force acting on tank walls and increase the stability of structures/vehicles which are coupled with liquid sloshing tanks for engineering applications. Therefore, a series of tests were carried out for the sloshing tank with a liquid depth of 0.5 m under sway amplitude of 2.5 mm and 8mm and a range of excitation frequencies (0.4 to 1.7 Hz). Baffles in the tank significantly reduced wave motion and improved damping through energy dissipation. In the test series, baffles with 10% porosity at a distance of 1/6 m were found to be optimal to suppress the resonant waves.

*Yu et al. (2019)* conducted an experimental investigation on slatted screens performance in a sloshing tank under a range of excitation frequency, which covers up to the fifth sloshing mode. The test results show that, the number of screens in the tank can influence the effectiveness of screens in suppressing the sloshing oscillations for particular modes.

*Yu et al. (2020)* carried out parametric sloshing in the tank without and tank with vertical slatted baffles of each 40% porosity. Explored the damping mechanism and effectiveness of baffles in suppressing liquid motion by varying the number and



position of baffles in the sloshing tank. The tank was vertically excited using six degree-of-freedom motion platform with specific excitation frequencies and amplitudes. The number of baffles had a strong influence on slosh reduction in the baffled tank for all sloshing modes. In the test series, it was observed that the tank with three baffles was more effective in reducing amplification due to the first five modes, whereas the two baffles and one baffle performed less effectively in the case of odd (first and third) and even sloshing modes (second, fourth, and fifth), respectively.

*Yu Y M. (2021)* carried out a study on the performance of two porous floating baffles in a rectangular sloshing tank with different liquid fill levels rates (30%, 50%, and 70%). The perforated two baffles are positioned in the tank at 1/6 and 5/6 of the tank length. The series of shake table tests were carried out under a harmonically excited tank (surge motion) with excitation amplitude of 0.002, 0.004, and 0.005  $m$  and frequency of 0.6 to 1.1  $Hz$  with a 0.05  $Hz$  increment. The maximum sloshing reduction (82% to 86%) was observed in the baffled tank with a 30% filling rate compared to 50% and 70% fill rates.

### **2.3.2 Analytical and numerical investigation**

*Warnitchai and Pinkaew (1998)* proposed an analytical model based on dynamic equations for sloshing to study the performance of different flow-dampening devices performance in the rectangular sloshing tank. A gravitational flow test was performed for the damping behaviour of the wire mesh screen device in the sloshing tank. The shake table tests were performed to validate the model test results of the tank with a wire mesh screen. The results exhibit higher sloshing damping at lesser wave amplitudes and negligible effect on sloshing frequency. The experimentally evaluated effects of the tank with flow damping devices results are well agreed with model predictions.

*Chen and Nokes (2005)* developed a finite difference method to analyze coupled, viscous and nonlinear sloshing motion in the tanks. In the method, the sloshing oscillations at the end walls climb proportionally with the Reynolds number for a given excitation frequency.

**Maleki and Ziyaeifar (2008)** presented an analytical expression based on Laplace's differential equation to evaluate the damping ratio in a sloshing tank fitted with baffles for varying fill levels subjected to horizontal excitation with amplitudes ranging from 0.4 to 1.5mm. Using this method, the dissipated fraction of overall sloshing oscillation energy induced by flow separation around the baffles was estimated. To validate the theoretically expected damping ratio, a series of tests were carried out on a shake table with a tank model.

**Goudarzi and Danesh (2016)** investigated the suppressing effects of vertical baffles in a rectangular tank under random excitations (earthquake) numerically using ANSYS CFX. The validity of an analytical model of a full-scaled tank was investigated. The rectangular tank in the simulations had an aspect ratio (ratio of static liquid depth to tank length) of 0.3, 1, and 2. Baffles in the tank significantly reduced wave motion in all tanks except the tank with an aspect ratio of 0.3, and higher damping was observed in the baffled tank as the baffles moved near the center of tank.

**Wu et al. (2012)** investigated the sloshing phenomenon in the baffled tank using a time-independent finite difference scheme and fictitious cell approach. The research mainly focused on baffles size, flow movement around the baffles, and resonant frequency in the tank under surge motion. The study includes varying positions and numbers of vertical baffles and the influence of baffle height in the tank with varying fill levels. In the test series, the highest damping was observed in the tank with two baffles positioned at a distance 0.2 times the length between those. The numerical approach was found to be more effective to obtain natural frequency in the case of a tank fitted with bottom-mounted baffles. Experimentally observed wave motion characteristics in the baffled sloshing tank well predict the numerical results.

**Cavalagli et al. (2016)** studied liquid participation in the rectangular tank, with a focus on wave motion, damping, energy dissipation characteristics, and hydrodynamic forces for civil structures to control vibration. A numerical simulation based on CFD (computational fluid dynamics) under harmonic motion was performed for a sloshing tank with varying excitation amplitudes, frequencies, and fill levels. During the experimental investigation, minimum energy dissipation characteristics were observed

near the resonance. In the study, the CFD model accurately predicts the sloshing absorber characteristics and was found to be effective in predicting energy dissipation.

**Cheng et al. (2016)** conducted a numerical simulation to explore the baffles performance in the moving liquid filled tank. In the numerical tests results, when the porosity of the perforated screens decreases, the sloshing behavior gradually changes from that of a non-compartment tank to that of a compartment tank. Further, it was observed that a low porosity is favourable to the first natural sloshing mode

**Zand et al. 2019** studied liquid dynamics in the porous baffled rectangular tank to enhance the stability of the tank and prevent the hydrodynamic forces on the tank walls at resonant excitation. The various geometry of porous baffles were considered in the sloshing tank along with vertical baffles by changing the baffle's porosity, baffles length, the position of baffles, and the number of baffles. A potential flow model formulated using the Boundary element method with Green's function. Using varying geometry of the baffles, authors observed a unique behavior to suppress the sloshing motion as well as forces. In the simulation, the vertical baffles were found to be significant when the baffle was mounted at the top.

**Bellezi et al. (2019)** studied how efficient perforated swash bulkheads are at reducing sloshing in a box-shaped tank. Numerical simulations were performed to account for the effects of the bulkhead's open-area ratio, the tank's filling level and, the excitation frequency using the Lagrangian particle-based method. To know the effectiveness of perforated screens to minimize sloshing in the tank with three distinct fill levels ( $h/L = 0.167, 0.33$  and  $0.50$ ) considered. With test results authors proposed an empirical equation for optimum porosity as a function of tank fill level

**Poguluri and Cho (2020)** performed both numerical and experimental study on sloshing tank with varying porosities (9.64%, 19.68%, and 30.22%) of screens and, it was found that, the use of fully submerged screen in a tank reduced the amplification factor and pressure at the tank wall. The screen with 19.68% found be more effective to reduce the liquid motion and pressure in the tank. Figure 2.1

*George and Cho (2020)* used eigenfunction expansion and VOF methods to study the performance of vertical porous baffles of varying porosities and submerged depths in a rectangular sloshing tank. The results are validated with experimental tests. The findings explore how the porous baffles functions as an anti-sloshing device in a tank and efficient it is designed to dissipate energy.

## **2.4 TUNED LIQUID DAMPER**

Sloshing tanks so called Tuned Liquid Dampers (TLD) is widely used for tall structures to reduce the vibration of the structure. It has also been regularly used in the shipping industry to keep massive ships from rolling. TLD research is an interesting topic for many researchers because of its importance and wider application. Significant literature has been addressed in the current work to improve the performance of TLD to reduce structural vibration.

*Lee et al. (1982)* documented the performance of offshore platforms using Liquid Vibration Absorber (LVA) so-called liquid sloshing by frequency tuning. Platform response was very sensitive to the variation of cylinder radius, fill level variation in the cylinder which corresponding to natural frequency and damping of the LVA. The performance of the offshore platform with TLD was significantly good with effective parameters.

*Bauer (1984)* studied the motion of immiscible liquid in a rectangular tank to reduce the structural vibration and the author suggested that this can also be used for suppressing the vibration of buildings, bridges, etc. Necessary liquid theory and mathematical mechanical model are presented for the cantilever beam subjected to the oscillation.

A high-rise hotel called the “Shin Yokohama Prince” Japan was first introduced to understand the performance of liquid damper as vibration control of tall structure. Wakahara et al. (1992) investigated the optimum TLD design for tall building safety and serviceability. Theoretical and experimental parametric studies were conducted to estimate the quantities of the TLD and effective TLD parameters for the dynamic behaviour of the building. Numerical simulations are used to validate the experimental

results. Tamura et al. (1995) demonstrated the effectiveness of TLD by measuring the wind-induced reactions of four buildings at full scale. Under severe wind, the acceleration of buildings with TLD was reduced by up to 50% more than that of buildings without TLD when the water mass ratio to total mass of buildings was about 1/350-1/150.

*Sun et al. (1992)* studied liquid damping effect in a rectangular TLD through wave breaking. The empirical damping and frequency shift coefficients were considered for nonlinear behaviour in the mathematical model. A shake table test for sloshing in the tank was carried out to validate the model results. The response of structure-TLD interaction was experimentally studied and it was found satisfactory in reducing the acceleration of the structure.

*Sun et al. (1995)* conducted experimental tests on liquid sloshing in varying geometry of TLDs under regular sinusoidal excitation. The TLD mechanical properties are constructed using a Tuned Mass Damper (TMD) analogy from experimental data. Using the TMD analogy, the amplitude-dependent effective mass, damping ratio, and natural frequency were obtained from non-linear TLD and important TLD properties are discussed based on these results.

*Koh et al. (1995)* conducted a study on multiple-mode liquid dampers to minimize the response of structure. Also investigated the multiple liquid dampers for different vibration frequencies of the structure by tuning the damper for particular mode. It was shown that multiple TLDs with varying modal frequencies are better in vibration control than TLDs with particular concentrated frequency. Furthermore, the study demonstrates the effectiveness of TLD dependency on excitation frequency content, as well as the significant effect of TLD position and optimal mass proportions on vibration response.

*Modi et al. (1997)* investigated the nonlinear behaviour of passive rectangular nutation dampers numerically. It considers wave propagation, wave-tank interaction, particle interactions at the free surface, and wave-breaking. The impact characteristics of the wave striking the tank wall and wave breaking at lesser water depth are not taken into

account in the analysis. As a result of the ratio of liquid depth to tank width, there is a significant difference between numerical and experimental results.

**Reed et al. (1998)** studied the dynamic characteristics of liquid dampers through shake table tests. The test results are compared with numerical modeling based on non-linear shallow water wave equations under a range of frequencies and amplitude. TLD response frequency increases as excitation amplitude increases, and TLD functions as a hardening spring system. The findings show that the performance of TLD is improved even when the damper frequency is slightly mistuned.

**Warnitchai and Pinkaew (1998)** proposed a theoretical model for TLDs with flow-dampening devices. By theoretical study, it is observed that flow-dampening devices in the sloshing tank causes the additional damping. The test findings are confirmed by shake table test on TLD. The TLD with porous screen of wire mesh type found more effective to produce the higher damping. Experimentally evaluated effects of TLD with flow damping devices results are well agreed with model predictions.

**Yu et al. (1999)** conducted a study on the non-linear numerical model of TLD. The system was developed as an equivalent TMD to capture the behavior of the TLD system adequately under different loading conditions. It features the TLD's stiffness hardening characteristic under large amplitude excitation as well as wave breaking. The Nonlinear-Stiffness-Damping (NSD) modeled as a Single-Degree-of-Freedom (SDOF) system with stiffness and damping parameters. These are calculated from an energy matching procedure (energy dissipation provided by the NSD is equivalent to that of the TLD). It was demonstrated that the model can accurately predict the behaviour of the TLD during wave breaking and large amplitude excitations.

**Kaneko and Ishikawa (1999)** conducted a study on TLD-structure interaction to mitigate horizontal structural vibration. Based on nonlinear shallow water wave theory, an analytical model was given that could account for the dissipation energy related to liquid motion as well as the effect of submerged nets on TLD behaviour under harmonic excitations. Theoretically obtained energy dissipation results were confirmed by

experiments. It was shown that the optimal damping factor can be achieved by nets and the structural vibration was reduced to a greater extent in presence of nets.

**Kaneko and Yoshida (1999)** proposed an analytical model for deep-water type rectangular TLD with submerged nets to mitigate horizontal structural vibration and are validated with experimental results. It was observed that good accuracy in energy dissipation by TLD with a submerged net at the center. The authors suggested that a net with an appropriate resistance coefficient be inserted in a rectangular tank to get the optimum dampening effect.

**Yamamoto and Kawahara (1999)** used the Arbitrary Lagrangian-Eulerian (ALE) form of the Navier-Stokes equations to anticipate the motion of the liquid. The Navier-Stokes equations in space were discretized and solved using improved balancing-tensor-diffusivity and fractional-step approaches. The TLD structural interaction response was predicted using Newmark's technique in the time domain. It was established that the technique described in this work is appropriate for the analysis and that the TLD is effective at reducing oscillation. However, no experiments were conducted to validate the model.

**Banerji et al. (2000)** explained the structural response under earthquake ground motions can significantly be reduced by properly designed TLD. Further, it was understood that the effectiveness of a rectangular TLD depends on the tuning ratio, depth ratio, and mass ratio. The numerical simulations and analysis of various SDOFs were shown that a maximum depth ratio of 0.15 and a low mass ratio of 1 to 4% for a TLD is more successful at minimizing structural response. The authors also suggested a practical TLD design procedure to control the seismic response of structures.

**Gardarsson et al. (2001)** examined the effectiveness of a sloped-bottom liquid damper with a 30° angle to the horizontal. It was found that the hardening spring behavior exhibited by box-shaped TLD and softening spring exhibited by sloped-bottom TLD. The amplitude dispersion effect and the wave run-up effect, respectively, were responsible for these phenomena. Also, it was shown that in the sloped-bottom

condition, more liquid mass contributes to the sloshing force, resulting in a greater loss of energy.

*Li et al. (2002)* presented a simple shallow rectangular TLD model to control the structural vibration under forced horizontal oscillation and solved continuity and momentum fluid equations for shallow liquid using the finite element method. The three-dimensional problem was reduced to a one-dimensional problem and the formula for calculating the control force was supplied in order to streamline the computation process for the design and analysis of shallow rectangular TLD. Experiments, however, weren't performed to validate the model.

*Li and Wang (2004)* conducted a theoretical and experimental investigation to reduce the multi-modal vibration characteristics of elevated structures with TLDs. To decrease the multi-modal reactions of elevated structures under random excitations, it was advised to use multiple TLDs. TLD sloshing periods were set to the first few natural periods of the structure for efficient vibration control. Theoretical and experimental research have revealed that the mass ratio of single and multiple TLDs with a structure is the same and that multi-TLDs are more efficient at reducing structural motion by up to 40%.

*Ju et al. (2004)* described TLD characteristics using number of screens and small blocks connected to the wall. For the corresponding damping ratio of the TLD, the authors suggested an equation. The mass ratio, the number of wire screens, and the various fill levels in the tank are also taken into consideration when conducting an experimental programme on the interaction of tank coupled with a structure during seismic excitation. It was found that a model with a heigerr mass ratio of 0.02, three wire mesh screens, and a larger filling ratio (length of the tank to the height of water) of 6 can provide higher damping.

*Tait et al. (2005)* conducted experimental tests using both linear and non-linear models. In the TLD with slatted porous baffle, the free surface motion, base shear forces, and energy dissipation were examined. It was found that the linear model can only provide a preliminary estimate of the energy-dissipating characteristics of a TLD, but the



nonlinear model can precisely represent the response characteristics within the spectrum of excitation amplitudes. Also, the outcomes of the experiments are used to test the flow models using various screens.

*Tait et al. (2005, 2007)* conducted a study on bidirectional TLDs behavior with four vertical screens two along each principal axis. The slatted screens of slat nearly  $5\text{mm}$  wide, spaced at  $7\text{mm}$ , and the resulting solidity ratio of 0.42 was considered for energy dissipation due liquid motion in the tank. The free surface motion, the resultant base shear force, and energy variation due liquid sloshing were used to describe the TLD response. The application and performance two dimensional square and rectangular tanks for TLDs was explored, and it was also demonstrated that a decoupled behaviour for the 2D TLD simultaneously minimises the structural reactions in two modes of vibration with the appropriate aspect ratio.

*Tait (2008)* conducted a study on structure-TLD systems to reduce the dynamic response of tall structures. The detailed design approach for TLDs was explained. TLD damping is performed by inserting dampening screens into the sloshing tank. For both sinusoidal and random excitations, the damping ratio formulation was presented using an analogous displacement variable. The model has been validated using experimental data.

*Xin et al. (2009)* proposed a density variable sloped bottom TLD (tank filled with water and fine sand). Conducted experimental shake table tests on structure-TLD with appropriate scale factors for models. The density-variable control system was found to be more effective and stable than TLD without any damping elements in the tank in reducing structural storey drift and floor motion history.

*Deng and Tait (2009)* studied the theoretical modelling of TLD by changing the tank bottom geometry. The energy dissipation through dampening screens was modelled using the virtual work approach using tank equivalent mechanical parameters. The parabolic-bottom tank and the sloped-bottom tank were proven to be more effective with their mass ratio than the triangular-bottom and flat-bottom tanks. Furthermore, the

authors proposed equivalent mechanical models for TLD tank geometries for practical applications.

**Ikeda (2010)** studied the dynamic response of the elastic two-story structure with two rectangular TLD configurations by both theoretical and experimental programs. In structure-TLD interaction the author considered three different cases of TLD installation: In the first case, one tank was installed at the top and another at the second storey, in the second case one tank was kept at the top and, in the last configuration both tanks are placed at the top. It was concluded that multiple tanks are less effective in reducing structural response.

**Samanta and Banerjee (2010)** conducted a study on modified TLD to control structural vibration. The researchers proposed a modified TLD configuration and discussed the interaction of the TLD structure with a spring system. Large sloshing was noticed through the spring connection when compared to the conventional arrangement. TLD was found to be more successful than typical fixed bottom with structure in minimizing structural response during earthquakes.

**Cassolato et al. (2011)** presented a method for calculating the energy dissipation by inclined screens in the tank. The efficiency of slanted slat-screens in enhancing the damping ratio of TLDs was examined. To anticipate the liquid response, a mechanical model was developed. The model results are validated using the experimental shake table test data. It was observed that changing the screen angles in the TLD causes a variation in the damping ratio. The varying damping ratio is useful for to achieve required level of damping in the tank as a TLD.

**Molin and Remy (2013)** conducted experimental and numerical studies on liquid dampers with vertical perforated baffles to minimize the dynamic response of land buildings under wind /earthquake excitation. Performed the experimental test on baffled TLD tank (800mm x 500mm x 600mm) and  $h=320mm$  liquid depth under forced sway and roll motions. During the testing, the baffle porosity remained constant (18%) while the motion amplitudes and frequencies were changed. With increased mass and damping coefficients, the hydrodynamic loads in the tank were reported. The proposed

numerical model's estimated hydrodynamic coefficients agreed well with the experimental data. Molin and Remy (2015) expanded on previous research by varying the size and shape of screen openings while keeping the porosity constant. The experimental and numerical hydrodynamic coefficients agreed very well.

*Soliman et al. (2015)* investigated the effective position of TLDs on the structure. By taking into account the coupled sway and torsion responses, a whole system model under dynamic excitation was presented. The dynamic analysis structure-TLD system was addressed, and the FE model results were compared to the experimental data. The structure-TLD system's results were found to be in good agreement with experimental test values.

*Kumar and Sinhamahapatra (2016)* suggested installation and optimum position of baffles in TLDs to reduce the ill effect by sloshing on end walls and to achieve dynamic stability without reduction in damping of TLD. To investigate the dynamic impacts of single-opening slotted baffles and slat screens, a computational approach based on finite element pressure formulation was developed. Natural frequency, slosh damping phenomenon, base shear variation, overturning moment, and free surface elevation were computed and investigated as effects of porosity on free and forced dynamic properties. A partially perforated baffle was found to have good dynamic advantages and a reduced weight penalty without compromising the advantages stiffness.

*Nguyen et al. (2018)* investigated the time domain dynamic response of the multi degrees of freedom system under the earthquake excitation. To minimise the dynamic response structure, a variable number of liquid dampers with slatted porous baffles were used. The effect of different liquid fill levels on the frequency ratio, mass ratio, damping ratio, damping coefficient, displacement, and shear force was studied. The authors proposed that using an ideal tuning ratio for a structure with multiple TLDs is effective in reducing dynamic response under different ground accelerations.

*Tsao et al. (2018)* developed a liquid damper with porous media to document the additional damping force sloshing tank. The TLD is modeled as an equivalent mechanical system considering the damping due to porous media to study the linear

dynamic response of fluid in a tank. The equivalent masses, frequency, and, damping ratio for the application of vibration control in structure-TLD interaction problems were derived without using any empirical formulas. The design procedure of TLD with porous media was explained in detail.

*Tuong et al. (2020)* conducted a study on MTLDs in controlling the vibrations of a single-storey framed structure under dynamic loadings by two numerical methods: lumped mass method and the finite element/ volume method. By use of MTLDs, the top displacement of the structure was reduced from 45mm to 2 mm under harmonic loading and 42mm to 23 mm underground motion. The shake table test was conducted to verify the numerical results.

## **2.5 SUMMARY OF LITERATURE REVIEW**

The literature survey shows the performance of linear and non-linear characteristics of sloshing in the tanks to suppress the sloshing oscillations under varying excitations by experimental, analytical, and numerical approaches. Sloshing in the tank performance depends on and sensitive (Lee et al.,1982; Sun et al.,1992; Modi et al.,1997; Yu et al., 1999) to geometry, liquid height, ratio of liquid depth to tank length/width, mass, frequency, wave breaking, wave dispersion, boundary layer at the wall, flow particles interaction at free surface and damping. To increase the damping, authors tried for energy dissipation by using the slopped bottom tank and tank with fine sand (Gardarsson et al., 2001; Xin et al., 2009). Furthermore, researchers have started using flow damping devices such as solid, porous baffles/screen in the tanks towards achieving required damping; tanks with circular poles, flat-plate, and the wire-mesh screen was used (Warnitchai and Pinkaew. 1998); the effect of submerged nets was studied (Kaneko and Ishikawa. 1999; Kaneko and Yoshida. 1999); Ju et al. (2004) used porous screen of wire type and damping blocks to the wall; Tait et al. (2005, 2008) and Soliman et al.(2015) investigated tank with slat screen behavior; Cassolato et al. (2010) used inclined slated screens in a tank for damping ratio; Faltinsen and Timokha (2011) studied the natural sloshing frequency and modes in a rectangular TLD with vertical porous baffle at the tank centre; Molin and Remy (2013) conducted an both experimental and model investigation on tanks fitted with vertical circular opening steel

plates, further extended the work with vertical slots and circular holes [Molin and Remy (2015)]; Kumar and Sinhamahapatra (2016) studied the optimum position of single slotted baffles in tanks to reduce the ill effect by sloshing on end walls and to achieve dynamic stability without a reduction in damping; Cho and Kim (2016) used two porous baffles in the liquid tank to suppress the liquid motion.

## **2.6 KNOWLEDGE GAP**

The magnitude of the damping ratio depends on the dissipation of energy in a tank due to flow damping devices in it. In the structure-TLD problems, the liquid sloshing frequency to be properly tuned to the natural frequency of structure's vibration mode which is to be suppressed. In these conditions tank with suitable flow damping devices is necessary. In this regard, it is understood that hardly any attempt has been made to use porous baffles and varying porosity percentages (solidity ratio). Therefore, the performance of the number of porous screens in a liquid-filled tank will be used to suppress the sloshing oscillations at resonant modes under range of sway excitations, which is the main objective of the present study.

## **2.7 OBJECTIVE OF THE PRESENT STUDY**

The objective of the present work is to investigate sloshing dynamics in the porous screened tank through the analytical and experimental program.

1. To determine the drag coefficient of porous screens by the experimental investigation.
2. To develop an analytical model for vertical porous screens performance in a sway excited rectangular sloshing tank.
3. Conduct an experimental shake table investigation on vertical porous screens performance in a swaying rectangular sloshing tank to compare the analytical test results.
4. To study the performance of porous baffles in the tank for structure-TLD interaction.

### EXPERIMENTAL SET-UP AND INVESTIGATIONS

---

#### 3.1 INTRODUCTION

In general, laboratory studies are referred to as experimental investigation and physical model studies because they give a knowledge about physics behind the works, real application in engineering aspects, collection of data and analysis more practically than natural methods and can be interpreted.

The proposed experimental study aims to explore the performance of number of porous baffles in the liquid sloshing tank with varying liquid filling levels. The concept of porous baffles in the tank is introduced to enhance tank stability by controlling the hydrodynamic loads on the tank walls. The porous baffles of different porosities, the number of baffles, and the position of baffles in a sloshing tank are considered to explore the energy dissipation/damping characteristics in a baffled sloshing tank.

The experimental test series also involved a tank with liquid alone (clean tank/ without baffle condition). Tank without baffle condition involved varying fill levels in the tank to explore the effect of fill level under the range of sway motions. By comparing the baffled condition, this test can help to document the percentage of attenuation of sloshing motions, forces, and other dynamics parameters. Investigations on the proposed concept of the porous baffle's performance in the sway-excited sloshing tank are primarily achieved by the laboratory shake table experiments. A unique shake table with a ballast mass concept setup is arranged in the Marine Structures laboratory of the Department of Water Resources and Ocean Engg. Further, the experimental test are explored and test results are compared with analytics liquid sloshing model.

#### 3.2 RECTANGULAR TANK

A rectangular sloshing tank of length ( $L$ ) of 1.0 m, width ( $b$ ) of 0.4 m, and 0.65 m height ( $H$ ) is used in the test investigation. The tank is made of a 12mm thick acrylic sheet in order to prevent hydro elastic implications on the tank walls. A metal frame was also

constructed for the sloshing tank to prevent it from bulging with high filling levels. According to the position of the baffles in the tank, a number of groove are made to arrange the baffles in position and proper fixity in the tank walls along the larger dimension of the tank. Two runup wave probes are attached to both end walls, as shown in Fig 3. 1. Care was taken to reduce catching effect by elevated amplitude caused by wall reflection during sloshing. The capacitance-type wave probes are placed at equal distances using a cradle frame to document the wave elevations in the sloshing tank. All wave probes are connected to a data acquisition system (EMCON).



Figure 3.1 View of rectangular sloshing tank

Wave probe of capacitance and amplification units is used to capture waveform data in the sloshing tank. To measure the run-up due to wave movements or water disturbances. The sensor can be aligned to the waves and once the waves start forming across the sensor, the water starts moving forward and backward on the structures (tank walls). The sensor which is placed at the same location of observation also will experience the same water movement and thus express the information as the distance of water in the direction of waves. For testing purposes, the shake table motion varied with various amplitudes and frequencies. A Linear Variable Differential Transformer (LVDT) is also connected with the table bottom larger platform to ensure the accuracy of the amplitude

and frequency. The shake table's acquired displacement time history is used to assure the forcing frequency.

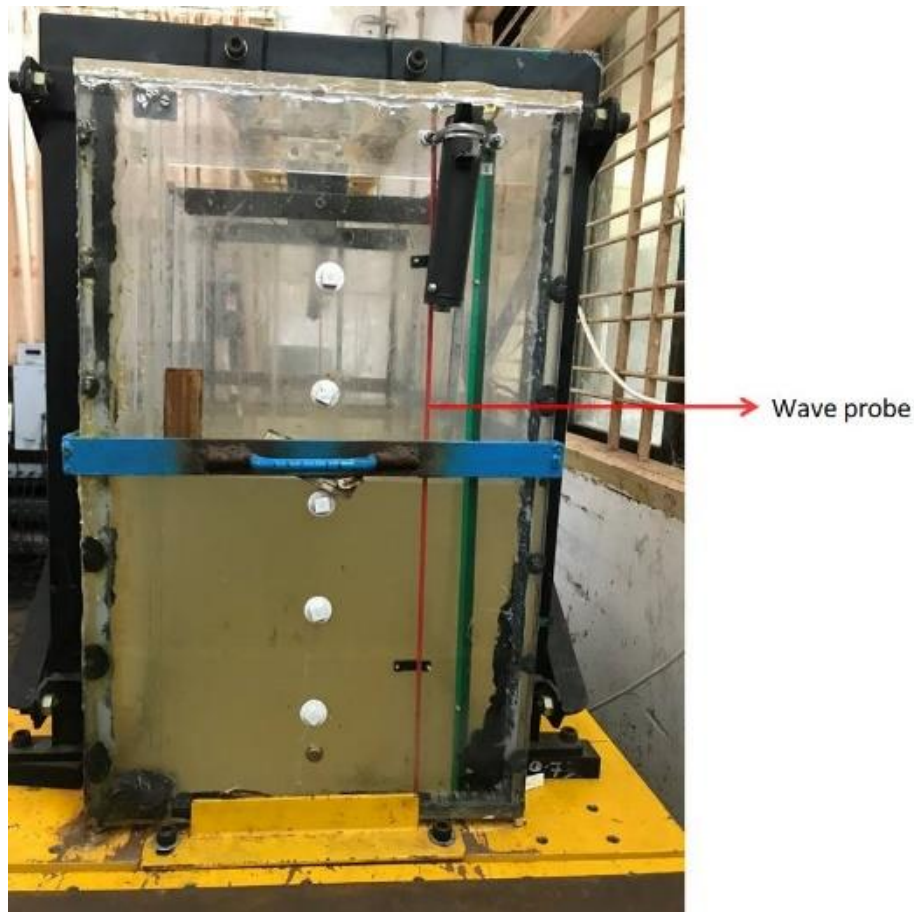


Figure 3.2 A view of Runup probe at near the tank wall

### 3.3 INSTRUMENTATION AND CALIBRATION OF INSTRUMENTS

#### 3.3.1 General

The present investigation has carried out sufficient experimental tests in the laboratory of marine structure of the Water Resources and Ocean Engineering department, NITK-Surathkal, India. A set of experiments are conducted using the rectangular tank to study the liquid participation and dynamics in the tank. A shake table is used to conduct sloshing test in the rectangular tank.

Instruments are calibrated in order to convert the measured output voltage into mechanical properties, instruments. It is done by being aware of a sensor's voltage



output for given values of an input physical quantity. A graph depicts the output data for several known input values. The slope of the best-fit line is then used to compute the calibration coefficient. To reduce calibration errors in the experiments, calibration of all instruments is done for each set of tests. The sensors will be calibrated using DAQ-specific bench Analysis software. During calibration, all sensors must connect to the DAQ in the way described in the manual and follow the step-by-step procedure.

### 3.3.2 Wave Probes



Figure 3.3 View of the Runup Probe

The wave probes in the tank will be acquiring wave elevations at different locations by providing the fluctuations in voltage. The variation in the voltages by the change in the depth of liquid in the sloshing tank is captured by the data acquisition system. Using the appropriate equipment, the wave surface heights in the tank and at the tank walls caused by sloshing in the tank are transformed into an electrical signal. The laboratory wave recorder software provided by EMCON (Environmental Measurements and Controls) converts the digital voltage signals into wave heights with time intervals. The sensor measures the capacitance caused by the sensor rod. The higher the water level, the more would be capacitance. This change in capacitance is recorded at fast intervals of about 25 values per second and sent to a dedicated microprocessor for converting the change in capacitance to meaningful information in the form of linear voltage for a range of 0 to 5 volts, with power + 12 Volt DC. The voltage is further fed to computer software through RS232/USB port format into a dedicated software namely, EMCON Lab wave software which presents the information as the distance of travel in the units of centimetres or millimetres. Run-up will be displayed on a computer screen and

recorded on the computer simultaneously. The runup probes (Figure 3.3) in the test series are 75 cm long, 1 cm wide, and constructed of glass epoxy with a rubber coating.

For the purpose of obtaining the calibration constants, the probes are calibrated in a static environment. The wave probe is attached to a tank and immersed with known water depth, and by balancing the wave probe's bridge circuit, the water level is initially noted as zero reading. The proportionate output voltages are then recorded as the probe is slowly submerged at varying depths with constant intervals. Similarly, the probe is positioned above the level of still water, and the corresponding output voltage is recorded. The area covered by this depth of submersion of the wave probe for calibration is sufficient to capture the wave surface elevation profile. Plotting the voltage indicated for known water level immersion and the slope of the best fit line yields the calibration constants. Figure 3.4 represents typical calibration charts obtained for the probes used in this study.

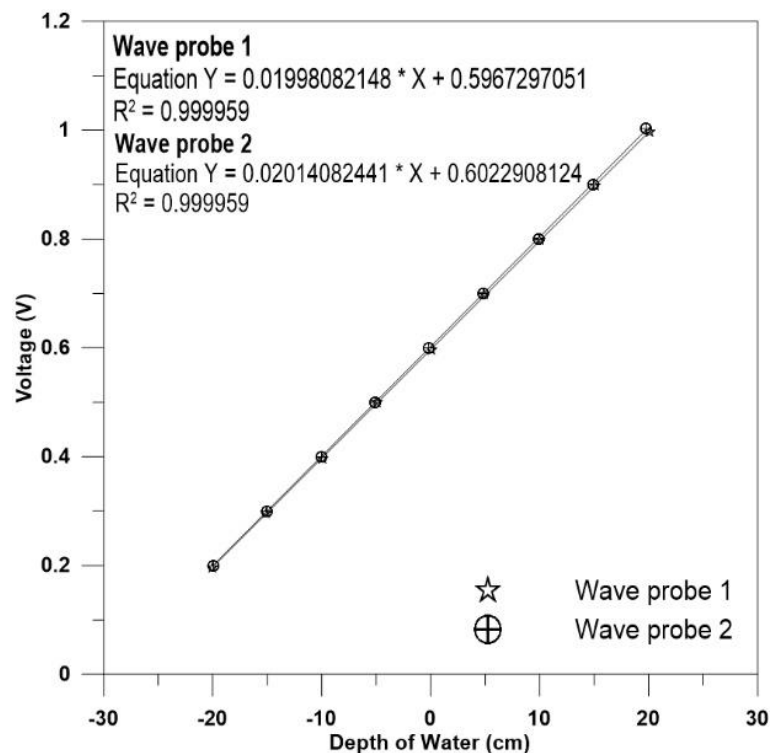


Figure 3.4 Calibration chart for the Probes

### 3.3.3 Load Cell

In the present study, S-type load cells are used. The photograph the load cell is shown in Figure 3.5. These load cells are basically used to measure tensile and compressive force measurement for many engineering applications. In present works, these are helpful to measure the force exerted by two platforms under harmonic excitations. The spring configuration is made in the load cell's center beam. Under load, this spring element deforms elastically and recovers once the load is removed. Spring element strain gauges detect this deformation and convert it to an electrical signal.



Figure 3.5 View of the S-type Load cell

The S Type load cell operates on the following principle: when subjected to external force, the elastic body (sensitive beam) deforms, causing the resistance strain gauge (conversion element) pasted on its surface to deform as well. When the resistance strain gauge is deformed, its resistance increases. The value changes (increases or decreases), and the resistance change is converted into an electrical signal (in voltage) by the corresponding measuring circuit, completing the process of converting the external force into an electrical signal. The load cells are used as force transducers and are calibrated in kilograms. Calibration was performed with various weights in 0.5 kg increments, and corresponding voltages were recorded. Furthermore, in the software,

enter the required value in the dedicated box. The two different load cell calibration charts as shown in Figure 3.6.

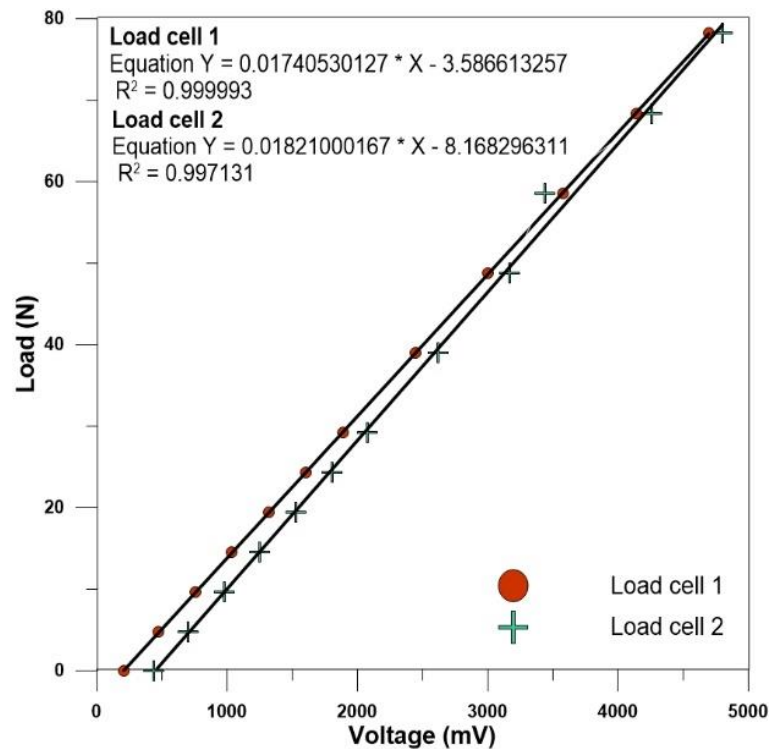


Figure 3.6 Calibration chart for the Load cells

### 3.3.4 Linear Variable Differential Transformer (LVDT)

An LVDT is a type of electromechanical position transducer or sensor that offers accurate and frictionless positional feedback data regarding the linear physical motion of a table displacement. The view of LVDT is shown in Figure 3.7. It operates on the same principles as an AC transformer, but instead of supplying a voltage, it measures linear movement using basic transformer principles of mutual inductance. In a setup, a soft iron ferromagnetic core known as a plunger is free to move in a straight line inside a central hollow tube with a spring connection will give the result of the displacement of the table. The magnetic linking of the coils causes the movement of the core to increase or decrease the voltage induced in the coil. constructing a linear displacement measuring device with a precise output proportionate to the position of its movable core. Further, Excitation amplitude and frequency accuracy are assured by the time signal from the LVDT.

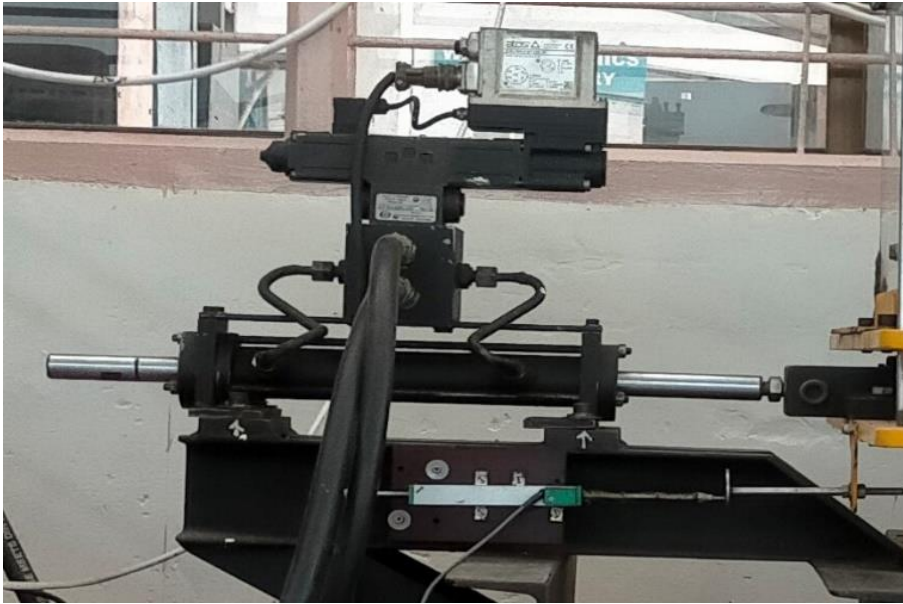


Figure 3.7 View of LVDT connected with edge of the shake table larger plate

To calibrate the LVDT, connect the LVDT cable pins to the instrument sensor using the correct colour code (Primary start: Red, Primary finish: Green, Secondary start: Yellow, Secondary finish: Black), and set the display to zero. This is known as null balancing, and the reading should be recorded. Give the displacement of a 2.5 mm interval from the null position and take note of the voltage variation and distance. The corresponding range of voltage and distance of the core during the calibration test are plotted and shown in Figure 3.8.

### 3.3.5 Shake Table

A unidirectional servo-hydraulic shake table arrangement is used for the present experimental investigations. Figure 3.9 shows a schematic diagram of the experimental shake table setup. The shake table has a 500 kgf payload capacity, which can operate at frequencies up to 10 Hz. And, Figure 4 shows the photograph of the experimental test setup. It consists of two platforms: a larger platform measuring 110 cm by 65 cm on the left of the table setup and a shorter platform measuring 40 cm by 65 cm on the right of the machine. The rectangular sloshing tank is fixed on the left side of platform (Table plate-1) and the equivalent 'ballast' weights arrangements are made on the right-side shorter platform (Table plate-2). The ballast mass concept is mainly used to evaluate base shear and liquid force in the tank.

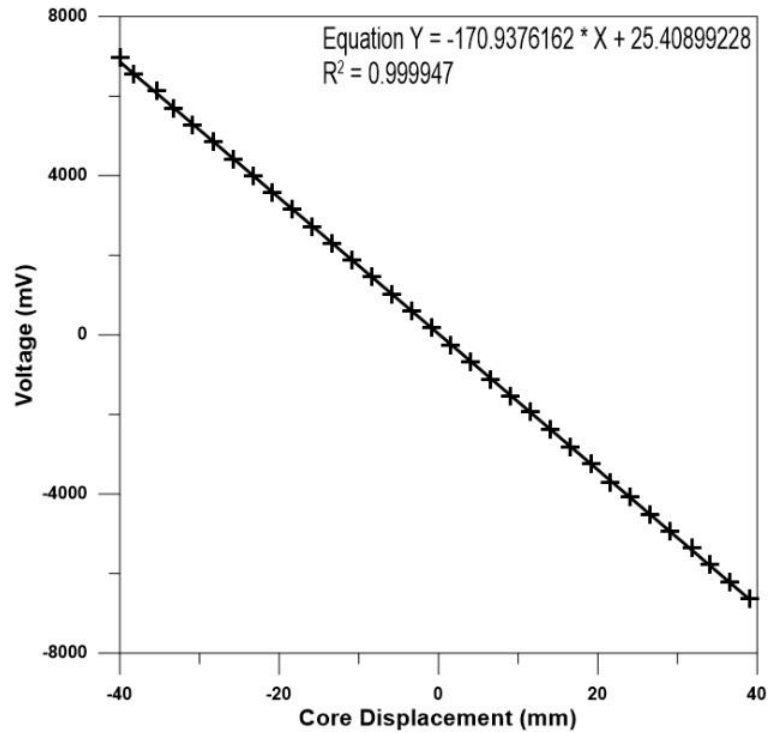


Figure 3.8 Calibration chart for the LVDT

A cradle model is framed on the shake table platform-1 to attach the wave probes at various positions inside the tank. The platform-1 force transducers measured the platform inertial forces, which included the platform mass, mass of the sloshing tank, cradle arrangement mass, sloshing water mass, and other instrumentation mass. The ballast mass was chosen so that the mass of the left side platform (platform-1) and the ballast mass equals the total mass linked into the platform force transducers above, including the still water mass. The platform-2 force transducers measured the platform inertial forces, including the platform mass and ballast mass. A larger single plate is designed in the shake table beneath the two platforms, and it is connected to the hydraulic rod (piston) and an LVDT (Linear Variable Displacement Transducer).

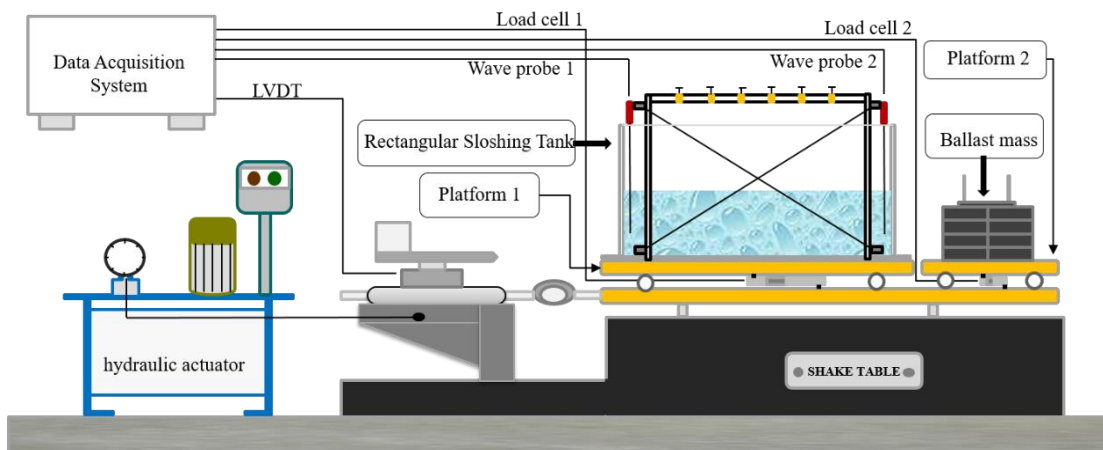


Figure 3.9 Schematic diagram of the experimental shake table setup



Figure 3.10 view of experimental shake table setup

Through a hydraulic actuator, the larger plate will produce displacement based on known input displacement through piston rod movement. In the setup, the piston position and movement are operated using a position controller (Figure 3.11). Before the experiment starts, set the proper position of the table using piston movement through the position controller to move the table in the correct range and adjust the offset value in the controller to be equal to the value of the position of the piston. The assembled shake table system is placed and secured on a 1.25 m long strong concrete bed.



Figure 3.11 View of the Position Controller



Figure 3.12 View of the Wave generator

In the current work, an arbitrary waveform generator is used to generate waveforms over a wide frequency range. Figure 3.12 show the photo of wave generator equipment. To generate waveforms, an arbitrary waveform generator uses the direct digital synthesis technique. An arbitrary waveform generator can also instantly switch between different frequencies. A generator capable of producing sine, square, and triangle outputs with variable amplitude and adjustable DC offset. The wave amplitude is measured based on peak-to-peak voltage. In the system, the sine wave is mathematically represented as  $V(t) = A \sin(2\pi ft + \phi)$ , where  $A$  is the amplitude in volts,



$t$  is the time in seconds,  $V$  is the vertical axis in volts, and  $f$  is the sine wave frequency in  $Hz$  and  $\phi$  is the sine wave's phase.

As discussed on top, through a connection to load cells, the two platforms are firmly attached to the test frame. The platform forces on the left and right will be measured using the load cells. the two S-type load cells, namely the first load cell and second load cells, which are connected at the bases of platform- 1 and platform- 2 respectively. The base shear force from each platform through load cells is recorded as a base shear force- F1 and base shear force- F2. the base shear force-1 includes The inertial forces caused by the rectangular sloshing tank mass ( $p_1$ ), the inertial forces caused by the mass of liquid occupied in the sloshing tank ( $p_2$ ), and the additional force which is caused by the liquid participation in the sloshing tank named as  $p_3/F_s$  The second load cells connecting the ballast mass to the second platform of the shake table measure the base shear force-F2, which is equivalent to the sum of  $p_1$  and  $p_2$ .

An empty tank test is carried out to verify and calibrate the shake table setup. In the empty tank test, the empty rectangular tank (tank without liquid) is placed on platform- 1, and an equal weight of platform-1 is arranged on platform-2 with known weight (ballast mass). The shake table setup is excited with different frequencies and amplitudes using an empty tank. Since no liquid is contained, the total base shear force (the difference in forces owned by two load cells) should be zero.

### **3.3.6 Data Acquisition System (DAQ)**

A Data Acquisition System (DAQ) is on the other side of the shake table. Two data acquisition systems are used for the sloshing investigation, namely Bench and EMCON. The Bench is used for the shake table tests, is supplied by GEOTRAN, and runs on software called "Bench Analysis," which requires a window-based operating system (XP, Windows 7, 8, Vista) and nearly 100 Mb of installation space. The DAQ operates with a power input of 100 - 240VAC (47-63Hz). When a DAQ is connected to a PC through the use of USB and the user starts software, a led that indicates data transfer to the PC and blinks during strain configuration will be visible. DAQ can easily be connected to PC using USB supplied along with DAQ connect the USB to DAQ and then connect the other ends of the USB to the PC. 16 channels of a data logger with 16-

bit resolution make up the DAQ. The transducers, such as load cells and accelerometers, and linear variable displacement transducers (LVDT) are connected via the channels.

EMCON (Environmental Measurements and Controls) was used to record wave elevation in the sloshing tank. EMCON's laboratory wave recorder software is used to convert digital voltage signals into wave heights. The system includes a capacitance-based high-sensitive wave sensor, a multichannel data logger (LAOWR), and Windows-based data acquisition software. The data acquisition frequency is 30 Hz. With power + 12 Volt DC, the data protocol sensor input ranges from 0 to 5 volts.



Figure 3.13 view of porous baffles with hole arrangements

### 3.3.7 POROUS BAFFLES

In the experimental investigation for the tank with porous baffles conditions, there are three different porosities are considered for the present investigation. The porous baffles of 4.4%, 6.8%, and 9.2% porosities are considered. the photograph view of porous baffles shown in Figure 3.13. In view of hydraulic efficiency and dispersion effects in screened sloshing tanks, circular hole arrangements (Cho and Kim (2016); Molin and Remy (2013)) are planned to construct porous baffles with selected porosities. The holes in the porous baffles maintained a constant of 1.5 cm for flow through screens of varying porosities. Further, porous baffle plates 5mm thick are selected based on the tank dimensions. The 5 mm thick plates are may sufficient to withstand hydrodynamic loads in the sloshing tank for our condition. The holes in the

porous baffle of varying porosities are built in a 45-degree scattered arrangement. The configuration of pores arrangement in the baffles is shown in Figure 3.14. Figures 3.14 a, b, and c refer to 4.4%, 6.8%, and 9.2% porosities respectively.

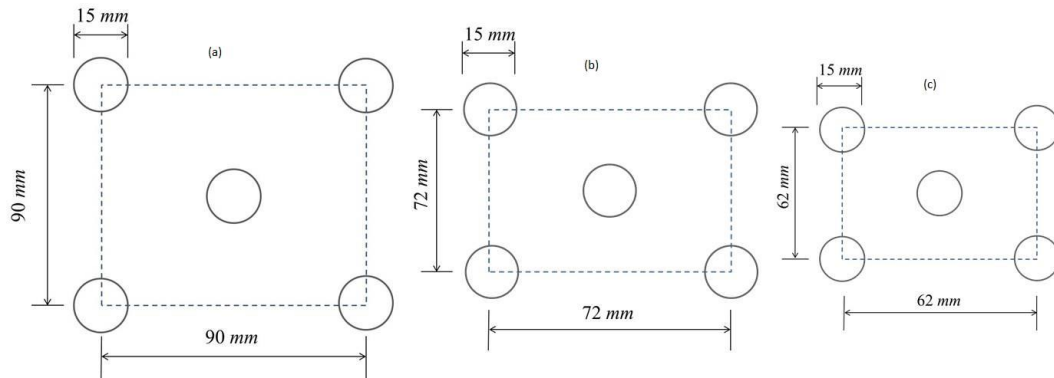


Figure 3.14 Hole arrangements in the porous baffles

### 3.4 GRAVITATIONAL FLOW TEST

#### 3.4.1 Model details

The experimental setup consists of two reservoirs/tanks of the same cross-sectional area of  $45\text{ cm} \times 45\text{ cm}$  in plan view and height of  $100\text{ cm}$ . The two tanks are fabricated using an acrylic sheet of  $12\text{ mm}$  thick. The care was taken to avoid liquid linkages at plate junctions and corners. The two tanks are connected by using an acrylic pipe of length  $60\text{ cm}$  and diameter of  $9\text{ cm}$ . The horizontal pipe connection arrangements between two tanks positioned at  $7.5\text{ cm}$  from two tank bases. The nomenclature diagram for the flow test setup is shown in Figure 3.15.

To determine the drag coefficient for porous screens and to document the variation of drag coefficient value for varying porosities of screens under non-oscillating flow conditions, there are six different porosities are considered. In the test series, the porous screens of porosities include 4.4%, 6.8%, 9.2%, 15%, 20%, and 25%. Five porous screens of each porosity are chosen for flow-through screens between two tanks. To create porous screens,  $0.5\text{ cm}$  circular discs of acrylic material are chosen. Six porous plates based on six porosities are prepared to construct the porosity in the discs. Further, the porosity configuration of each porosity is traced on discs from plates. The

porosities in the plates include constant circular pores 1.5 cm in diameter, and the pores in the screen of varying porosities are built in a 45-degree scattered arrangement. The porous screen discs are shown in Figure 3.17. In the test procedure, the five screens of each porosity are placed at regular intervals of 10 cm in horizontal pipe by employing PVC pipe couplings. Care was taken to ensure a tight fit when placing the screens inside the pipe, and screens are placed normal to flow by using pipe couplings so that screens do not tilt or oscillate while water flows from one reservoir to another.

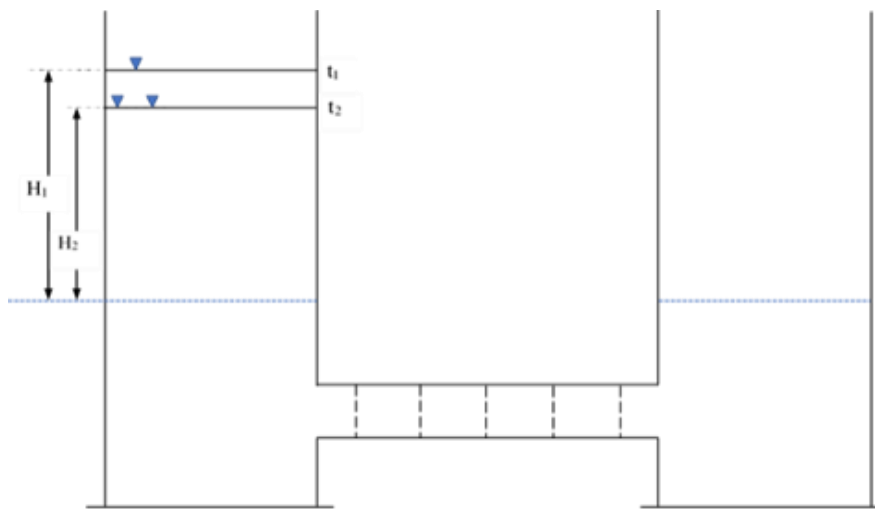


Figure 3.15 Nomenclature diagram for measurement of screen drag coefficient

### 3.5 EXPERIMENTAL PLAN

In order to achieve the objectives of the study, a series of gravitational flow tests for liquid movement between two tanks through porous screens and the experimental shake table tests are carried out in the rectangular sloshing in a clean tank and tank with porous baffles condition.

To begin, a series of gravitational flow tests will be performed between two tanks for drag coefficients of varying porosities in order to study the flow variation with time in the two tanks in terms of heads.



Figure 3.16 view gravity flow setup

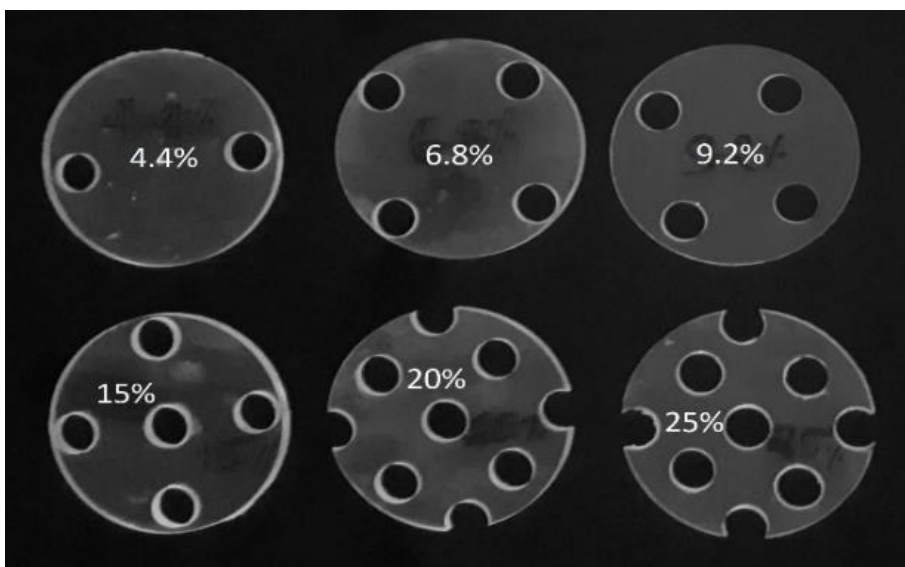


Figure 3.17 view of porous screens of six varying porosities

Secondly, a series of experimental shake table tests is being carried out to study the dynamics of liquid participation in the clean rectangular sloshing tank with varying fill levels under a constant excitation amplitude and the range of excitation frequencies. In the tests, three different filling depths ( $h$ ) in terms of tank depth ( $H$ ) of 25%, 50%, and 75% will be considered.

Thirdly, sloshing tests in the rectangular tank with porous baffles will be carried out to document the wave elevation, sloshing forces, and energy dissipation variations in the

baffled tank in comparison to the clean tanks. In all test cases, tanks with and without baffles for three different fill levels, the tank is subjected to sway motion for a range of excitation frequencies.

Fourthly, an analytical model will be formulated based on the dynamic equation of motion for a clean as well screened tank to compare/confirms the experimental test results.

### **3.6 EXPERIMENTAL PROCEDURE**

#### **3.6.1 The drag coefficient for the porous screens in a non- oscillating flow**

Potable water is introduced in the the reservoir/tank. During the experiments, initially, the water is stored in one tank (Tank-A) with a known head, say at time  $t = 0$  as shown in Figure 3.18. Then, it is allowed to flow through the pipe with five porous screens of known porosity into the other tank. For every 2.5cm fall in water level in the tank, time is recorded. Let  $H_1$  and  $H_2$  be the two successive elevations of 2.5cm head difference during time  $t_1$  and  $t_2$  and continued until it reaches its equilibrium state as shown in Figure 19. The same test procedure is repeated by varying heads in the tank and. The experimental data with a range of flow velocities are documented. Further, the test is carried out for remaining porous screens. The screen drag coefficient value under the range of velocities will be obtained by following the procedures below.

Let 'A' be the cross-sectional area of the tank /reservoir and 'a' the cross-sectional area of the screen passage. The velocity of liquid approaching the screens will be determined using the relation:

$$V = \frac{A H_1 - H_2}{a t_2 - t_1}$$

The head difference/loss of kinetic energy of the flow from the screen is:

$$\Delta H = (H_1 - H_2) \left[ 1 - \frac{V^2}{2g(H_1 - H_2)} \right]$$

The drag coefficient of the screen,  $C_d$  is calculated by the equation developed based on pressure difference at both ends of pipe is given as

$$C_d = \frac{2g\Delta H}{nV^2}$$



Figure 3.18 Experimental setup, water is stored in one tank with a known head



Figure 3.19 Experimental setup, water in the equilibrium state

The damping ratio of the porous screen can be estimated by a well-known energy-ratio formula (Isaacson et al. 2004; Miles et al. 1958). By considering the one period of liquid oscillation, the damping ratio shall be calculated as:

$$\xi = \frac{\Delta E}{4\Pi E}$$

Where,  $\Delta E$  is the total loss of energy, caused by any obstacle, during one cycle,  $E$  is its maximum gravitational potential energy. In the case of screen oriented normally to the flow, the energy is dissipated mostly by pressure drag. The drag force for small baffle areas,  $dA$ , can be expressed as (Stricklin and Baird, 1966)

$$dF = 0.5 \times \rho C_d V |V| dA$$

where  $\rho$  is the density of the fluid,  $C_d$  is the drag coefficient and  $V$  is the flow velocity with respect to the screen. Since  $C_d$  is a piece-wise function of  $V$ , using the above relation, the average energy dissipation rate of screens can be evaluated.

$$\Delta E = 0.5 \times \rho \iint C_d |V|^3 |dA dt$$

### 3.6.2 Sloshing test in the tank

Firstly, the experiments started with a clean tank with a 25 % fill level. The fill level in the tank equals  $(h/L)$  0.163. Care is to be taken exact fill level in the tank and tank fixity on the table platform. The ballast mass is maintained on another shake table platform by placing the known plate weights including the tank filling depths. The wave probes are fixed on both end tank walls and are connected to the EMCON. The shake table is positioned using a piston rod through the position controller. The known excitation frequency and amplitude for sway motion are given through a wave generator. The shake table all sensor connected the bench-DAQ. Both data acquisition systems are connected to laptops to check the corresponding signals and are stored for further calculations. Care has also been taken to start DAQ at the same time. Before starting the experimental shake table test for the clean tank, the instruments are calibrated according to the set of procedures. The tank is excited through a shake table for a range of excitation frequencies which covers first four resonant frequencies. The excitation frequencies are selected based on the tank filling level and are listed in Table 1. For each test, the table motion with each excitation frequency with an excitation amplitude of  $(A/L)$  of 0.0075 will be run up to 90 seconds. The time response of all sensor signals will be recorded and saved. Similarly, the shake test on rectangular tank with all fill



level will be performed under range excitation frequencies. The same procedure has been continued for porous baffle condition. The tank with baffled condition, firstly single porous baffle positioned at tank centre with all porous screen baffles performance will be checked, further, two baffle condition will be performed. In the two baffle condition, the baffles are positioned at equal distance from tank walls i.e. each baffle is positioned at  $L/3$  distance from both tank walls.

Table 1 Frequency range for shake table experiments

Frequency in <i>Hz</i> for three different fill levels		
<i>25% Fill level</i> ( $h/L = 0.163$ )	<i>50% Fill level</i> ( $h/L = 0.325$ )	<i>75% Fill level</i> ( $h/L = 0.488$ )
0.457	0.457	0.457
0.494	0.536	0.553
0.531	0.616	0.650
0.569	0.696	0.747
0.606	0.776	0.843
0.770	0.927	0.978
0.933	1.078	1.112
1.097	1.229	1.247
1.218	1.328	1.341
1.339	1.428	1.436
1.460	1.527	1.530
1.553	1.607	1.609
1.645	1.687	1.688
1.738	1.767	1.767
1.813	1.836	1.837

1.888	1.906	1.906
1.964	1.976	1.976

### 3.6.3 Wave surface elevations

The experimental wave surface elevation in the sloshing tank at both end walls will be listed for all sway motion frequencies. In the experimental test results, the wave response at the left tank wall will be considered for further simulation. The steady-state response will be chosen in the time history signals to obtain the maximum free surface oscillation heights. The transient response is not considered for analysis, and it is found based on the natural time period in the overall response signal. Further, the maximum free surface elevation values are normalised by excitation amplitude ( $A$ ).

### 3.6.4 Sloshing force

Under each excitation, the force transducer (load cells) senses the force generated by the sloshing tank and ballast mass movements. The two platforms signals are recorded in DAQ both in kilograms and newtons with each time step. The time history of force signals is saved on the laptop. The sloshing force will be obtained by taking the difference between two base shear forces from platform force transducer signals. The experimental procedure to obtain sloshing force is as follows.

$$F1(t) = p1(t) + p2(t) + p3(t)$$

$$F2(t) = p1(t) + p2(t)$$

$$Fs(t) = F1(t) - F2(t)$$

Where,

$F1(t)$  = Force by the platform 1 force transducer

$F2(t)$  = Force by the platform 2 force transducer

$p1(t)$  = Inertial force caused by the empty sloshing tank

$p2(t)$  = Inertial force due to mass of liquid in the tank

$p3(t)$  or  $F_s$  = Inertial force caused due liquid sloshing in the tank / Sloshing force

### 3.6.5 Energy dissipation

In the tank without any baffle or flow damping diveices, the energy due liquid sloshing force in tank is dissipated by wave tank interaction /viscous boundy conditions. The dissipated energy related to the sloshing forces and displacement of the tank for one complete cycle. In present work, the dissipated energy of the sloshing force, will be determined by integrating the area delimited by the sloshing force in the hysteresis plot.

### 3.7 ANLYTICAL MODEL FOR LIQUID SLOSHING IN A TANK

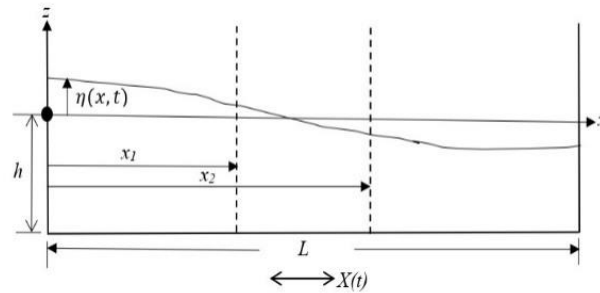


Figure 3.20 Sloshing tank with porous baffles

The 2-D liquid sloshing oscillations in the rectangular tank with two vertically fixed porous baffles were investigated. Figure 3.20 shows a definition sketch of porous baffles in a rectangle tank of length  $L$  and static liquid fill level in the tank is  $h$ . The Cartesian coordinate is attached to the left tank wall, where  $x$ - axis aligned along excitation direction,  $z$ - axis pointing along vertical direction and  $z = 0$  refers the static liquid level in the tank. The liquid in the assumed to be inviscid and incompressible, and the wave movement in the are small, allowing linear flow theory to be used.

The liquid particle movement with time can be described by the gradient of a velocity potential  $\phi(x, z, t)$ , which satisfy the Laplace equation.

$$\frac{\partial^2 \phi}{\partial x^2} + \frac{\partial^2 \phi}{\partial z^2} = 0 \quad 3.7$$

The kinematic boundary conditions for the fluid velocity at the tank walls:

$$u(x, z, t) \Big|_{x=0, x=L} = \frac{\partial \phi}{\partial x} \Big|_{x=0, x=L} = 0 \quad 3.71$$

$$w(x, z, t) \Big|_{z=-h} = \frac{\partial \phi}{\partial z} \Big|_{z=-h} = 0 \quad 3.72$$

$$\frac{\partial \phi}{\partial z} \Big|_{z=0} = \frac{\partial \eta}{\partial t} \quad 3.73$$

The infinite summation of sloshing modes in a rectangular tank expresses the velocity potential as:

$$\phi(x, z, t) = \sum_{n=1}^{\infty} \dot{q}_n(t) \cos\left(\frac{n\pi x}{L}\right) \frac{\cosh\left[\frac{n\pi(z+h)}{L}\right]}{\left(\frac{n\pi}{L}\right) \sinh\left(\frac{n\pi h}{L}\right)} \quad 3.74$$

The surface level can be expressed as: 3.75

$$\eta(x, t) = \sum_{n=1}^{\infty} q_n(t) \cos\left(\frac{n\pi x}{L}\right). \quad 3.76$$

Where,  $q_n(t)$  is a liquid surface elevation of the  $n^{\text{th}}$  sloshing mode. The above equation, will be used to determine the free surface elevation of liquid sloshing at any point in a total tank length.

Energy of a system due to the liquid sloshing motion inside the tank can be expressed in terms of the gravitational potential as

$$V = \frac{1}{2} \rho b g \int_0^L \eta^2(x, t) dx \quad 3.78$$

and the kinematic potential as

$$T = \frac{1}{2} \rho b \int_{-h}^0 \int_0^L \left[ \left( \dot{X} + \frac{\partial \phi}{\partial x} \right)^2 + \left( \frac{\partial \phi}{\partial z} \right)^2 \right] dx dz \quad 3.79$$

where,  $\dot{X}$  is the velocity of the tank in horizontal direction.

In the formulation,  $C_m$  refers the inertia coefficients,  $C_d$  is the coefficient of drag, and  $C_l$  denote loss coefficients by flow through screen. The porous screens of varying porosity,  $P$  defined as

$$P = 1 - S \quad 3.8$$

The overall kinetic energy of the sloshing liquid can be expressed as (Tait, 2008)

$$T = \frac{1}{2} \rho A_{cs} C_m \sum_{j=1}^{ns} \int_{-h}^0 \left( \frac{\partial \phi}{\partial x} \Big|_{x_j} \right)^2 dz \quad 3.81$$

$$T = \frac{1}{2} \rho A_{cs} C_m \sum_{j=1}^{ns} \sin^2 \left( \frac{n\pi x_j}{L} \right) \int_{-h}^0 \left( \frac{\cosh \left[ \frac{n\pi(z+h)}{L} \right]}{\sinh \left( \frac{n\pi h}{L} \right)} \right)^2 dz \dot{q}_n^2 \quad 3.82$$

where  $ns$  is the total number of screens and  $A_{cs}$  is the cross-sectional area of the screen with  $t_b$ , and  $t_b$  refers the screen dimension in the direction of the flow it is expressed as

$$A_{cs} = ht_b S \quad 3.83$$

The non-conservative nonlinear damping forces in the direction of  $q_n$  are given as

$$Q_n = -\frac{1}{2} \rho b C_l \sum_{j=1}^{ns} \sin^3 \left( \frac{n\pi x_j}{L} \right) \int_{-h}^0 \left[ \frac{\cosh \left[ \frac{n\pi(z+h)}{L} \right]}{\sinh \left( \frac{n\pi h}{L} \right)} \right]^3 \times dz |\dot{q}_n| \dot{q}_n \quad 3.84$$

Lagrange's equation with the non-conservative forces:

$$\frac{d}{dt} \left( \frac{\partial T}{\partial \dot{q}_n} \right) - \frac{\partial T}{\partial q_n} + \frac{\partial V}{\partial q_n} = Q_n, \quad n = 1, 2, 3, \dots \quad 3.85$$

The resulting equation of motion for liquid sloshing in a tank:

$$m_n^* \ddot{q}_n(t) + c_n^* \dot{q}_n(t) + m_n^* \omega_n^2 q_n(t) = \gamma_n^* \ddot{X}(t) \quad 3.86$$

where,

$$m_n^* = \frac{1}{2} \frac{\rho b L^2}{n\pi \tanh\left(\frac{n\pi h}{L}\right)} \quad 3.87$$

$$k_n^* = m_n^* \omega_n^2 = \frac{\rho b L g}{2} \quad 3.88$$

$$\omega_n^2 = \frac{n\pi g}{L} \tanh\left(\frac{n\pi h}{L}\right) \quad 3.89$$

The dynamic equation of motion for liquid sloshing in a rectangular tank with no screens and a tank with porous screens were solved using Newmark's method in the MATLAB® application.

and the excitation factor in the above equation can be expressed as

$$\gamma_n^* = \rho b L^2 \frac{[1 - \cos(n\pi)]}{(n\pi)^2} \quad 3.9$$

### 3.7.1 Tank with no screen (clean tank)

The damping ratio for the tank with no screen case can be estimated as:

$$\zeta_w = \left(\frac{1}{2h}\right) \sqrt{\frac{\nu}{2\omega_n}} \left(1 + \frac{2h}{b} + SC\right) \quad 3.91$$

Where,  $\nu$  is the fluid viscosity and  $SC$  is the surface contamination in the liquid tank,  $SC=1$  (Miles 1967).

### 3.7.2 Tank with screens

$$c_n^* = C_l \frac{4\rho bL}{3\pi^2} \Delta_n \Xi_n q_n \omega_n \quad 3.92$$

The screen parameters in the above equation can be expressed as:

$$\Delta_n = \frac{1}{3} + \frac{1}{\sinh^2\left(\frac{n\pi h}{L}\right)} \quad 3.93$$

$$\Xi_n = \sum_{j=1}^{ns} \sin\left(\frac{n\pi x_j}{L}\right)^3 \quad 3.94$$

In the above equation, the ‘ $C_l$ ’ refers the screen loss coefficient, which is determined by using the following procedure.

$$C_l = C_d (1 - P) \quad 3.95$$

Where,  $P$  is the screen porosity. The drag coefficient ( $C_d$ ) is related to energy dissipations phenomenon by porous baffle. In the present work the drag coefficient for the all screen of porosity will be considered based on the study on gravitational flow between two reservoirs with six different porosities. In test series the value of  $C_d$  is equal to

$$C_d = C(Re)^{-m} \quad 3.96$$

Where,  $Re$  is Reynolds number,  $C$  and  $m$  are constants in the above empirical equation. Furthermore, Baines and Peterson (1951) proposed an equation to calculate the loss coefficient based on screen porosity and Tait et al. (2005) suggested an equation determines the contraction coefficient for screen with varying porosity in Baines and Peterson (1951) equation. The  $Cd$  from this procedure also considered in the present analytical model.

$$C_l = \left(\frac{1}{PC_c} - 1\right)^2 \quad 3.97$$

$$C_c = 0.405e^{\pi(P-1)} + 0.595 \quad 3.98$$

The sloshing force is calculated by multiplying the acceleration of the fluid's center of mass by the fluid mass (Love and Tait. 2010). The center of mass (centroid) of the sloshing fluid is given by (Faltinsen and Timokha. 2001).

$$x_c = -\frac{L}{\pi^2 h} \sum_{n=1}^{\infty} q_m(t) \frac{1}{n^2} [1 + (-1)^{n+1}] \quad 3.99$$

$$F_s = -m_w \frac{L}{\pi^2 h} \sum_{n=1}^{\infty} \ddot{q}_n(t) \frac{1}{n^2} [1 + (-1)^{n+1}] \quad 3.99a$$

The normalized energy dissipation per cycle can be expressed as:

$$E_w' = \frac{E_w}{0.5m_w A^2 \omega^2} \quad 3.99b$$

The energy dissipated by sloshing force ( $F_s$ ) per cycle is expressed as.

$$E_w = \int_t^{t+T} F_s dx(t) \quad 3.99c$$

### 3.8 STRUCTURE-TLD WITH POROUS SCREEN INTERACTION MODEL

The TLD with porous screen as the TMD model attached to the structure modeled as a generalized single degree of freedom system representing the mode of vibration being suppressed, which is shown in Figure 1.8a and Figure 1.8b respectively. As the TLD tank moves with the structure due to the external excitation the contained fluid will exhibit a sloshing response motion. The coupled equations of motion of the structure-TLD with and without porous screens as two degrees of freedom system can be expressed as

$$\begin{pmatrix} M_s & 0 \\ 0 & m_{eq} \end{pmatrix} \begin{Bmatrix} \ddot{X}_s \\ \ddot{x}_r \end{Bmatrix} + \begin{pmatrix} C_s + c_{eq} & -c_{eq} \\ -c_{eq} & c_{eq} \end{pmatrix} \begin{Bmatrix} \dot{X}_s \\ \dot{x}_r \end{Bmatrix} + \begin{pmatrix} K_s + k_{eq} & -k_{eq} \\ -k_{eq} & k_{eq} \end{pmatrix} \begin{Bmatrix} X_s \\ x_r \end{Bmatrix} = \begin{Bmatrix} F(t) \\ 0 \end{Bmatrix} \quad 3.8a$$



where  $M'_s$ ,  $C_s$  and  $K_s$  are the mass of the main structure with a mass of fluid that does not participate in the sloshing motion of the fluid, damping and stiffness of the structure, respectively. The equivalent mass,  $m_{eq}$  is the portion of the fluid that contributes to the fundamental sloshing of the contained fluid.

$$M'_s = M_s + m^{non} \quad 3.8b$$

where  $m^{non}$  is the mass of non-participating component of the liquid, which can be expressed as

$$m^{non} = \rho b h L - m_{eq} \quad 3.8c$$

The equivalent mass, damping and, stiffness of the TLD with porous screens, corresponding to the fundamental sloshing mode, which develops dynamic forces equal to the forces exerted by the sloshing fluid in the rectangular tank, are used to represent an equivalent mechanical system, given by (Tait, 2008) as follows.

$$m_{eq} = \frac{8\rho b L^2}{\pi^3} \tanh\left(\frac{\pi h}{L}\right) \quad 3.8d$$

$$c_{eq} = C_l \frac{256\rho b L}{3\pi^5} \tanh^3\left(\frac{\pi h}{L}\right) \Delta \Xi \omega x_r \quad 3.8e$$

$$\zeta_{eq} = C_l \frac{16}{3\pi^2} \tanh^2\left(\frac{\pi h}{L}\right) \Delta \Xi \frac{x_r}{L} \quad 3.8f$$

$$k_{eq} = \frac{8\rho b L g}{\pi^2} \tanh^2\left(\frac{\pi h}{L}\right) \quad 3.8g$$

$$\omega_{eq}^2 = \frac{\pi g}{L} \tanh\left(\frac{\pi h}{L}\right) \quad 3.8h$$

The design of TLD with porous screens by TMD analogy is more effective if TLD can be expressed as an equivalent TMD by introducing a displacement variable. The equivalent displacement variable,  $x_r$ , is introduced as (Tait, 2008)

$$q = \Gamma x_r \quad 3.8i$$

where, the modal participation factor

$$\Gamma = \frac{2}{n\pi} (1 - \cos(n\pi)) \tanh\left(\frac{n\pi h}{L}\right) \quad 3.8j$$



RESULTS AND DISCUSSIONS

4.1 GRAVITY FLOW TEST FOR DRAG COEFFICIENT FOR POROUS SCREENS

The test results are presented in terms of head loss ‘*H*’ as a function of strain rate ‘*V/d*’ for all screen porosities. It is observed that *H* is not only a function of *V/d*, but also depends on screen porosities. Figure 4.1 shows the screen porosities of 6.8% and 9.2% exhibit identical nature, more correlation with those maximum strain rate, whereas the value of *H* correlates well with the lesser value of *V/d* with all porosity of screen.

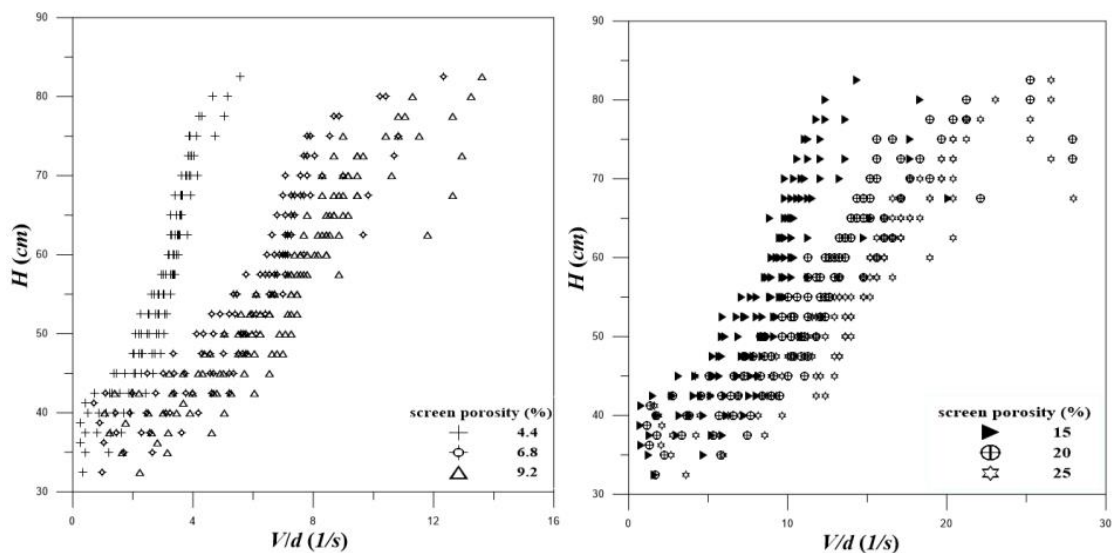


Figure 4.1 Head against strain rate

The drag coefficient of the screen with varying porosities over a wide range of flow velocities are derived and found to be a function of the Reynolds number. The experimental test data for screen of 4.4% porosity is given the Table 3.

$$C_d = C \left( \frac{Vd}{\nu} \right)^{-m} \quad 4.1$$

Table 2 Details of empirical relation

Screen Porosity (%)	Constants in empirical relation with Reynolds numbers	Coefficient of determination (R <sup>2</sup> )
4.4	$C = 4 \times 10^6, m = 1.625$ for $Re < 300$	0.93
	$C = 3 \times 10^7, m = 2.007$ for $300 < Re < 1273$	1
6.8	$C = 1 \times 10^6, m = 1.47$ for $Re < 565$	0.84
	$C = 3 \times 10^7, m = 2.03$ for $565 < Re < 3050$	1
9.2	$C = 3 \times 10^7, m = 2.039$ for $1 < Re < 4231$	1
15	$C = 3 \times 10^6, m = 1.652$ for $Re < 1009$	0.96
	$C = 5 \times 10^7, m = 2.081$ for $1009 < Re < 4523$	1
20	$C = 4 \times 10^6, m = 1.747$ for $Re < 1600$	0.97
	$C = 7 \times 10^7, m = 2.137$ for $1600 < Re < 4684$	1
25	$C = 3 \times 10^6, m = 1.717$ for $Re < 1987$	0.95
	$C = 1 \times 10^8, m = 2.172$ for $1987 < Re < 4684$	1

The constants  $C$  and  $m$  are summarised in Table 2 for a different range of Reynolds number,  $Re$ . Figures 4.2a to 4.2f show the screen drag coefficient ( $C_d$ ) for the different Reynolds number ( $Re$ ) in logarithmic coordinates. The experiments are repeated for two trials and the repeatability is checked. The bar chart for 4.4% and 25% porous screens corresponding to 85 cm head are shown in Figures 4.3a and 4.3b respectively. It is observed that the magnitude of  $C_d$  decreases with increasing values of  $Re$ . In the region of large Reynold number,  $Re > 1000$ , the experimental results by the use of the screen with 4.4, 6.8, 15, 20, and 25 percentage porosity show maximum fit and are given by a straight line, whereas, in the moderately large Reynolds number ( $Re = 100$  to 1000) the experimental data are scattered and are approximated by a straight line. In the case of a screen with 9.2% porosity, gives a straight line for the entire range of Reynolds number. From observation, this conforms with the general expectation that the larger the porosity, the larger the flow through the screens, yields less normal pressure on screens. When Reynolds number is extremely low ( $Re < 100$ ), drag force is directly proportional to velocity due to viscous shear force at the circumference of the pores and hence the drag coefficient is inversely proportional to Reynolds number. For all the porosities considered, the empirical formulation has good agreement with the experimental results which means Equation 4.1 is feasible to estimate the relation between  $C_d$  and  $Re$ .

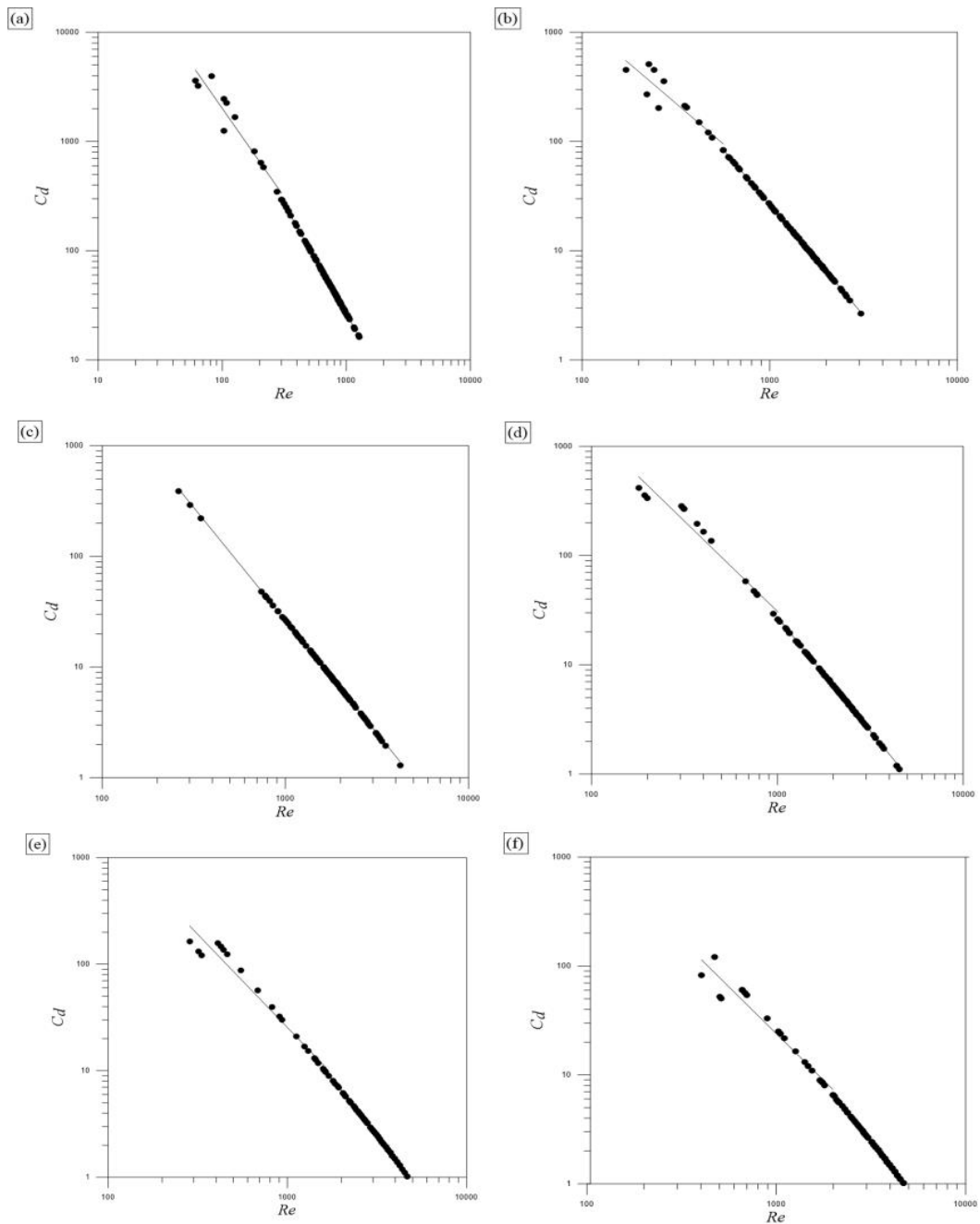


Figure 4.2 Variation of  $C_d$  with  $Re$  for different porosity of screens: (a) 4.4%, (b) 6.8%, (c) 9.2%, (d) 15%, (e) 20% and, (f) 25%

The damping ratio is evaluated by using the energy-ratio concept to describe the effect of porosity. The damping ratio for all porous screens drawn against the relative head (Figure 4.4). The energy loss due to flow rate and effect of viscous shear at tank interface and the porous hole may lead to damping ratios which are completely merged

for all porosities with low tank filling ratio, and are diverging with increasing tank filling ratio. Hence, despite the relatively small damping ratio with increasing in porosity and decreasing relative head.

Table 3 Experimental data

Head (cm)	Time (sec)	Head (cm)	Time (sec)	Head (cm)	Time (sec)
85	0	47.5	23.2	45	25.3
82.5	6.2	45	30.4	37.5	64.4
80	11.4	42.5	40.2	36.25	107.8
77.5	12.4	40	104.1		
75	13.6			70	0
72.5	13.6	77.5	0	67.5	13.5
70	14.6	75	11.2	65	14.9
67.5	15.6	72.5	13.4	62.5	15.2
65	16.2	70	14	60	15.7
62.5	16.2	67.5	14.6	57.5	16.3
60	16.6	65	14.8	55	16.3
57.5	18	62.5	15.1	52.5	17.3
55	20.3	60	15.4	50	18.4
52.5	21.2	57.5	16	47.5	19.4
50	25.5	55	18.4	45	23.1
47.5	26	52.5	19.2	42.5	26.5
45	38.4	50	21.3	40	31.1
42.5	72.6	47.5	24	37.5	41.8
		45	26	35	121.2
82.5	0	42.5	34.1		
80	10.3	40	61.3	70	0
77.5	10.5	38.75	102.4	67.5	13.5
75	13.7			65	14.9
72.5	13.8	75	0	62.5	15.2
70	14.1	72.5	13.4	60	15.7
67.5	14.5	70	13.5	57.5	16.3
65	15.4	67.5	14.7	55	16.3
62.5	16.1	65	14.8	52.5	17.3
60	16.7	62.5	14.9	50	18.4
57.5	17.6	60	15.3	47.5	19.4
55	19.7	57.5	15.7	45	23.1
52.5	23.4	55	17.7	42.5	26.5
50	24	52.5	18.6	40	31.1
47.5	26.5	50	20.9	37.5	41.8
45	36.8	47.5	22.9	35	121.2
42.5	43.4	45	25.4		
41.25	63.5	42.5	28.3	65	0

		40	47.5	62.5	13.9
80	0	37.5	126.4	60	15.9
77.5	12.6			57.5	15.9
75	12.9	72.5	0	55	16.2
72.5	13.1	70	12.8	52.5	17
70	13.7	67.5	14.5	50	17.4
67.5	14.6	65	14.8	47.5	18.2
65	14.6	62.5	15	45	19.9
62.5	15.6	60	15.1	42.5	21.9
60	15.8	57.5	15.6	40	27.7
57.5	17.2	55	17.5	37.5	33
55	18.6	52.5	18.5	35	43.6
52.5	20.8	50	19.1	32.5	160.5
50	23.2	47.5	20		

## 4.2 SLOSHING DYNAMIC IN THE RECTANGULAR CLEAN TANK

The experimental shake table tests on the sloshing tank begin with the tank without the screen. Before beginning the main study, the shake table performances were calibrated for the various stimulation frequency and amplitude combinations. And, the probes and LVDT are calibrated at regular intervals throughout the experiments. The second stage of experimental tests with number of vertical porous baffles of three varying porosities in the tank for three different fill levels were performed.

The analysis of sloshing in porous baffle tanks is concentrated on resonance conditions. Therefore, it is important to know about the dimensions, geometry, and liquid fill level of the sloshing tank. The present study includes one and two porous baffles in the tank; when these porous baffles are impermeable or watertight, the rectangular tank functions as three independent/separate tanks with no screen case. The three separate smaller tanks of each length ( $l/L$ ) 0.33 is defined as compartment tank. The first sloshing mode can be called as the first antisymmetric mode of the clean tank (non-compartment tank) with a wavelength of  $2L$ . For the second sloshing mode, it is referred to as the first symmetric mode and first antisymmetric mode of the non-compartment tank and compartmented tank respectively (standing wave with a wavelength of  $L$ ). The resonant frequencies for all sloshing modes ( $n$ ) in the clean tank with three different filling levels



can be estimated using the equation (Equation 4.2) proposed by Ibrahim 2005, and the estimated values are shown in Table 4.

$$f_n = \frac{1}{2\pi} \sqrt{\frac{n\pi g}{L} \tanh\left(\frac{n\pi h}{L}\right)}, n = 1, 2, 3... \quad 4.2$$

Where  $g$  is the gravitational acceleration and  $n$  is the sloshing modes number. A sway-oscillated rectangular tank with sway motion amplitude ( $A/L$ ) of 0.0075 and  $\omega=2\pi f$  is given as  $X(t)=A\sin(\omega t)$ .

Table 4 Natural frequencies of clean tank sloshing.

Modes	Values								
	<i>h</i> = 25% Fill level			<i>h</i> = 50% Fill level			<i>h</i> = 75% Fill level		
	$\omega$ (rad/sec)	$f$ (Hz)	$\omega/\omega_1$ ( $\beta$ )	$\omega$ (rad/sec)	$f$ (Hz)	$\omega/\omega_1$ ( $\beta$ )	$\omega$ (rad/sec)	$f$ (Hz)	$\omega/\omega_1$ ( $\beta$ )
1 <sup>st</sup>	3.807	0.606	1	4.872	0.776	1	5.298	0.843	1
2 <sup>nd</sup>	6.891	1.097	1.810	7.720	1.229	1.584	7.834	1.247	1.479
3 <sup>rd</sup>	9.176	1.460	2.410	9.595	1.527	1.969	9.615	1.530	1.815
4 <sup>th</sup>	10.918	1.738	2.868	11.099	1.767	2.278	11.103	1.767	2.096

#### 4.2.1 Analytical model validation

To validate the present analytical model, the surface elevation results are compared with the numerical results of Frandsen (2004) as shown in Figure 4.5a. The numerical work was performed for a tank with a  $h/L=0.5$  under amplitude of an excitation is  $A=0.005h$ , and an excitation frequency of  $0.7\omega_1$ . The present model is also compared with an experimental test conducted by Jin et al. (2014) as shown in Figure 4.5b. As explained in the authors experiment, sloshing tank with  $h/L=0.5$  is exposed to a forced vibration with an excitation amplitude of  $A=0.0025$  and a range of frequencies ( $\beta$ ) from 0.5 to 2. The analytical model runs for forty seconds, which is the same amount of time in experiments. The analytical results predict the experimental results with good agreement. The analytical model is also validated with an experimental work carried out by Faltinsen et al., (2011) to know the surface elevation variation in a sloshing tank

with a slat type porous baffle of porosity 0.0672 placed at  $L/2$  location as shown in Figure 4.5c. The analytical model predicts free surface response trends of experimental results with reasonable agreement.

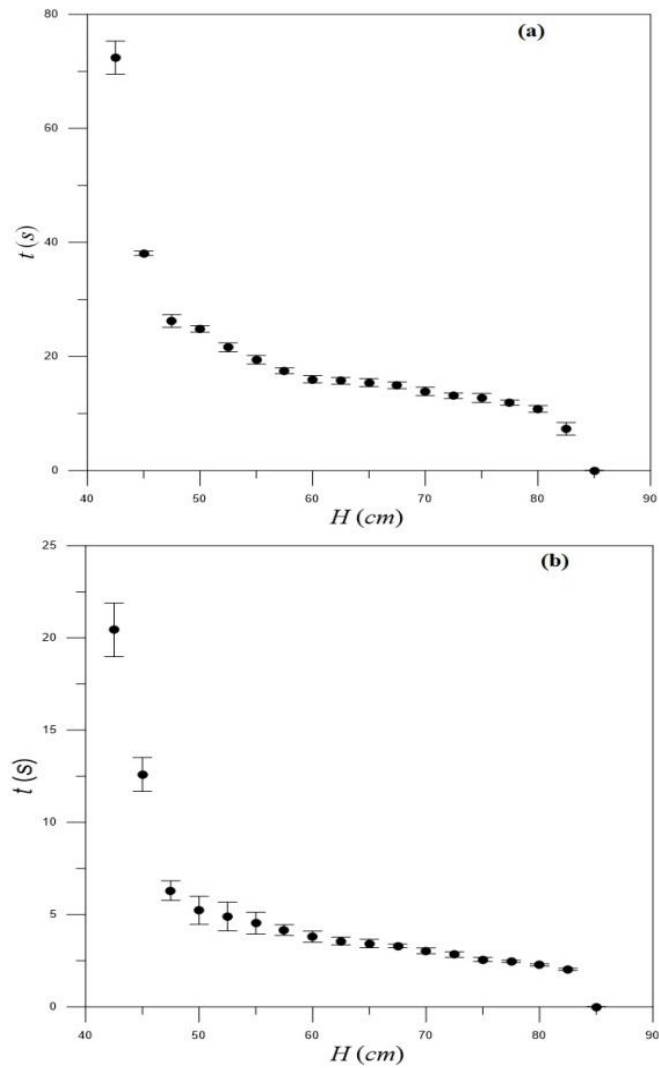


Figure 4.3 Error bar chart for screens of porosity: (a) 4.4% and, (b) 25%

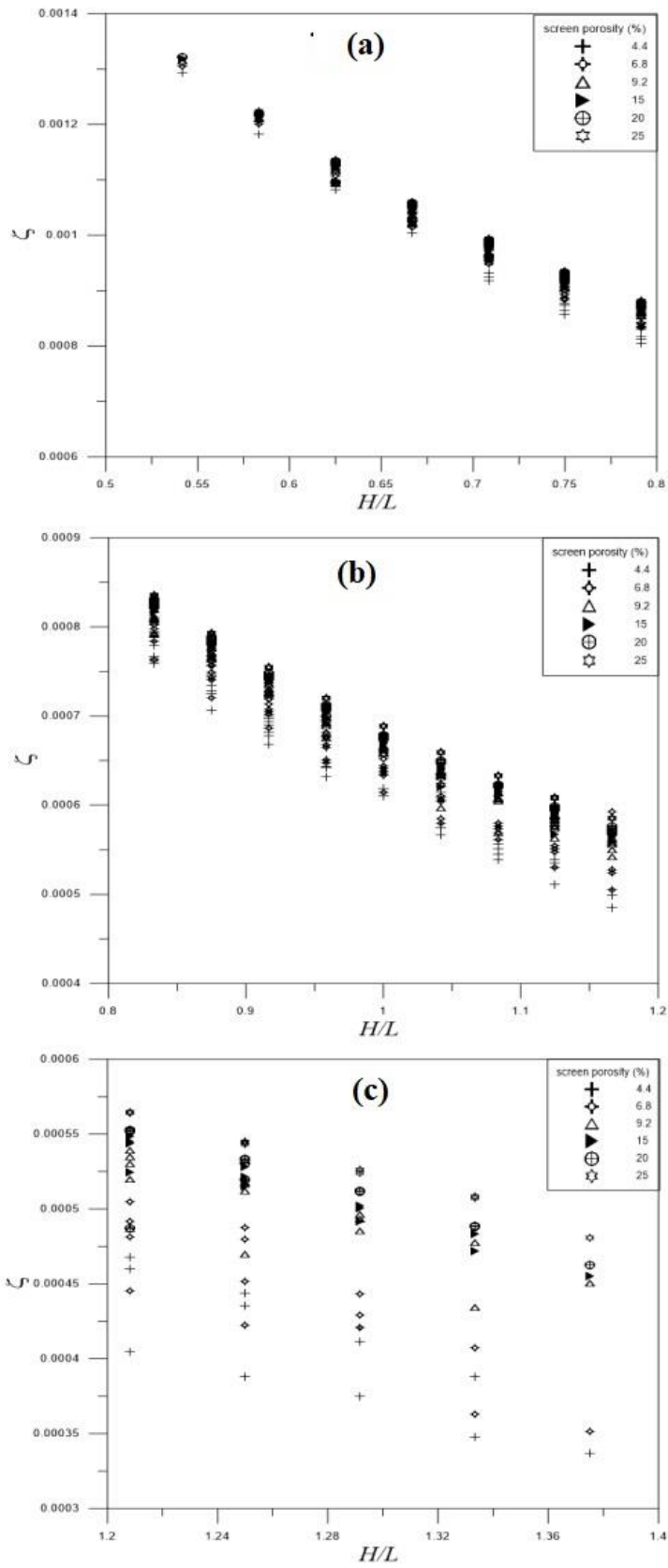


Figure 4.4 Variation of damping ratio of porous screens with filling ratio

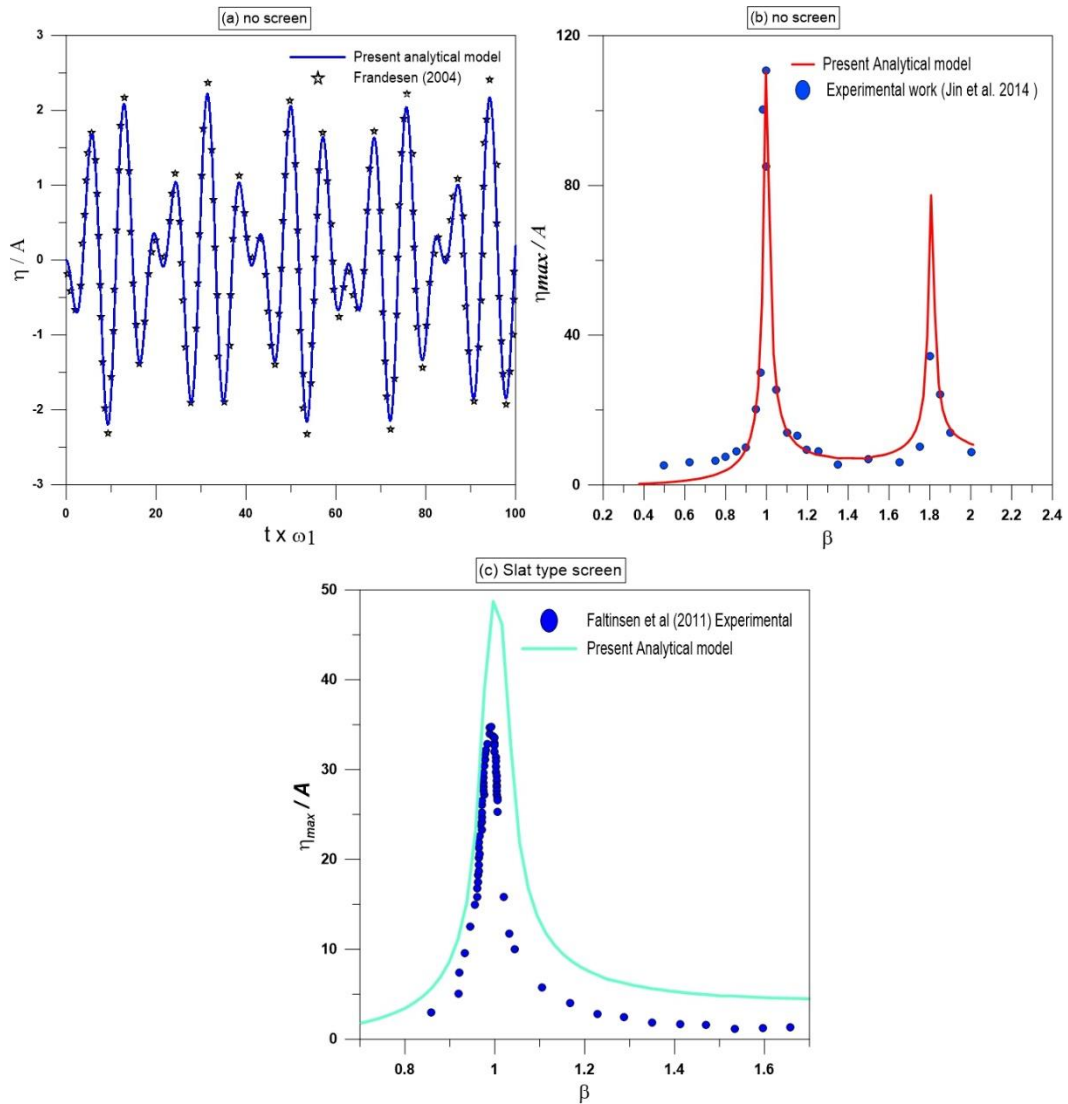


Figure 4.5 (a) The liquid free surface motion variation with the numerical results of (Frandsen, 2004). (b) The frequency response curve with the experimental results of Jin et al., 2014. (c) Maximum wave elevations with experimental results of (Faltinsen et al., 2011) [ $h/L = 0.5$ ,  $A = 0.005h$ ,  $P = 0.0672$  &  $\omega = 0.7\omega_1$ ]

#### 4.2.2 Maximum free surface motion

Significant sloshing peaks can be predicted if the tank motion or stimulation frequency is near to the natural frequencies of the liquid in the tank. i.e., Resonance will take place when both frequencies are relatively close to one another. The amplitude of free surface oscillation decreases due to damping effect produced by viscous effect at tank boundary layers and liquid interface during free oscillations. The damping effect in the no-screen

tank is mainly influenced by the kinematics viscosity of the liquid, sloshing tank dimensions, liquid fill levels, and excitation frequency. Therefore, the present investigation involved varied tank fill levels and tank excitation frequency to investigate the effects on free surface oscillation. The damping effect of viscous boundary layers is taken into account in the assessment of the free surface elevations response for the clean tank at all fill levels.

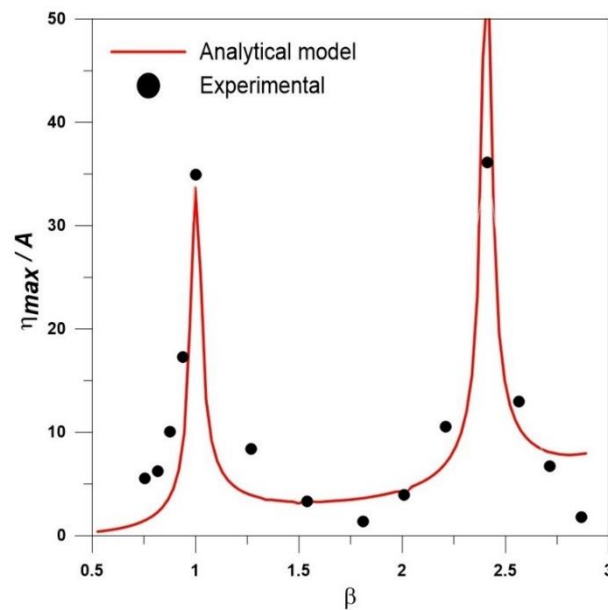


Figure 4.6 Maximum free surface elevation ( $\eta_{max}/A$ ) variations in a no-screen tank with 25% FL

The analytical test results of the normalized amplitude of maximum free surface elevation ( $\eta_{max}/A$ ) variation with frequency ratio ( $\beta$ ) in the clean sloshing tank with three different fill levels of 25%, 50%, and 75% are presented in Figure 4.6, Figure 4.7, and Figure 4.8 respectively.

The sloshing motion variation in the tanks was recorded as the sum of infinite sloshing modes in the tank during liquid sloshing under a range of excitation sway motions. The amplitude of free surface motion in the tank was measured near the left tank wall. From the figures, the response amplitude of maximum free surface motion is minimal when the frequency ratio ( $\beta$ ) is between 0.5 and 0.8. But as the frequency ratio increases from 0.8 to 1, the free surface motion significantly increases. Eventually, at  $\beta = 1$ , a higher peak is observed in the tank with all three filled levels. The peaks at the first frequency

ratio indicate the resonance frequency of the first resonant or fundamental sloshing mode. Further, the free surface motion dramatically decreases after  $\beta = 1$  and approaches the local minimum at  $\beta = 1.810, 1.584,$  and  $1.479$ , which correspond to the second sloshing modes in the tank of 25%, 50%, and 75% filled levels respectively.

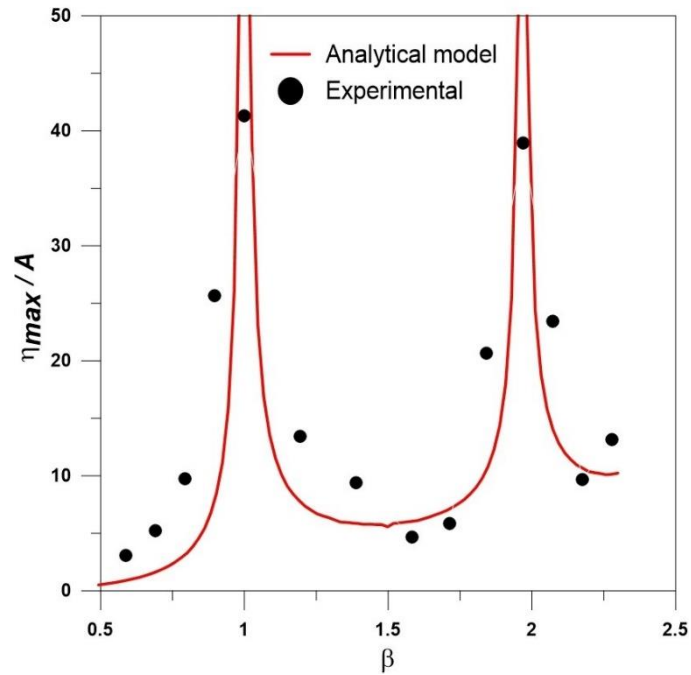


Figure 4.7 Maximum free surface elevation ( $\eta_{max}/A$ ) variations in a no-screen tank with 50% FL

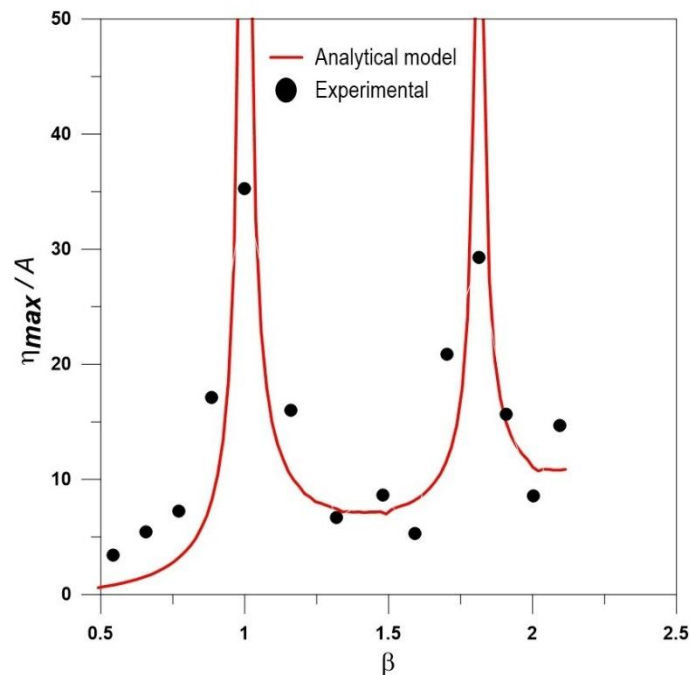


Figure 4.8 Maximum free surface elevation ( $\eta_{max}/A$ ) variations in a no-screen tank with 75% FL

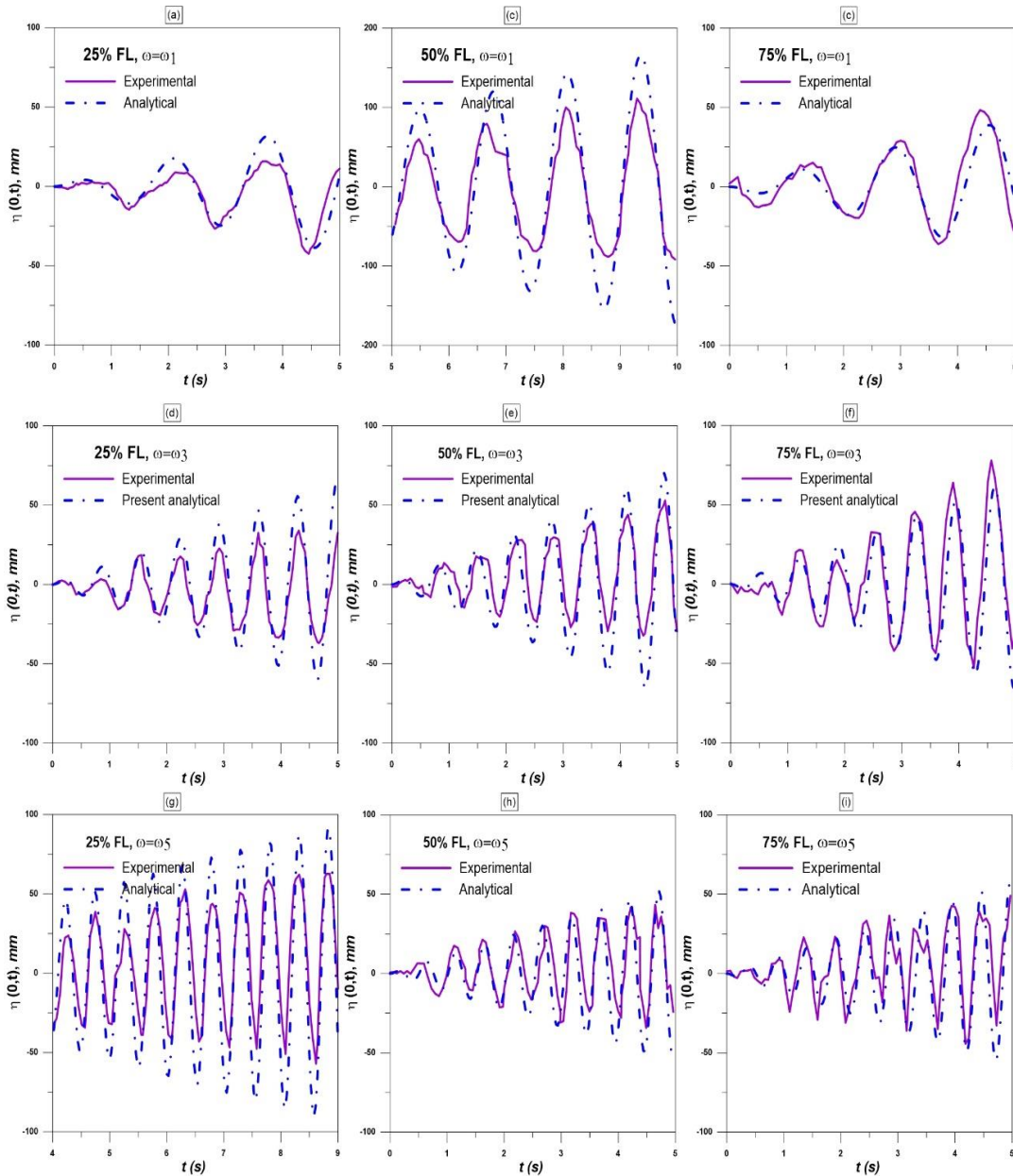


Figure 4.9 Time history of free surface elevation in a tank with no screen for 25%, 50%, and 75% fill levels at  $\omega = \omega_1, \omega_3$ , and  $\omega_5$ .

The amplitude of free surface liquid motion starts to increase (i.e., recovers) as the frequency ratio increases from the second resonant mode, and reaches the second maximum peak at frequency ratio,  $\beta = 2.410, 1.969$ , and  $1.815$ . The second maximum

response peaks in the tanks correspond to the third resonant mode of 25%, 50%, and 75% filled levels in a clean sloshing tank respectively. The analytical model results for resonant peaks in the liquid sloshing tank with three varying fill level conditions are confirmed by the experimental sloshing test. The test results for resonant peaks in the tanks are well correlated with each other.

### 4.2.3 Maximum sloshing force

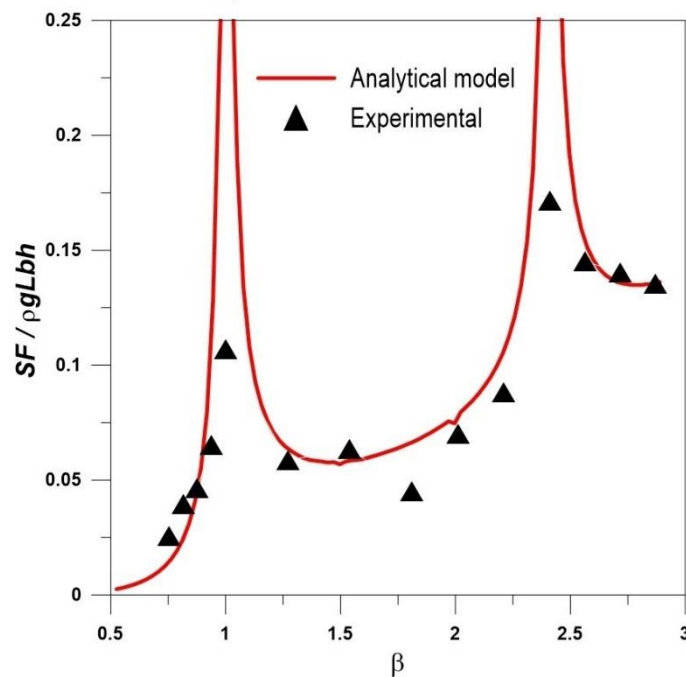


Figure 4.10 Maximum sloshing force variations in a no-screen tank with 25% FL

The magnitude of free surface elevation peaks in the liquid sloshing tank is varied with a change in the filled levels in the tanks. The analytical model test results show the magnitude of resonant peaks in the sloshing tank increases as the fill level increases in the tank. The amplitude of resonant peaks increases as the tank fill level increases may be the result of the simulation time span in the analytical model.

The resonant frequency at and/or near the first sloshing mode is a more important parameter in many practical applications for the sloshing tank with a range of liquid fill levels. In the present experimental investigation resonant frequency variation in tank with all three fill level show the exact phenomenon as we expected with a small quantitative difference. This peaks variations in the different filling levels in the tank



might happen as a result of the surface wave being duplicated by the wave that bounces off the end wall.

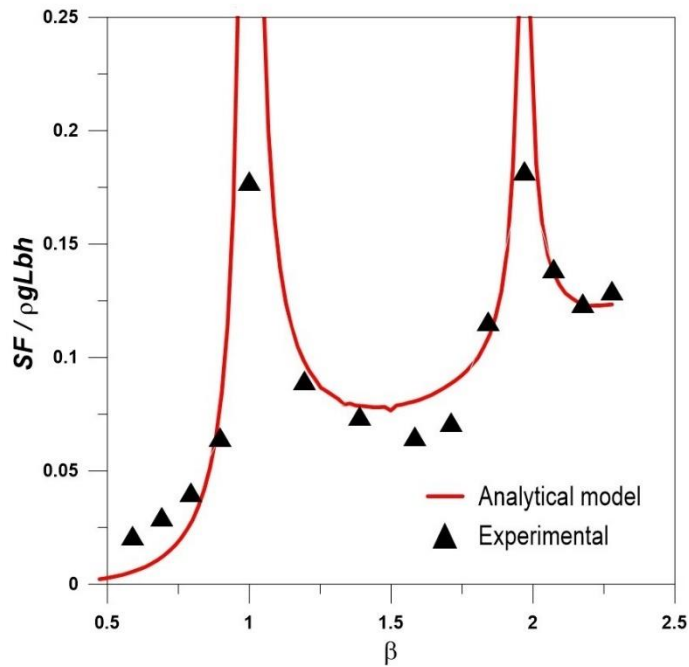


Figure 4.11 Maximum sloshing force variations in a no-screen tank with 50% FL

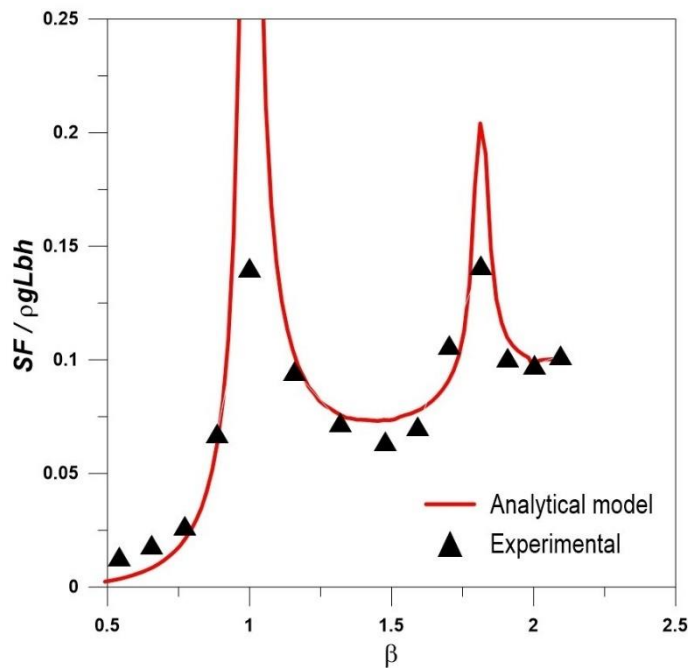


Figure 4.12 Maximum sloshing force variations in a no-screen tank with 75% FL

In the second resonant mode conditions, the maximum amplitude of surface elevation in the tank with all fill levels exhibits nearly the same variation and deposited the least response. The analytically obtained test results are confirmed by the experimental shake table test results within the range of excitation frequencies for the tank with all three different filled levels. The secondary peaks were observed in the tank at third resonant mode conditions for all liquid fill levels by both analytical and experimental investigations. At this resonant condition, the experimental test results exhibit exact phenomena with varying liquid fill levels in the tank. The discrepancy between the analytical and experimental test results is may due to sampling rate variation in the data acquisition system that we observed in experimental shake table tests.

#### 4.2.4 Energy dissipation

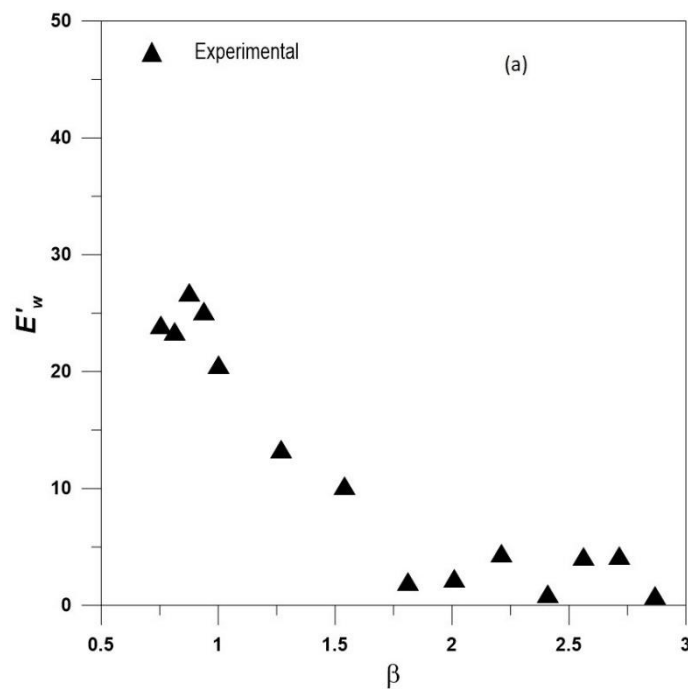


Figure 4.13 Energy dissipation variations in a no-screen tank with 25% FL

The experimental observation of waveforms of free surface motion is compared with analytical test results for a range of excitation frequencies. Figure 4.9 illustrates the time history of resonant wave free surface elevations in a sloshing tank with no screen. The results of the analytical model correlated well with the results of the experimental shake table.

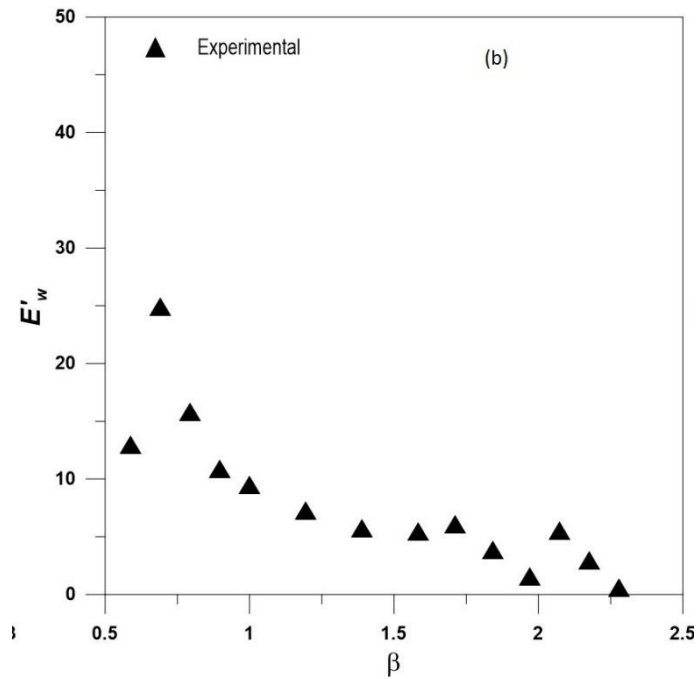


Figure 4.14 Energy dissipation variations in a no-screen tank with 50% FL

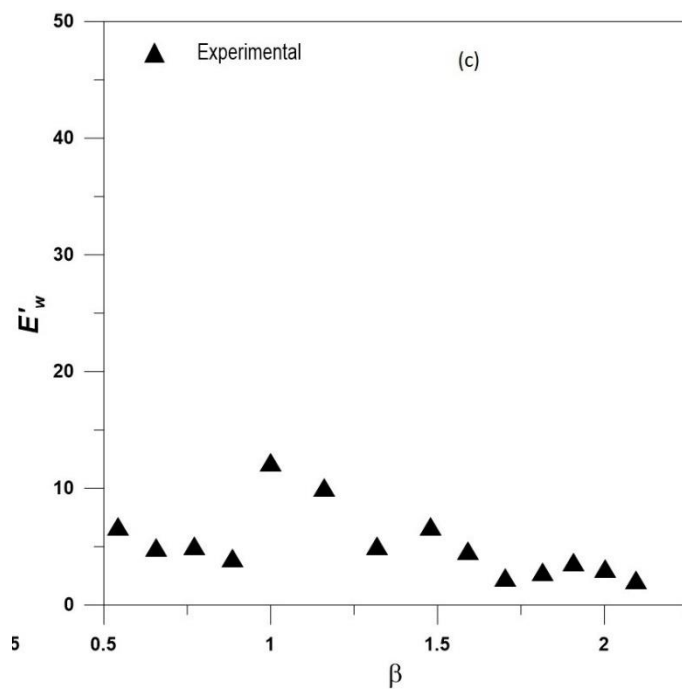


Figure 4.15 Energy dissipation variations in a no-screen tank with 75% FL

Figure 4.10, Figure 4.11, and Figure 4.12 shows the variation of dimensionless sloshing force under a range of excitation frequencies (frequency ratio) in a rectangular sloshing tank with no screens condition for 25%, 50%, and 75% fill levels respectively.

Analytical simulations were performed for all cases with an excitation amplitude of  $(A/L)$  0.0075 and a range of sway excitation motion that covered up to the first four lowest sloshing resonant modes. The maximum sloshing force peaks were observed as similar to the maximum free surface elevation near the resonance frequencies for the tank with all three fill levels.

In the case of the 25% fill level, the two peaks were observed at frequency ratio ( $\beta$ ) 1 and 2.41, corresponding to the first two odd resonant modes in the tank. The analytical model results well matched with experimental shake table test results. The response of normalized sloshing force is of 0.105, 0.05, and 0.16 observed at first three resonant modes by experimental tests and follows the exact trend remaining range of excitations.

Similarly, for tanks with 50% and 75% filled levels, the first two odd resonant modes were observed at frequency ratios of 1 and 1.97, and 1 and 1.82, respectively. For tank with 50% fill level, the response of normalized sloshing force is of 0.17, 0.06, and 0.18 observed at first three resonant modes by experimental tests which are slightly higher than in compare to the 25% fill level tank. This resembles that fluid participation in the tank with 50% fill is more compare to 25% fill level. In case of 75% fill level tank, it is observed that 0.14, 0.07, and 0.145 at first resonant modes.

For the tank with no screens, in all fill levels, large amplification in sloshing force range 0.15 to 0.18 times quasi-static response is observed from experimental tests at third mode natural frequency. And the response increases as fill level increase at first resonant mode. On other hand, for the third mode ( $n = 3$ ) case in the tank with no screen, the dynamic component of sloshing force reduces remarkably as filling levels increase. The present analytical test results well agreed with experimental test results. The variation of sloshing force in the clean tank shows same resonance behaviours similar to the free surface elevation variation in the clean tank for all fill levels.

Studied the energy response variation due to sloshing in the tank. For this, tank with and without porous baffles condition were considered. In the clean tank condition, the energy dissipated through the viscous effect during liquid tank interaction were observed. As excitation frequency increase the energy characteristics decreases in the

tank with all fill levels. At the first resonant mode, the magnitude of energy is observed maximum for all fill level case, and it is reduced further for higher excitation modes.

### 4.3 SLOSHING DYNAMIC IN THE RECTANGULAR TANK WITH TWO POROUS BAFFLES

#### 4.3.1 Maximum free surface elevation in a 25% FL tank with two porous baffles

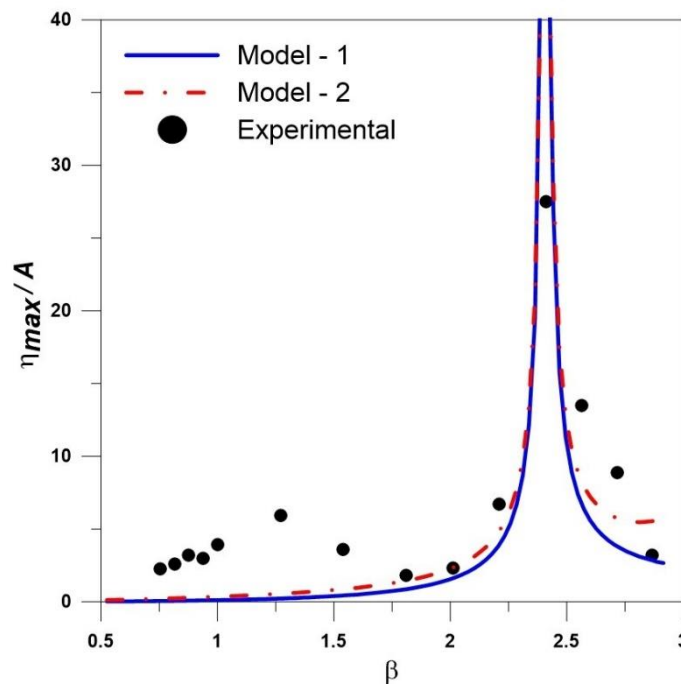


Figure 4.16 Tank with two porous baffle of 4.4% porosity

In the case of a sloshing tank with vertical porous screens, the damping effect caused by the flow through the porous screens, as well as the energy dissipated by the viscous action and viscous boundary layers, are considered. The energy dissipation characteristics of porous screens in the sloshing tank for free surface oscillations are mainly influenced by the type of screens and their loss/drag coefficient, screen porosity and position, liquid fill level, excitation frequency, and excitation amplitude. As a result, the maximum free surface oscillation variations were investigated in a rectangular tank equipped with two vertically fixed porous screens of 4.4% porosity positioned at  $L/3$  and  $2L/3$  distances from the tank's left wall. The two analytical model results were presented based on screen loss coefficients under a range of excitation frequencies. The maximum free surface elevation variations versus frequency ratio in

a tank with two porous screens for three different fill levels of 25%, 50%, and 75% are shown in Figure 4.16, Figure 4.19, and Figure 4.22 respectively.

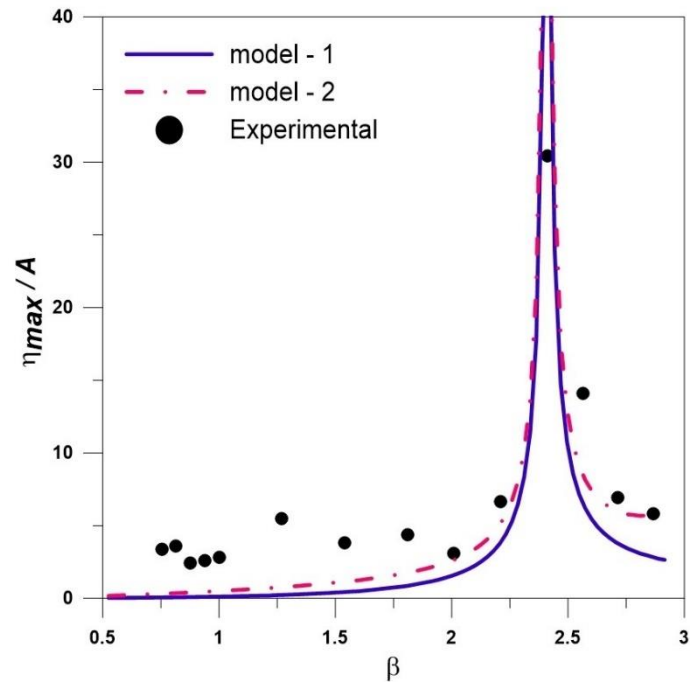


Figure 4.17 Tank with two porous baffle of 6.8% porosity

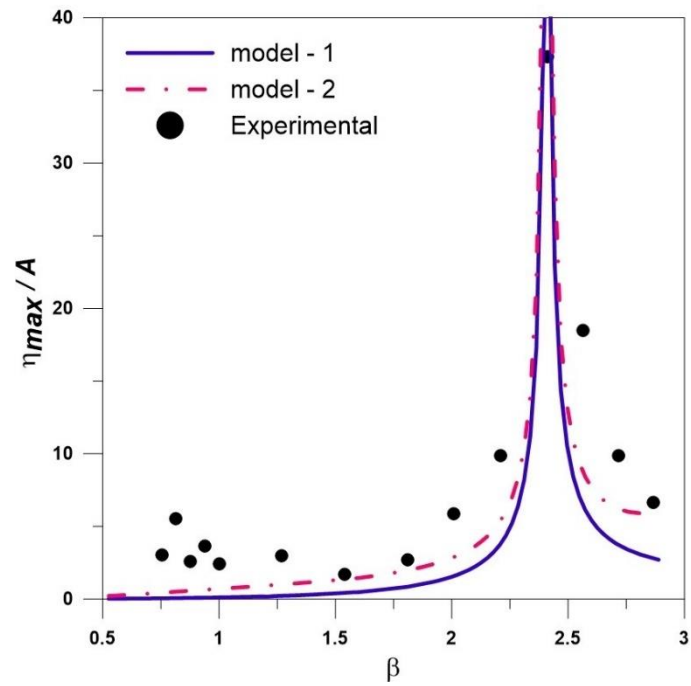


Figure 4.18 Tank with two porous baffle of 9.2% porosity

In the case of 25% filled level tank with two porous screens (Figure 4.16), the amplitude of maximum free surface elevation is minimal when the frequency ratio ( $\beta$ ) is between 0.5 and 2, but as increases from 2 to 2.410, the free surface significantly increases and reaches a maximum peak at third natural sloshing mode of the tank. Eventually, at  $\beta = 1$ , observed the lowest response i.e., the response of free surface oscillations in the screened tank were attenuated 99.67% compared to no-screen tank by model – 1 prediction and 98.96% by model – 2. When a tank with two watertight screens, the full tank (Length =  $L$ ) is considered into separates three smaller tanks (compartment tank) with no screen case. The smaller tank of length ( $l$ ) is equal to 0.33  $m$ . The first mode of natural sloshing frequencies of a smaller tank is equal to 1.469  $Hz$  for a 25% filled level. From the results, it is understood that at the low fill level (25% FL) the traveling wave present in the clean tank, and the two screens of the lower level of porosity (4.4%  $P$ ) in the sloshing tank can dampen the energy of sloshing oscillation and causes the resonant frequency shift. Due to this phenomenon, the sloshing elevations at end walls considerably reduced in the first resonant mode ( $\beta = 1$ ) and observed peak at the third resonant mode ( $\beta = 2.410$ ) in the screened tank, and which is the first resonant mode of compartment tank. The estimated curves from the analytical model -1 and model -2 exhibit same response within the range of frequency ratios. The two analytical models test results are compared with experimental shake table sloshing tests. The analytical models test results well correlate with experimental findings at and near the third resonant mode except near the first mode. Along with the precision of the data acquisition system, nonlinear and viscous effects may be responsible for the disparity between analytical models and experimental findings in the resonant mode.

In the case of 50% filled level tank with two porous screens (Figure 4.19), the amplitude of maximum free surface elevation is minimal when the frequency ratio ( $\beta$ ) is between 0.5 and 1.25, but as increases from 1.25 to 1.969 and reaches a maximum peak at third natural sloshing mode of the no-screen tank. Observed the lowest response at near  $\beta = 1$ . The response of free surface oscillations in the screened tank were attenuated 99.68% compared to no-screen tank response by model – 1 prediction and 98.85% by model – 2. It is concluded that the performance porous screens were shows

### 4.3.2 Maximum free surface elevation in a 50% FL tank with two porous baffles

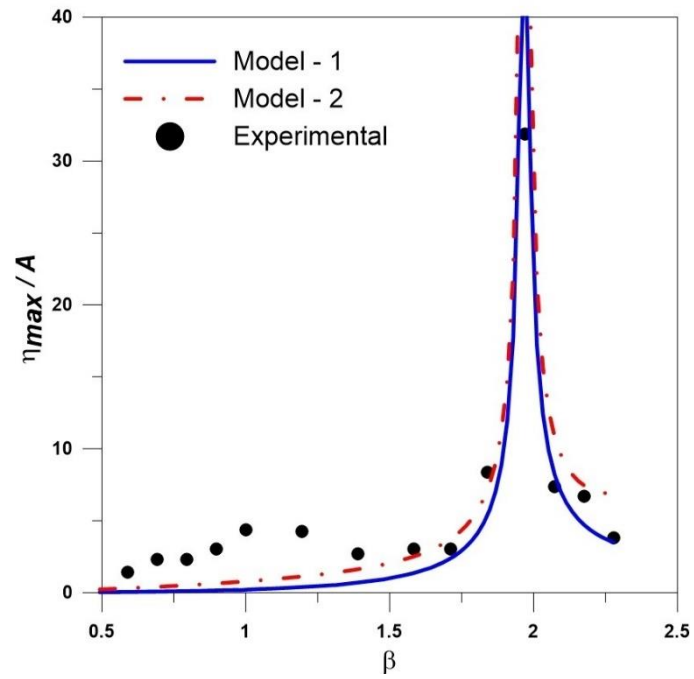


Figure 4.19 Tank with two porous baffle of 4.4% porosity

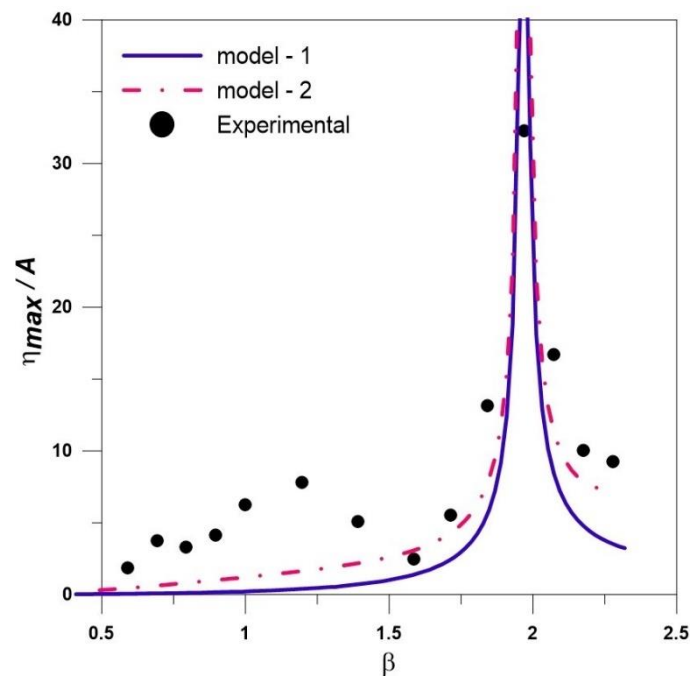


Figure 4.20 Tank with two porous baffle of 6.8% porosity



same behaviors as fill level increases. A small variation in porosity value can affect flow through the screens, resulting in a reduction in damping and an effect on free surface oscillations. The analytical model- 1 tests result well correlate with experimental findings at and near the third resonant mode compare to model -2 results. Similarly, to the 25% FL case, a large discrepancy is observed near the first mode.

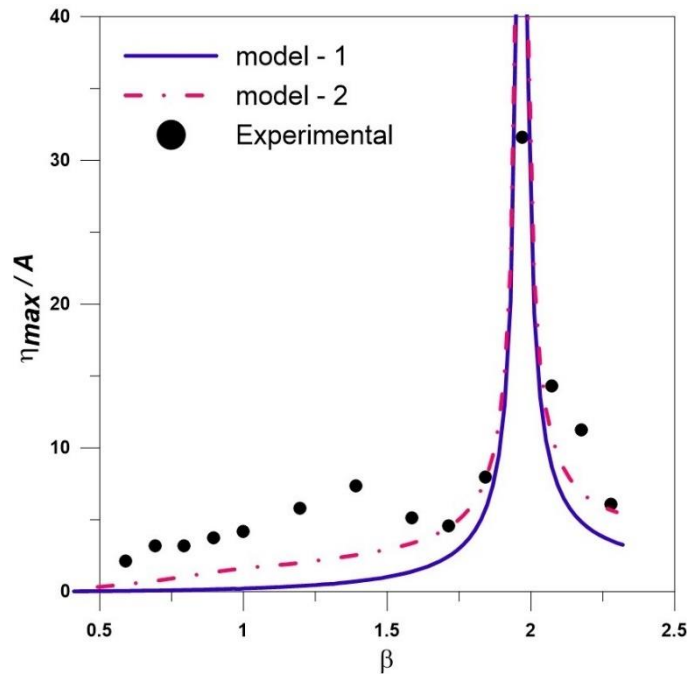


Figure 4.21 Tank with two porous baffle of 9.2% porosity

In the case of 75% filled level tank with two porous screens (Figure 4.22), the amplitude of maximum free surface elevation is minimal when the frequency ratio ( $\beta$ ) is between 0.5 and 1, but as increases from 1 to 1.815 and reaches a maximum peak at third natural sloshing mode of the no-screen tank. The response of free surface oscillations in the screened tank were attenuated 99.68% compared to no-screen tank response by model – 1 prediction and 98.71% by model – 2 at  $\beta = 1$ . The estimated curves from model-1 exhibit a good correlation with the results of model-2 within the range of frequency ratios. The discrepancy between the two model results near the first resonant mode can be summarized as follows, the Reynolds number ( $Re$ ) dependent drag coefficient for a screen depends on the velocity of liquid in the sloshing tank under sway excitation, and lower  $Re$  will lead to higher damping with large values of loss coefficient, whereas in the model-2, the loss coefficient is the function of the porosity,

### 4.3.3 Maximum free surface elevation in a 75% FL tank with two porous baffles

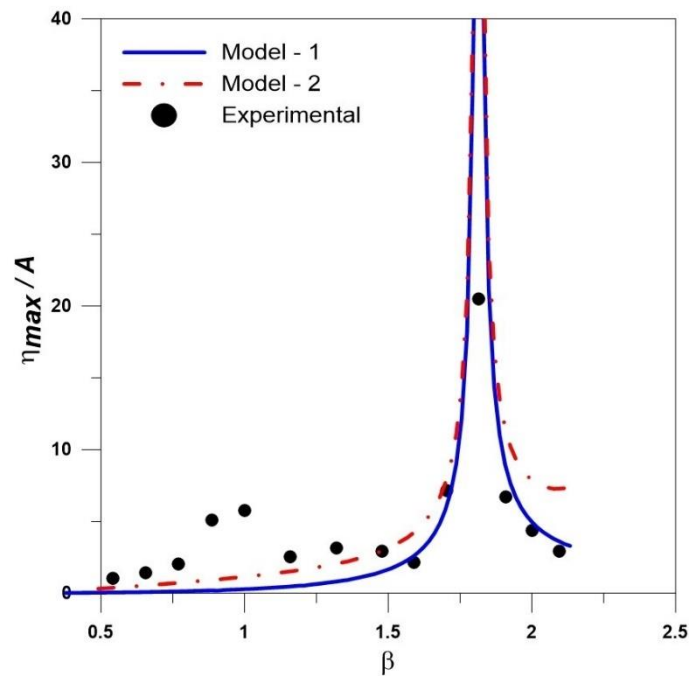


Figure 4.22 Tank with two porous baffle of 4.4% porosity

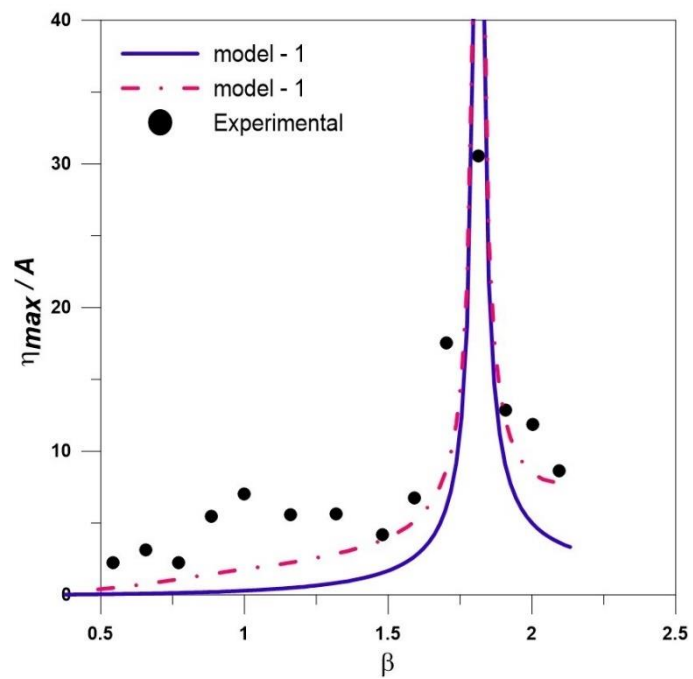


Figure 4.23 Tank with two porous baffle of 6.8% porosity

independent of  $Re$  i.e, the value of loss coefficient is constant with respect to the porosity of screens in the tank, and the value ( $C_l$ ) will not be influenced by excitation frequencies and any other parameters. The present two test models results are confirmed by experimental shake table tests. The test results well predict the results of model- 1 comparatively model -2 results. According to the model results, as the porosity of the screens increases, the flow increases and the damping effect decreases. As a result of this phenomenon, small peaks start to appear at the first resonant mode.

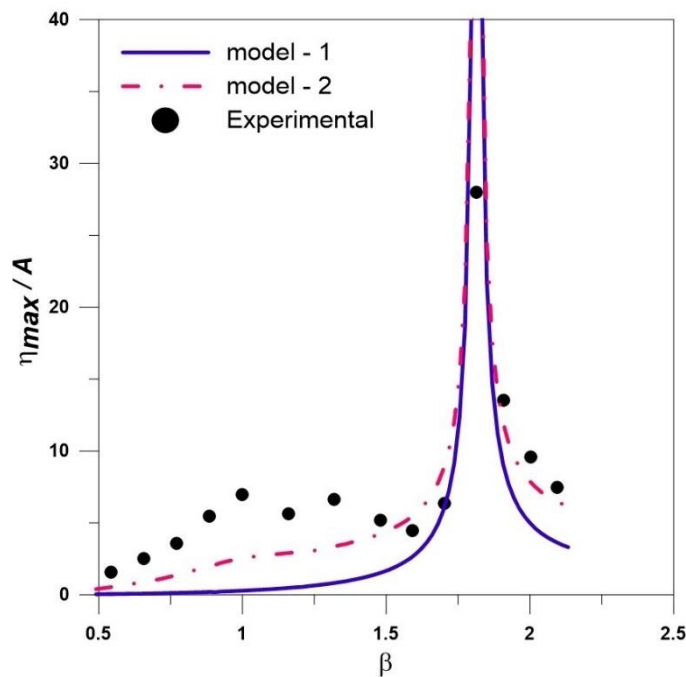


Figure 4.24 Tank with two porous baffle of 9.2% porosity

In the case of tank with effect two vertical porous baffles of 6.8%, the variation in sloshing elevation were observed in the sloshing tank due to the effect of tank geometry, fluid (water) density, liquid fill level in the tank, excitation frequency and amplitude, screens position and its porosity in the tank and screen damping effect. The screens are placed at  $L/3$  and  $2L/3$  distances from the tank's left wall, and two screens porosity of 6.8% were used throughout study. The screens damping effect in the present study mainly includes screen loss coefficient. In the analytical model – 1, the screen loss coefficient was adopted based on the test results on gravitational flow between two reservoirs with 6.8% porosity screens. In the test investigation, the screen loss coefficient depends on screen porosity and Reynolds number. Whereas in the model –

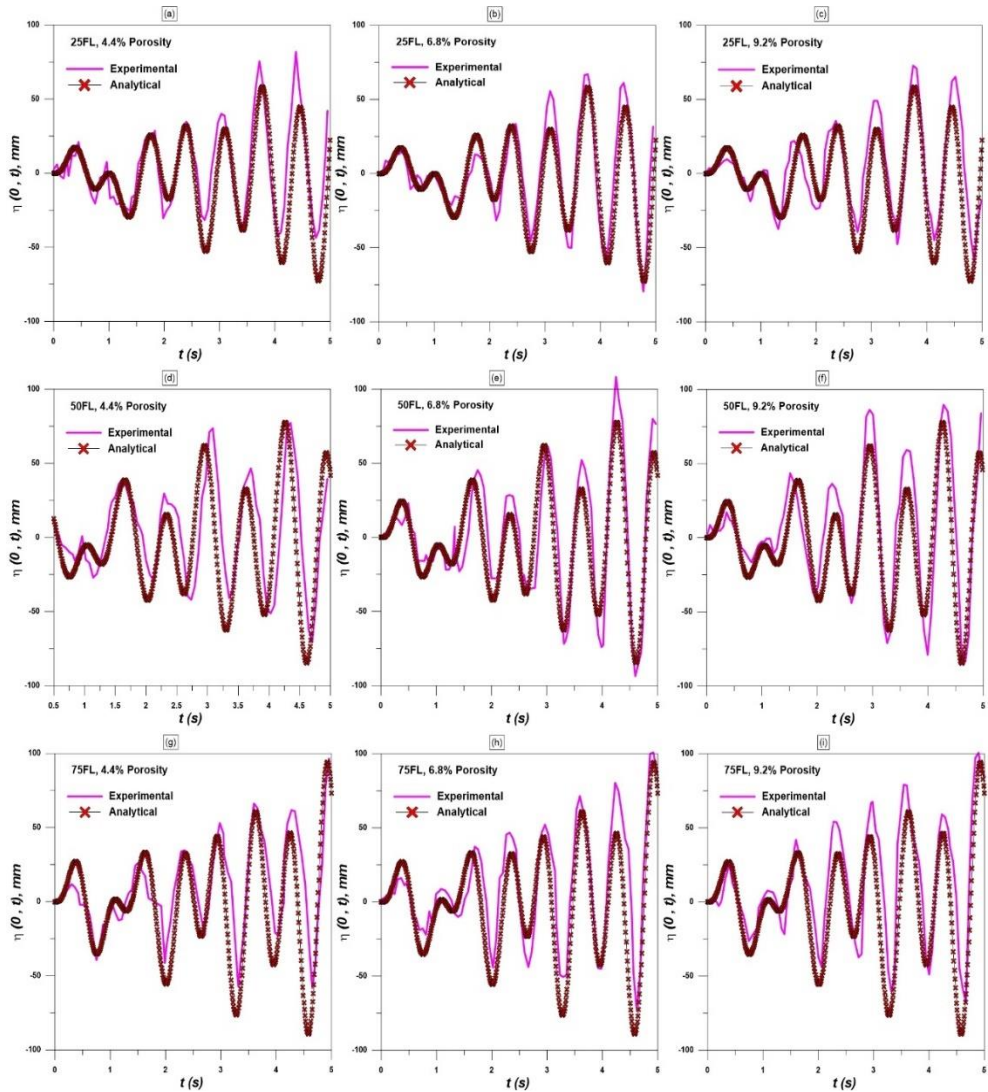


Figure 4.25 Time history of free surface elevation for the tank with baffles at  $\omega = \omega_3$ .

2, the screen loss coefficient dependent on porosity of screens and independent of Reynolds number (Baines and Peterson, 1951). The maximum free surface elevation variations versus frequency ratio in a tank with two porous baffles for three different fill levels of 25%, 50%, and 75% are shown in Figure 4.17, Figure 4.20, and Figure 4.23 respectively.

In the case of 25% fill level screened tank (Figure 4.17), the maximum free surface elevations observed least at lower frequency range and goes on increasing as frequency excitation increases, and reaches its peak at frequency ratio ( $\beta$ ) of 2.41, which is first antisymmetric mode of compartment tank ( $f_{n1} = 9.176 \text{ Hz}$ ) as well second antisymmetric

mode of non- compartment tank ( $f_{n3} = 9.176 \text{ Hz}$ ). This resonant frequency shift phenomenon was observed in both analytical models results, and it was caused by the low-level level porosity of the baffles screen in the tank.

#### 4.3.4 Maximum sloshing force variations in a 25% FL tank with two porous baffles

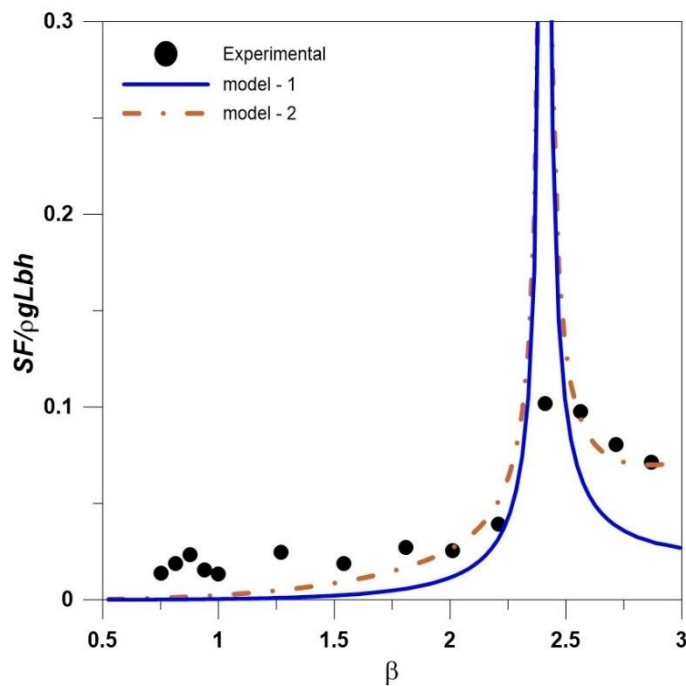


Figure 4.26 Tank with two porous baffle of 4.4% porosity

In the case of 50% fill level screened tank, the maximum free surface elevation responses by analytical model-1 were minimal between 0.5 and 1.25 frequency ratio and elevated from 1.25 to 1.969. But it is minimal up to 0.75 by analytical model-2, and surface elevation increases as excitation increases. Further, the responses by both models reached a maximum peak at the third resonant mode of the no-screen tank. Both the analytical model results show identical response pattern at third resonant mode, but shows difference in response amplitude quantitatively between two resonant modes. This difference may cause due to variation in the loss coefficient at lower range of Reynold numbers.

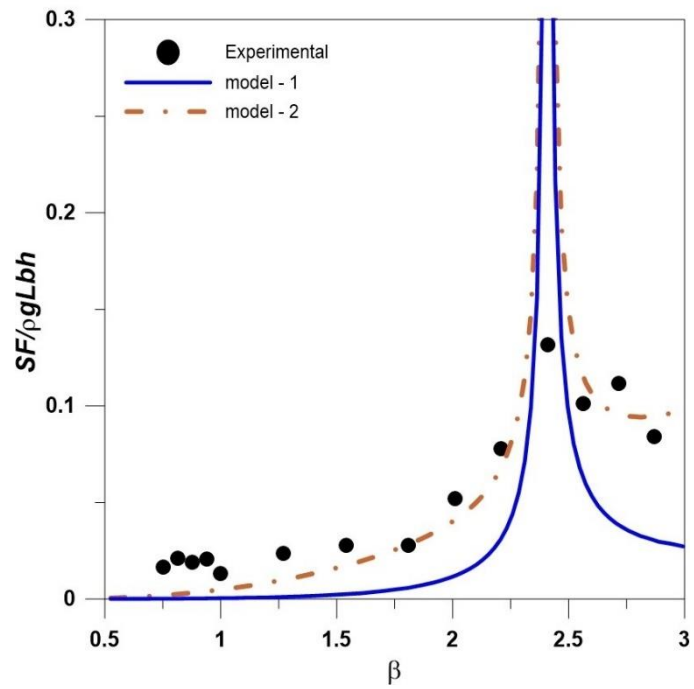


Figure 4.27 Tank with two porous baffle of 6.8% porosity

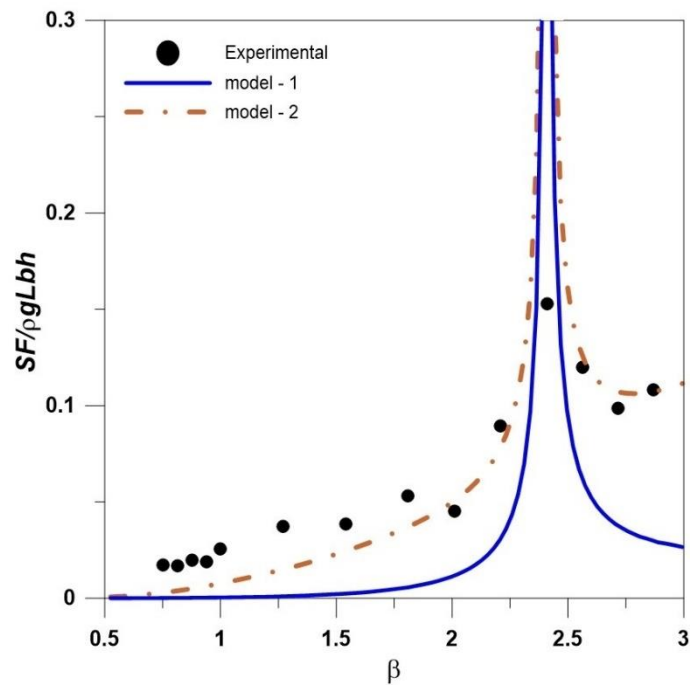


Figure 4.28 Tank with two porous baffle of 9.2% porosity

In the case of a 75% filled level tank with two porous screens (Figure 4.23), the amplitude of the maximum free surface elevation variation by model-1 is minimal

between 0.5 and 1 frequency ratio, but as it increases from 1 to 1.815, it reaches a maximum peak at the third natural sloshing mode of the no-screen tank. Whereas, the response of surface elevation starts increasing from frequency ratio of 0.5 and reaches its peak at third resonant mode.

#### 4.3.5 Maximum sloshing force variations in a 50% FL tank with two porous baffles

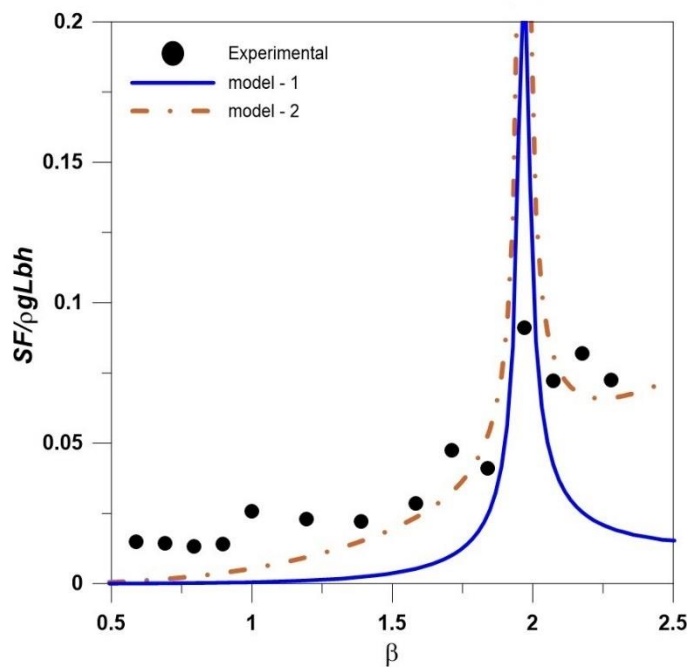


Figure 4.29 Tank with two porous baffle of 4.4% porosity

The fill levels have a significant impact on screen performance in the tank. All above response plots show that the resonant peak responses increase as the tank fill level increases. And, also observe that, as fill levels increases in the screened tank, causes the discrepancy between the two model results near the first resonant mode. This may occur due to the rebounding wave from the end wall duplicating the surface wave. The reduction in the wave elevation near the first resonant mode due the screens damping effect. In the analytical model – 1, the damping effect of porous screen depend on both screen porosity and flow which approaching the screens. The screen porosity of 6.8% gives a higher loss coefficient for lesser flow rate in the sloshing tank and as Reynold number increases the screen loss coefficient reduces and yields less damping. Where as

in the analytical model – 2, the damping depends only on magnitude of screens porosity. Therefore, the analytical model – 1 response for suppressing the wave elevation in the sloshing tank under range of excitation frequencies were found be more effective compare to analytical model – 2 test results for all three fill levels.

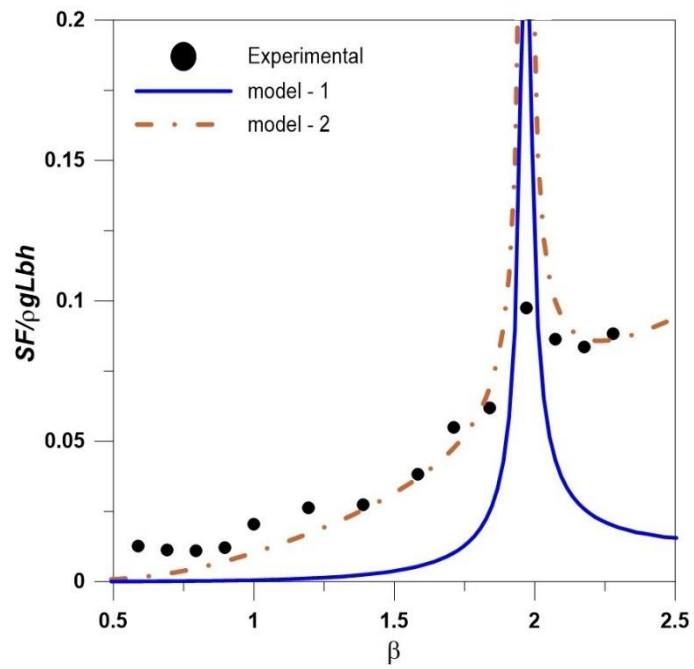


Figure 4.30 Tank with two porous baffle of 6.8% porosity

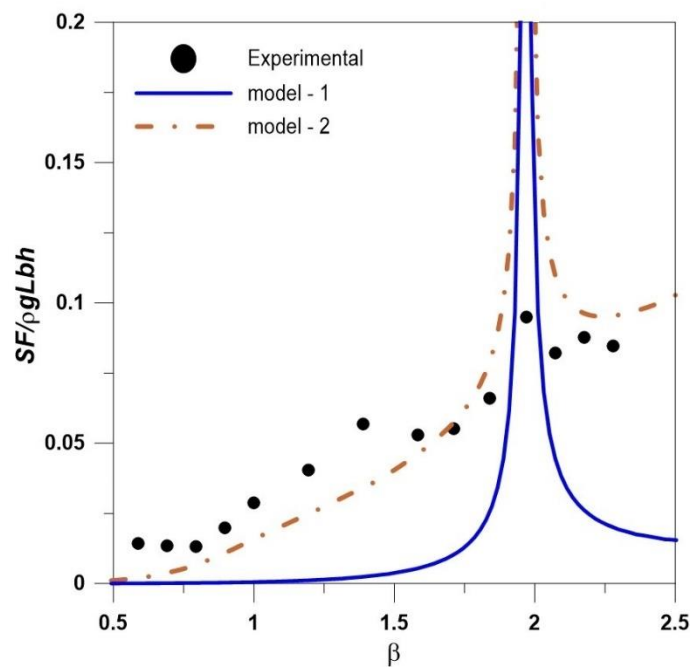




Figure 4.31 Tank with two porous baffle of 9.2% porosity

The maximum free surface elevation variations versus frequency ratio in a tank with two porous baffles of each one porosity 9.2% for three different fill levels of 25%, 50%, and 75% are shown in Figure 4.18, Figure 4.21, and Figure 4.24 respectively. The dynamics of free surface elevation variation in the sloshing tank were observed in the tank with 9.2% porosity screens for all fill level cases, similar to the 4.4% and 6.8% porosity screens in the tank. The resonant frequency shift phenomenon was also observed by the both analytical models.

#### 4.3.6 Maximum sloshing force variations in a 75% FL tank with two porous baffles

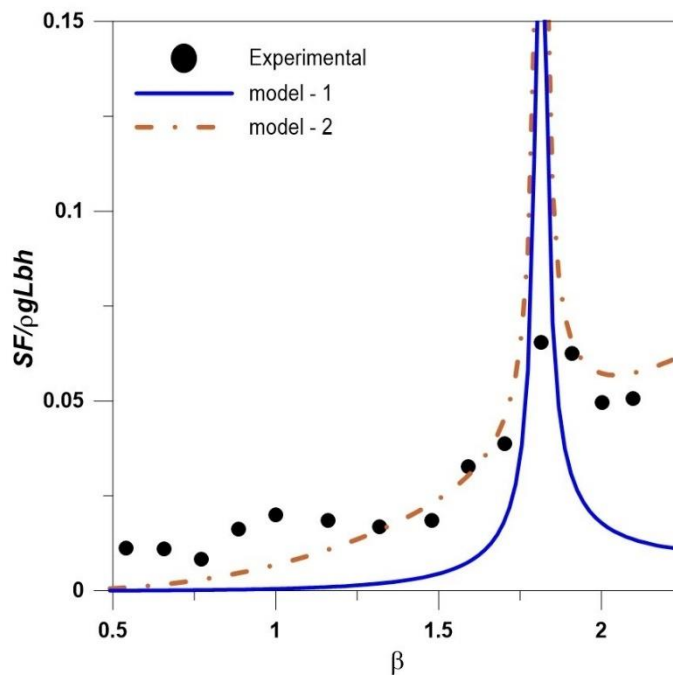


Figure 4.32 Tank with two porous baffle of 4.4% porosity

In addition to primary peaks at frequencies of 1.535 Hz, and 1.538 Hz in the case of porosity of 9.2% with 50% and 75% fill levels, a secondary peak is also observed at  $\beta = 1$ , which is the first mode sloshing frequency of the no screen tank. This is because the fluid can pass through the large porosity with more oscillation in the tank comparatively 4.4% and 6.8% of porous screens.

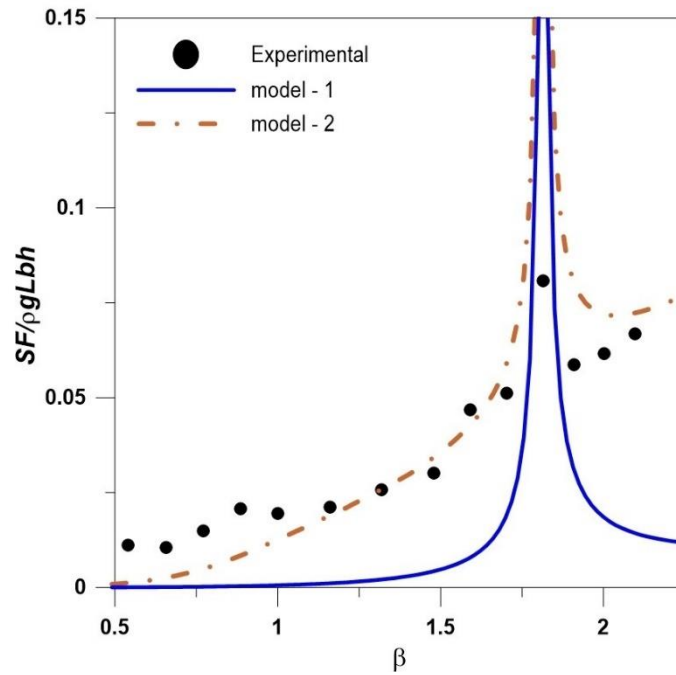


Figure 4.33 Tank with two porous baffle of 6.8% porosity

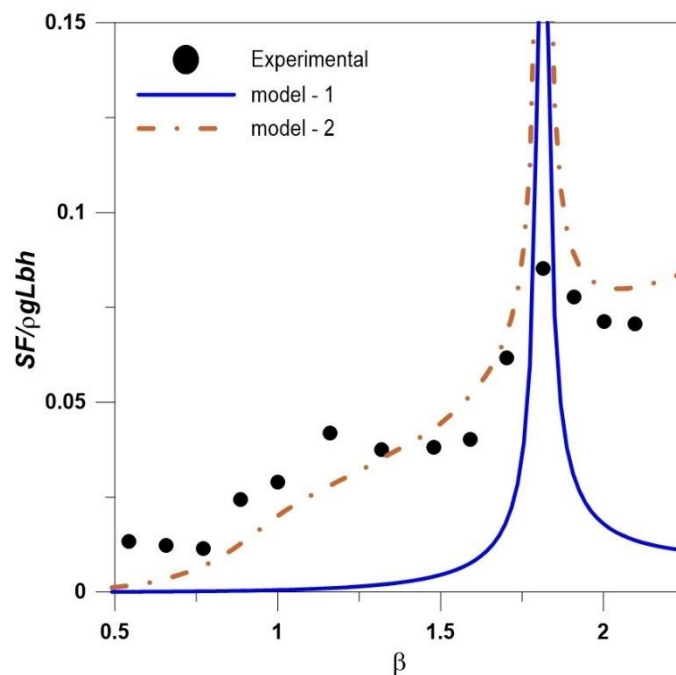


Figure 4.34 Tank with two porous baffle of 9.2% porosity

The sloshing force variation in the tank with two vertical porous baffles of three varying porosities of 4.4%, 6.8%, and 9.2% are discussed. The variation in sloshing force is observed in the sloshing tank due to the effect of the liquid fill level in the tank,

excitation frequency, and amplitude, screen position and screen porosity in the tank, and screen damping effect.

The screen damping effect in the present study mainly includes the porosity of the screen, screen drag coefficient, and placement of the screen in the tank. In the analytical model – 1, the screen loss coefficient is adopted based on the test results on the gravitational flow between two reservoirs with varying porosity of screens. Similar to the free surface elevation variation in the tank, two different screen loss coefficient is adopted to evaluate the sloshing force in the tank. As mentioned above, the screen loss coefficient depends on screen porosity and Reynolds number. Whereas in model – 2, the screen loss coefficient is dependent on the porosity of screens and independent of the Reynolds number (Baines and Peterson, 1951). The maximum free surface elevation variations versus frequency ratio in a tank with two porous baffles for three different fill levels of 25%, 50%, and 75%. In tank with all fill levels, the experimental test results well matched with model-2 results, where the loss coefficient is independent of Reynold number. But, two model test results follow the experiments test results at higher excitations frequency range. This behaviour may due to the fact, the drag coefficient values are nearly nonlinear at low level Reynold number range, but its liner at higher Reynolds range. Therefore, two model results show the similar trend at higher range of excitation.

In the case of 25% fill level screened tank, the sloshing force variation observed least at lower frequency range and goes on increasing as frequency excitation increases, and reaches its peak at frequency ratio ( $\beta$ ) of 2.41, which is first antisymmetric mode of compartment tank as well second antisymmetric mode of non- compartment tank. This resonant frequency shift phenomenon was observed in both analytical models result, and it was caused by the low-level level porosity of the baffles screen in the tank. The 4.4% porosity screens (Figure 4.26) are dampen the resonant sloshing frequency at first resonant mode, and deposited lesser force. This may more helpful for the tank where first resonant mode is concentrated. Further as porosity increase the force at near the first resonant mode increases, this may due large flow through the higher porous baffles (Figure 4.27 and Figure 4.27). Further, in the third resonant mode, the experiment and

two different model results show the same phenomenon and well correlate with each other.

#### 4.3.7 Energy dissipation variations in a 25% FL tank with two porous baffles

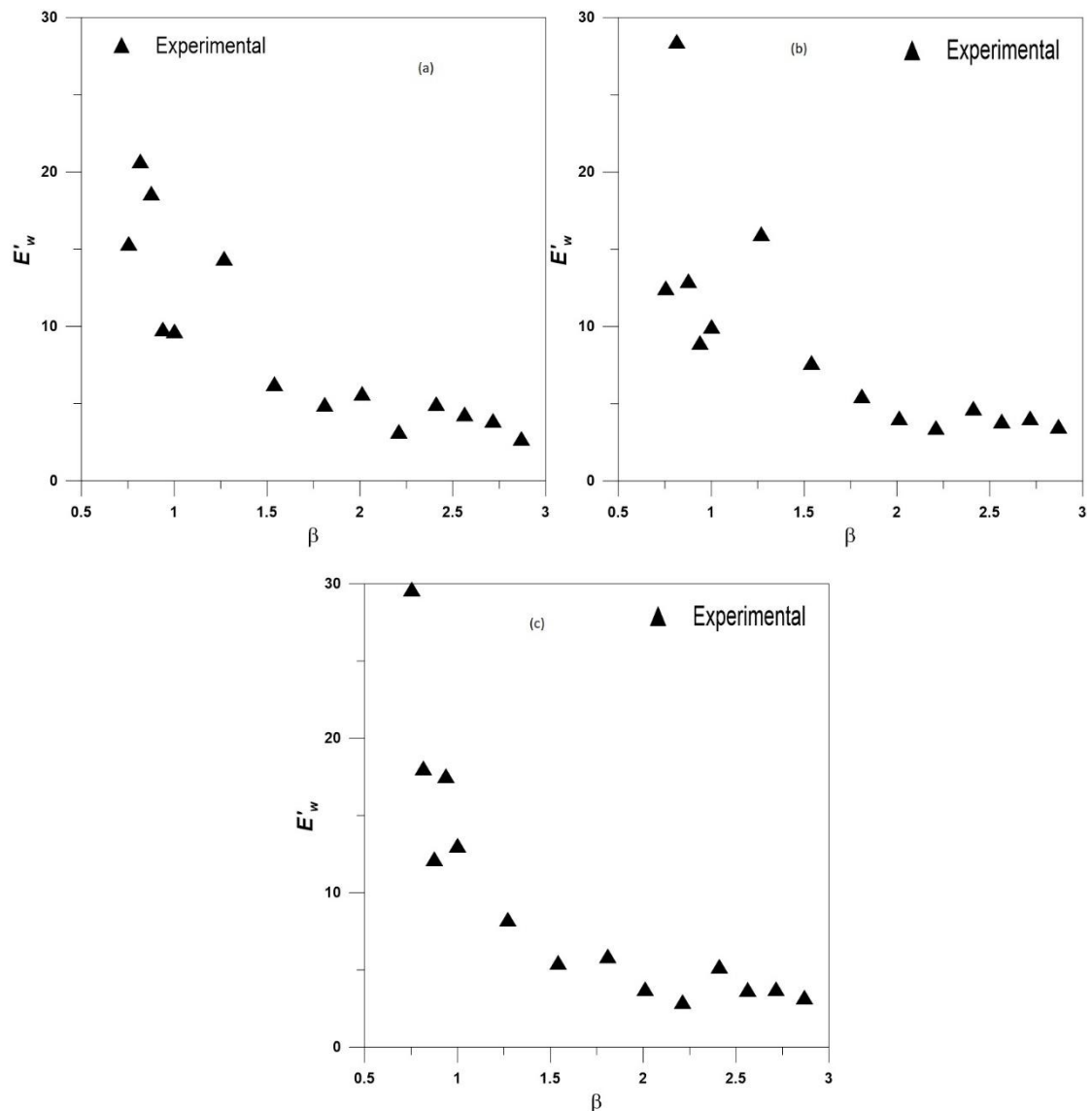


Figure 4.35 Tank with two porous baffles of (a) 4.4%, (b) 6.8%, and (c) 9.2% porosity

In the case of 50% fill level screened tank, the sloshing force responses by analytical model-1 were minimal between 0.5 and 1.0 frequency ratio and elevated from 1.0 to 1.969. But it is minimal up to 1.5 by analytical model-1, and surface elevation increases as excitation increases. Further, the responses by both models reached a maximum peak at the third resonant mode of the no-screen tank (Figure 4.29, Figure 4.30, and Figure

4.31). Both the analytical model results show identical response pattern at third resonant mode, but shows difference in response amplitude quantitatively between two resonant modes at first resonant mode. This difference may cause due to variation in the loss coefficient at lower range of Reynold numbers

#### 4.3.8 Energy dissipation variations in a 50% FL tank with two porous baffles

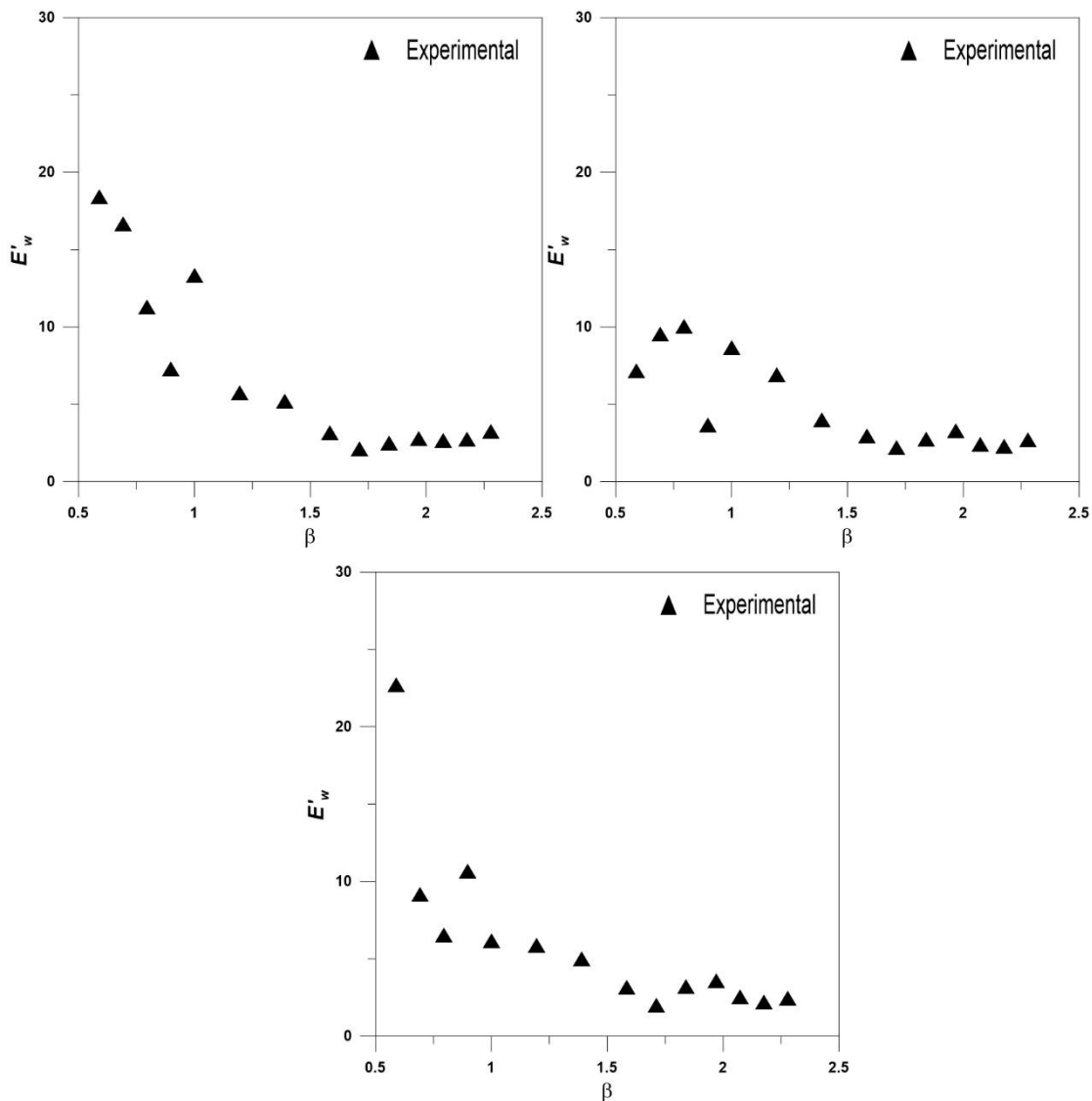


Figure 4.36 Tank with two porous baffles of (a) 4.4%, (b) 6.8%, and (c) 9.2% porosity

In the case of 75% fill level screened tank (Figure 4.32, Figure 4.33, and Figure 4.34), the force variation in the tank with all three porosities shows the same behaviour. But

by model-2, the tank with 9.2% porosities screens, a secondary peak is appearing near the first resonant mode and similar behaviour observed in the experimental results.

#### 4.3.9 Energy dissipation variations in a 75% FL tank with two porous baffles

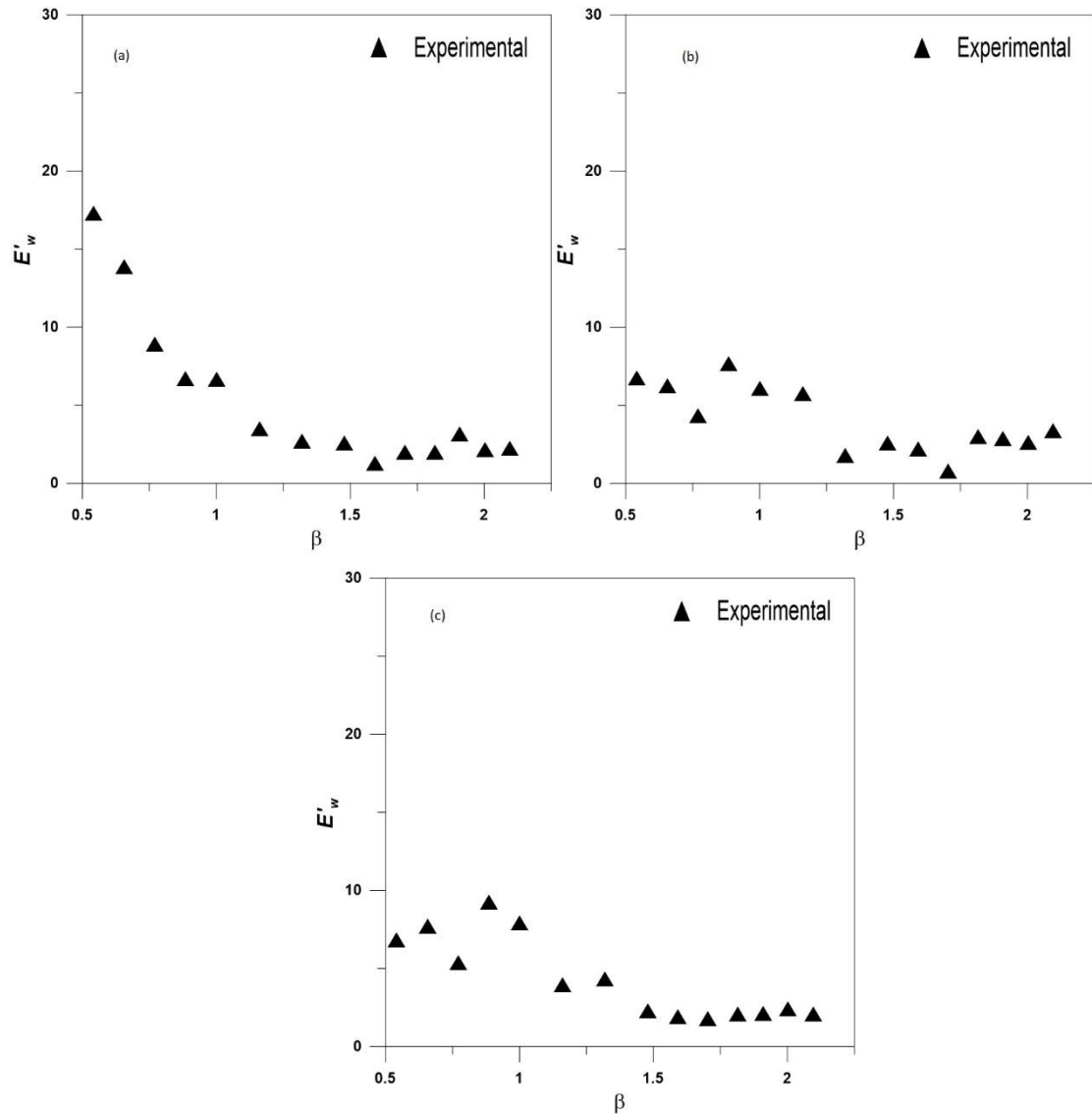


Figure 4.37 Tank with two porous baffles of (a) 4.4%, (b) 6.8%, and (c) 9.2% porosity

The viscous effect caused by the interaction of the liquid-tank and the flow through the porous baffles in the tank reduces the sloshing kinetic energy. The energy dissipation characteristic in the baffled tank with 25%, 50%, and 75% fill levels shown in the Figure 4.35, Figure 4.36, and Figure 4.37. In case of 25% fill level, the porous baffles of all porosities shows the similar behaviour, as excitation increases the magnitude of

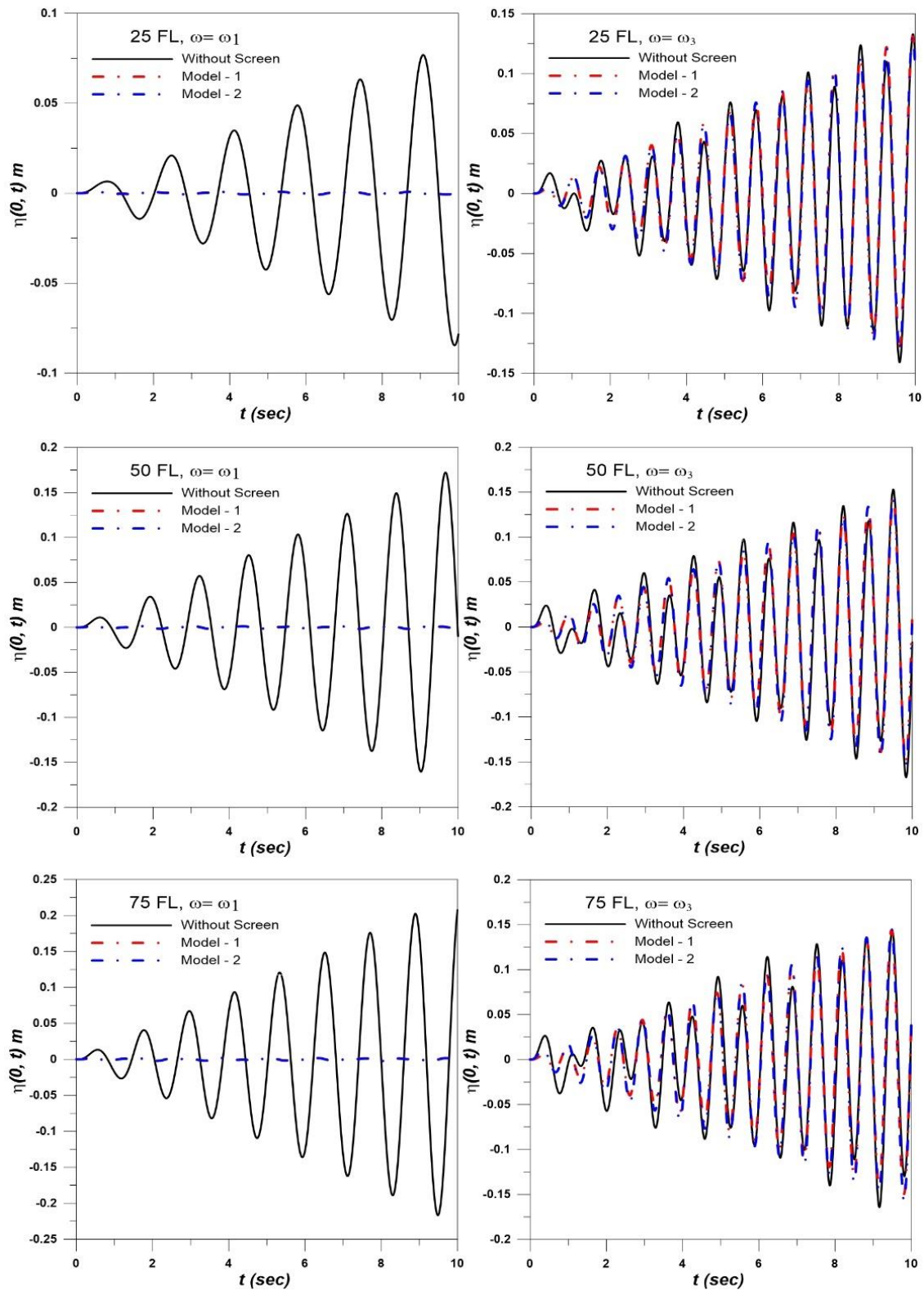


Figure 4.38 Time history of free surface elevation in a sloshing tank.

energy dissipation response reduces. In order to dissipate the kinetic energy, the free surface deformation produced by the presence of porous baffles and shear stress on the walls are particularly important.

The fundamental sloshing frequency is normally used to stimulate the tank to produce the most sloshing kinetic energy. In the present case a small amplification is observed near the first resonant mode. Due to the possibility of tank wall damage from large dynamic forces near the first resonant mode, dynamic force plays a significant role in tank design. In the present case, due to presence of porous baffle, the energy is reduced.

#### **4.3.10 Free surface elevation time series**

The purpose of this section is to relate the impacts of two porous screens in a rectangular sloshing tank to the sloshing mitigation under sway excitation. The plots in the Figure 4.38 show time history of free surface elevations in the tank with and without baffles. At first, the analytical work with a no-screen tank and tank with a porous screen for two different loss coefficients were carried out considering the frequency of excitation equal to the first two resonant modes of the no-screen tank for three different fill levels of 25%, 50%, and 75%. According to the obtained results, the maximum response of free surface elevations was observed in a no-screen tank with all three fill levels under two resonant modes ( $\omega=\omega_1, \omega_3$ ). In the case of the tank with a porous screen, the largest free surface elevations near the wall are completely suppressed for all fill levels in a first resonant mode ( $\omega=\omega_1$ ). Whereas, it is observed maximum as similar to the response of the no-screened tank under second resonant mode ( $\omega=\omega_3$ ) for all three fill levels. From the response, it is observed that both two models (models – 1 & 2) behave almost the same under resonant modes for all three fill levels.



## 4.4 SLOSHING DYNAMIC IN THE RECTANGULAR TANK WITH SINGLE POROUS BAFFLES

### 4.4.1 Maximum free surface elevation in a 25% FL tank with single porous baffles

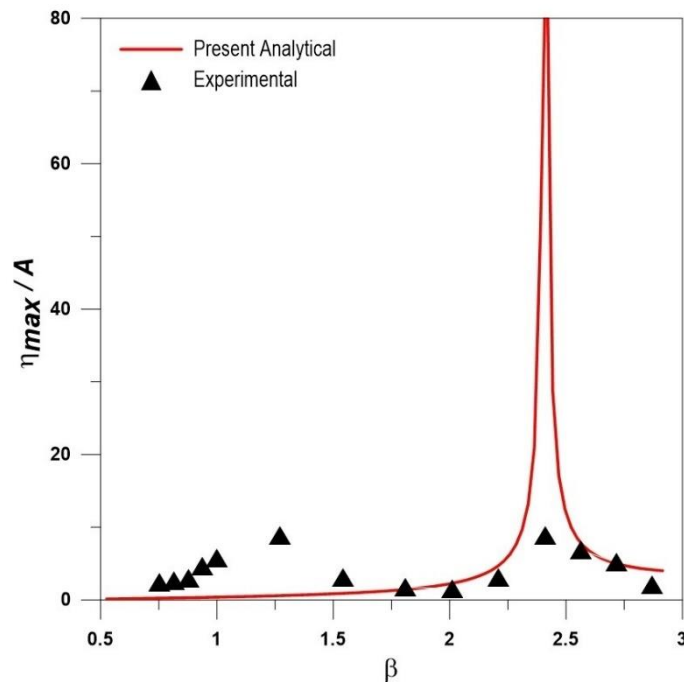


Figure 4.39 Tank with single porous baffle of 4.4% porosity

The sloshing elevation variation in the tank with effect single vertical porous baffles of all three porosities are discussed. The variation in sloshing elevation were observed in the sloshing tank due to the effect of tank liquid fill level in the tank, excitation frequency and amplitude, screens position and its porosity in the tank. The screen is placed at  $L/2$  from the tank's left wall i.e. centre of the tank. The screens damping effect in the analytical study includes screen loss coefficient based on the Baines and Peterson (1951) empirical relation. The maximum free surface elevation variations versus frequency ratio in a tank with single porous baffles for three different fill levels presented and discussed.

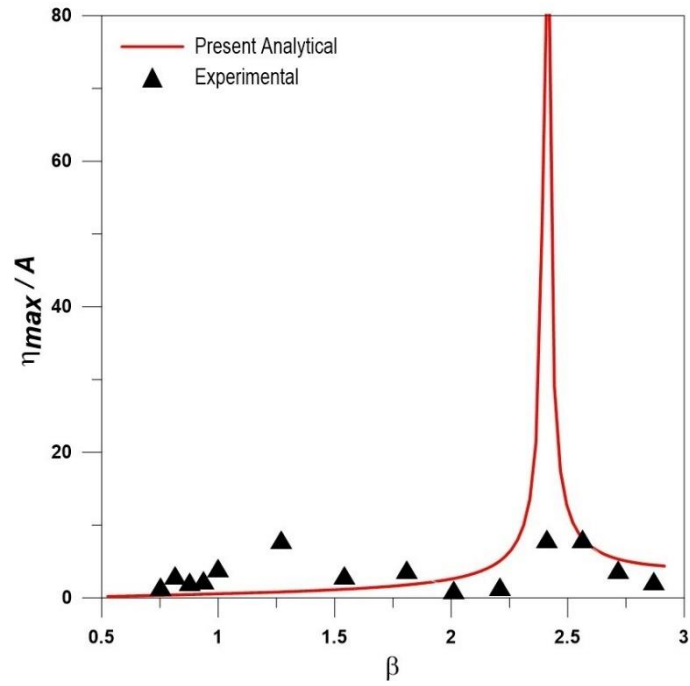


Figure 4.40 Tank with single porous baffle of 6.8% porosity

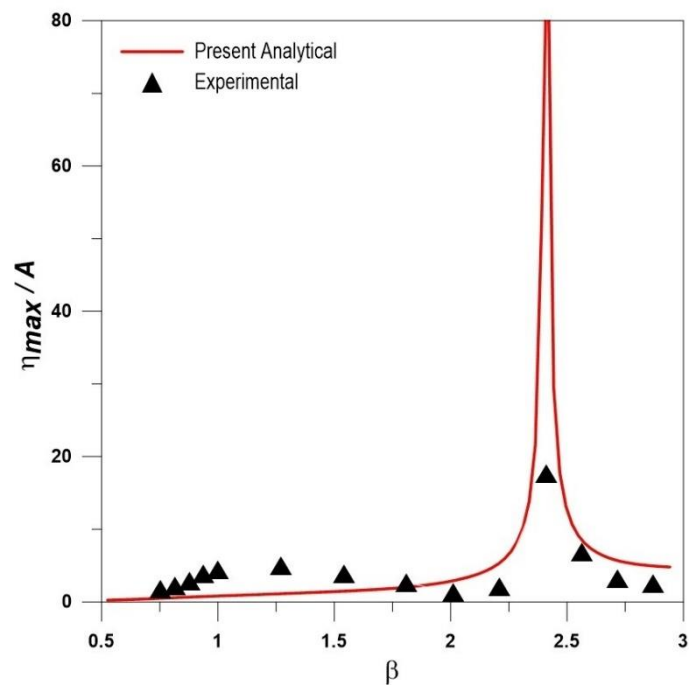


Figure 4.41 Tank with single porous baffle of 9.2% porosity

In the case of 25% fill level screened tank (Figure 4.39, 4.40, and 4.41), the experimentally observed maximum free surface elevations least at lower frequency

range and goes on increasing as frequency excitation increases, and reaches its peak at near the second resonant mode of tank. Whereas it least up to third resonant mode for analytical test results and reaches first peak at third resonant mode. The experimental test results show another peak at near the third resonant mode due presence of single porous baffle in the tank. The similar resonance phenomenon observed by both experimental and analytical test results in case of tank with 50% filled level. In the case tank with 75% fill level for all three porosities, the experimentally obtained free surface elevation results show the exact phenomenon as observed in the Wei et al (2015); Poguluri and Cho (2020) for tank single porous baffle condition comparatively other two fill levels.

#### 4.4.2 Maximum free surface elevation in a 50% FL tank with single porous baffles

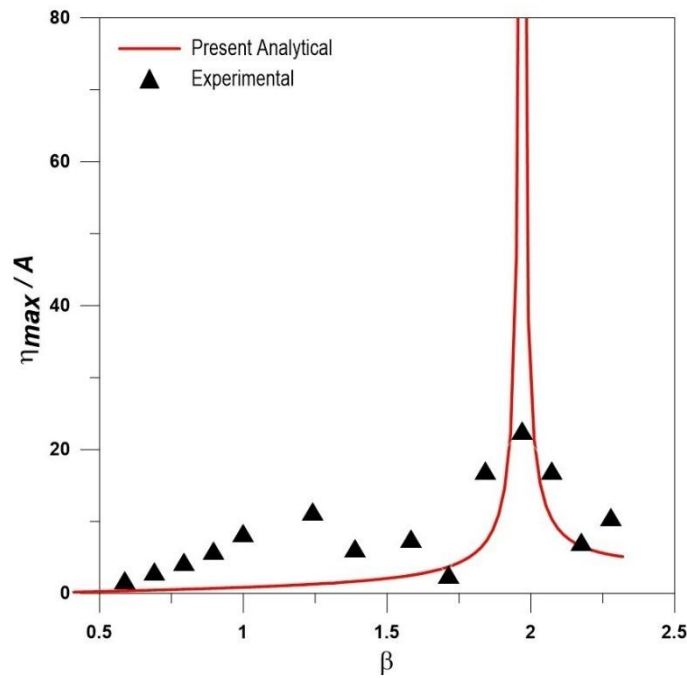


Figure 4.42 Tank with single porous baffle of 4.4% porosity

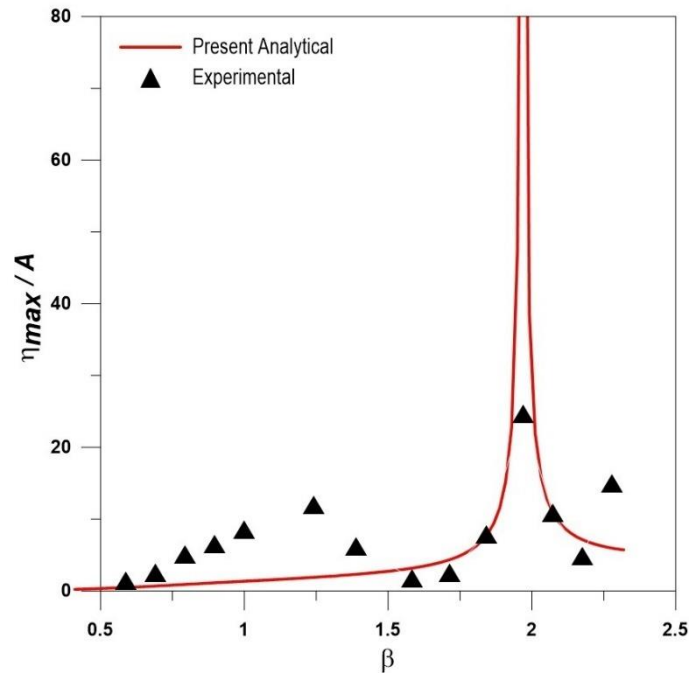


Figure 4.43 Tank with single porous baffle of 6.8% porosity

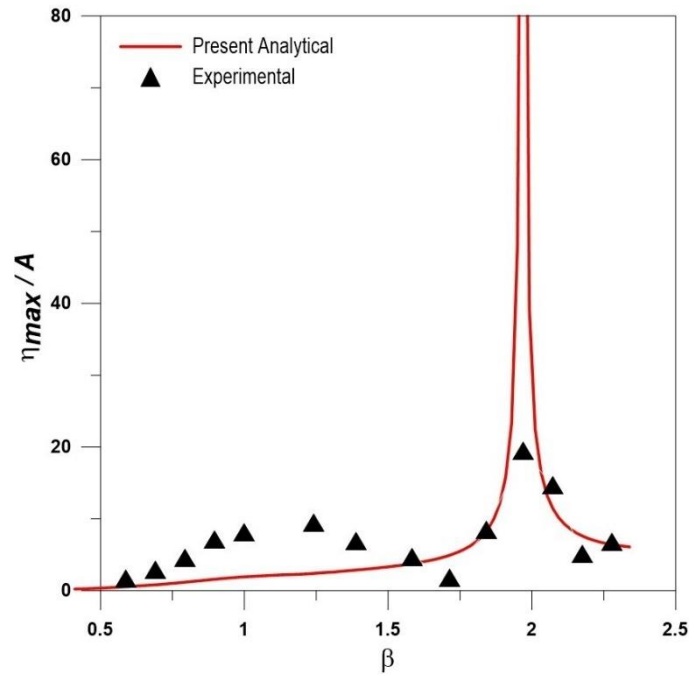


Figure 4.44 Tank with single porous baffle of 9.2% porosity

#### 4.4.3 Maximum free surface elevation in a 75% FL tank with single porous baffles

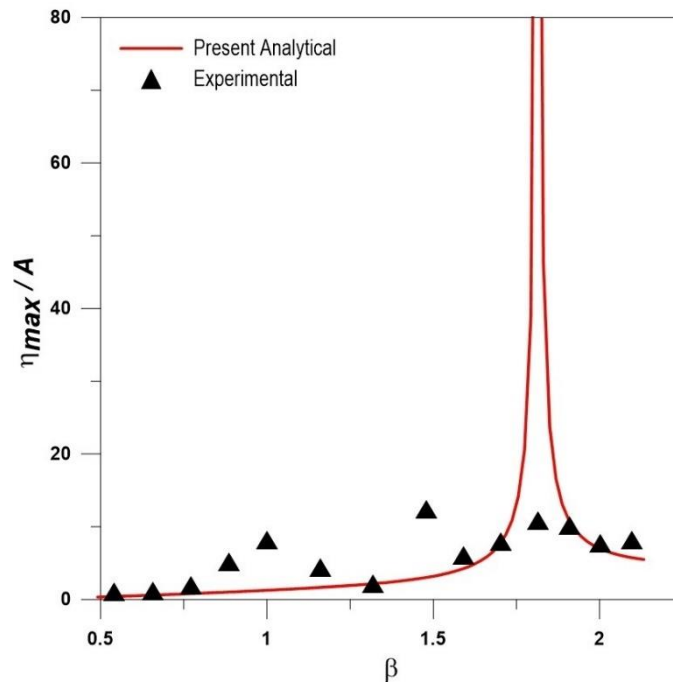


Figure 4.45 Tank with single porous baffle of 4.4% porosity

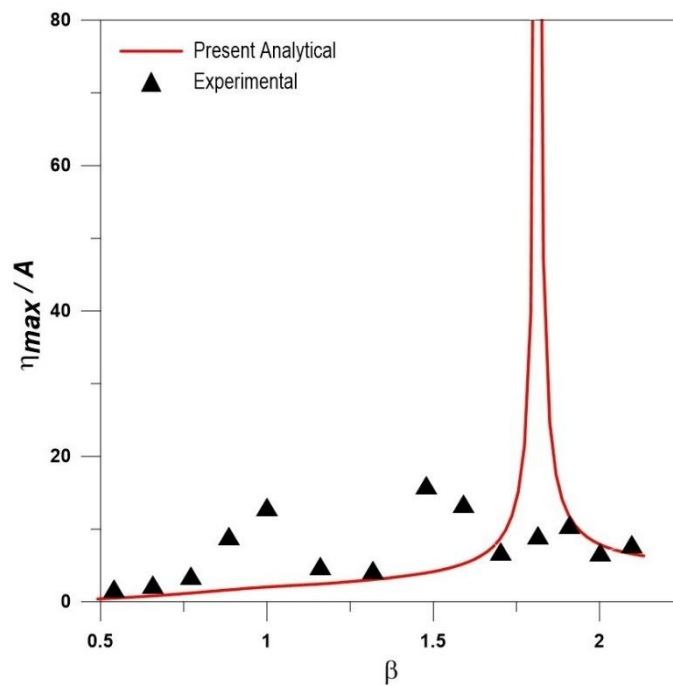


Figure 4.46 Tank with single porous baffle of 6.8% porosity

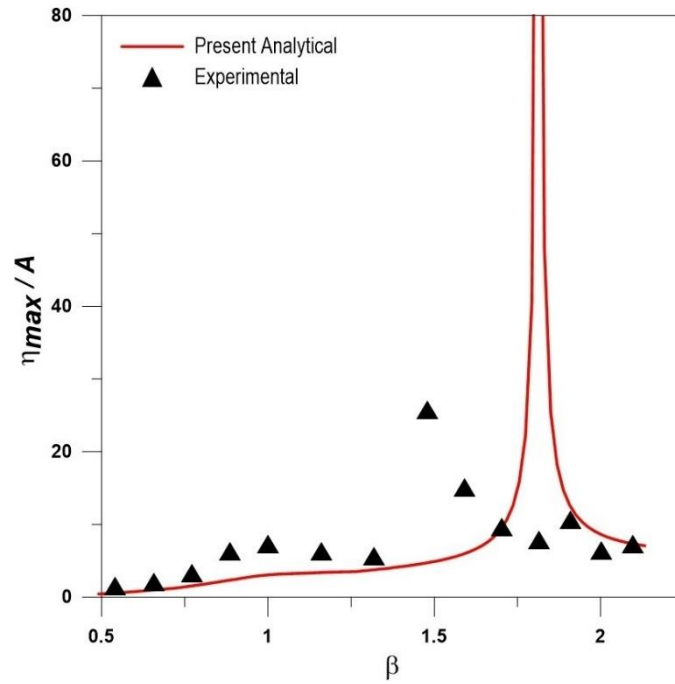


Figure 4.47 Tank with single porous baffle of 9.2% porosity

**4.4.4 Maximum sloshing force variations in a 25% FL tank with Single porous baffles**

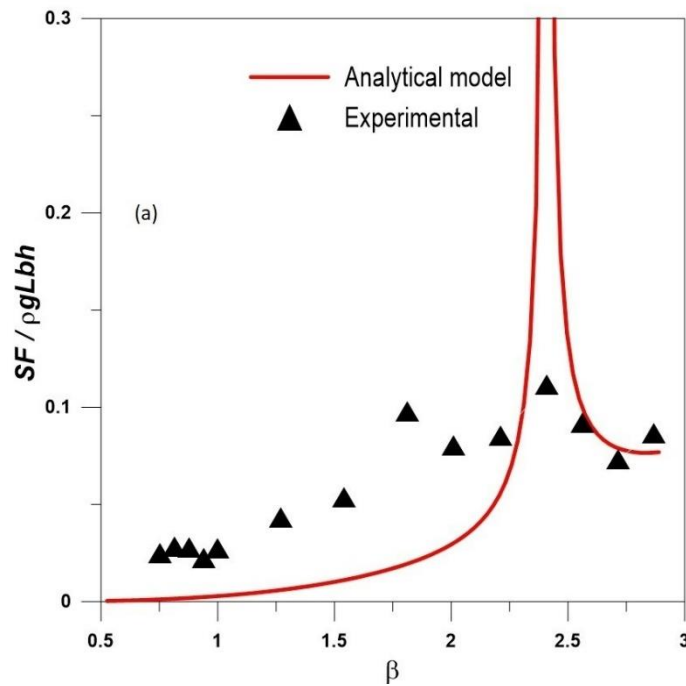


Figure 4.48 Tank with single porous baffle of 4.4% porosity

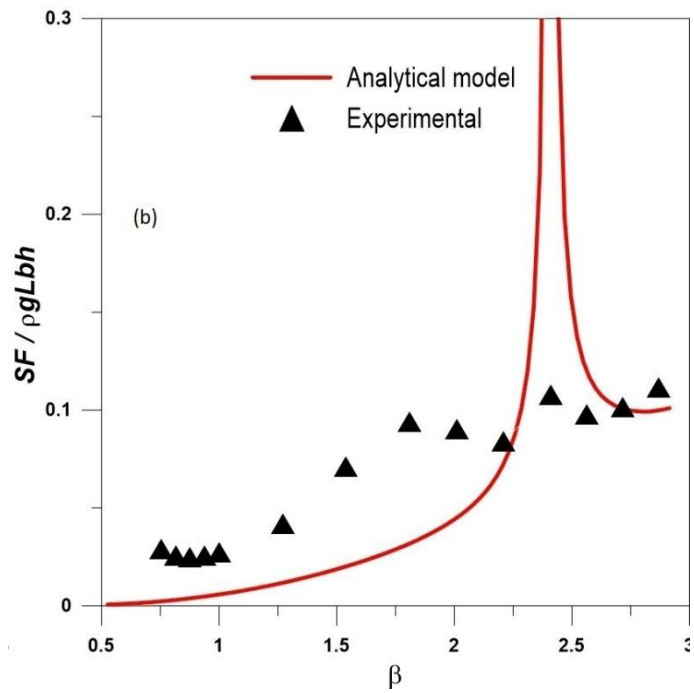


Figure 4.49 Tank with single porous baffle of 6.8% porosity

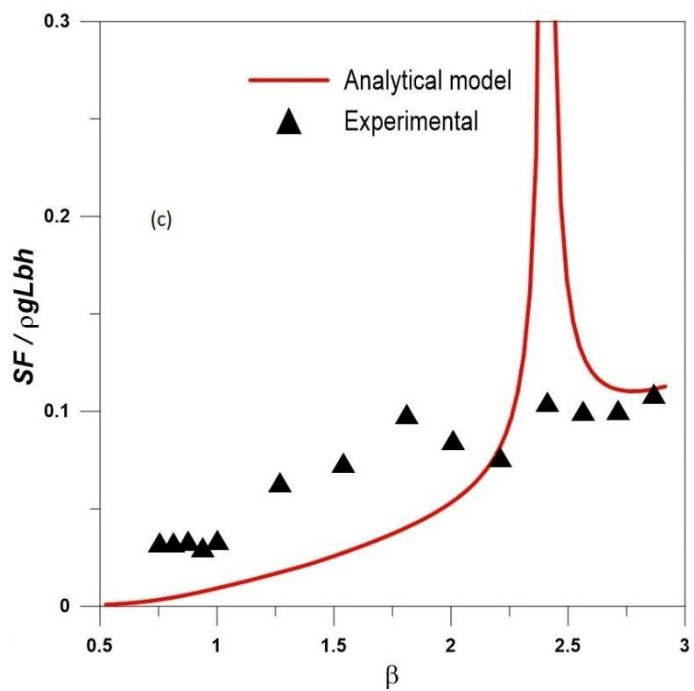


Figure 4.50 Tank with single porous baffle of 9.2% porosity

In case of sloshing force variation in the tank with 25% filled level (Figure 4.48, 4.49, and, 4.50), the maximum normalized sloshing force reduces near the first resonant

mode of tank with all three porous baffles and it is observed around 0.03. As excitation frequency increase the response increases in the experimental test results, and reaches maximum peak at second resonant mode and its observed nearly 0.1 for all three porous baffled conditions. The analytical model results for this condition fail to have a correlation with experimental findings. Behind second resonant mode both model exhibits same response with small peak near the third resonant mode for all porous baffled conditions.

In case of 50% filled level (Figure 4.51, 4.52, and 4.53), response of maximum sloshing force variation by 4.4%, 6.8%, and 6.8% shows the similar behaviours as observed in the 25% filled level condition. In the 50% filled level case the resonant

#### 4.4.5 Maximum sloshing force variations in a 50% FL tank with Single porous baffles

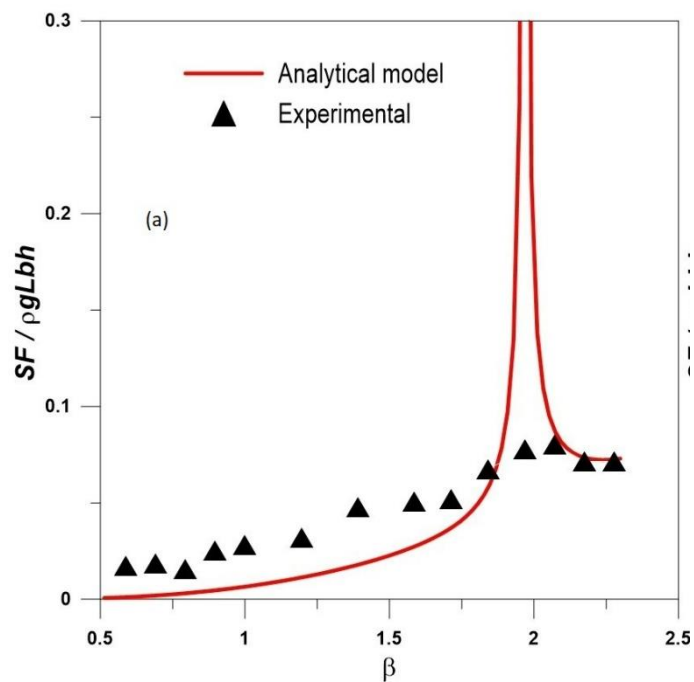


Figure 4.51 Tank with single porous baffle of 4.4% porosity



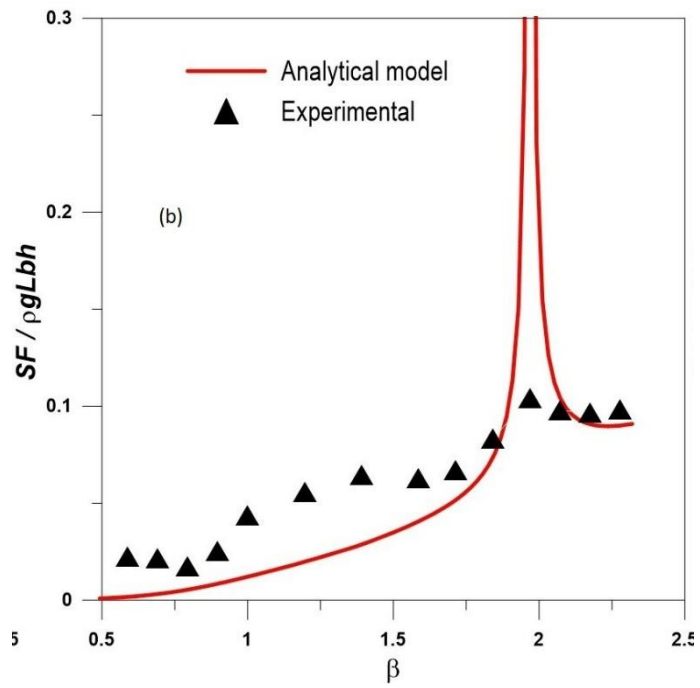


Figure 4.52 Tank with single porous baffle of 6.8% porosity

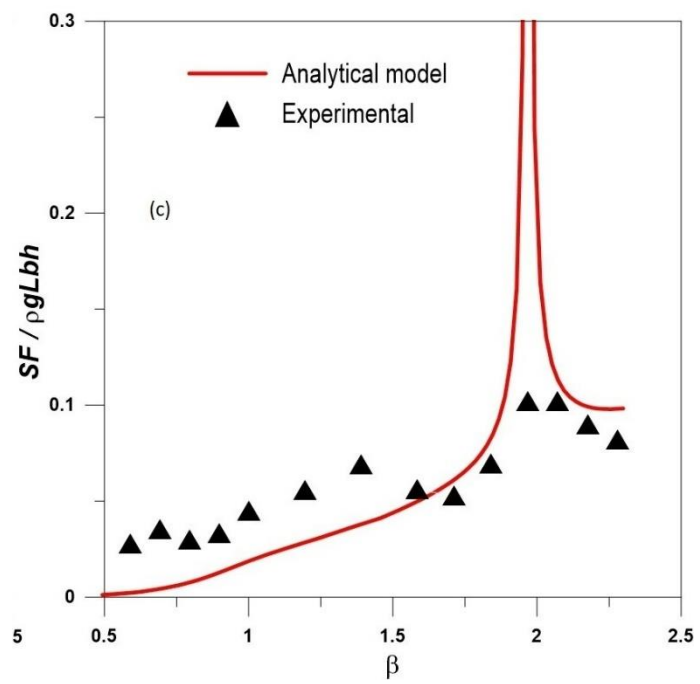


Figure 4.53 Tank with single porous baffle of 9.2% porosity

#### 4.4.6 Maximum sloshing force variations in a 75% FL tank with Single porous baffles

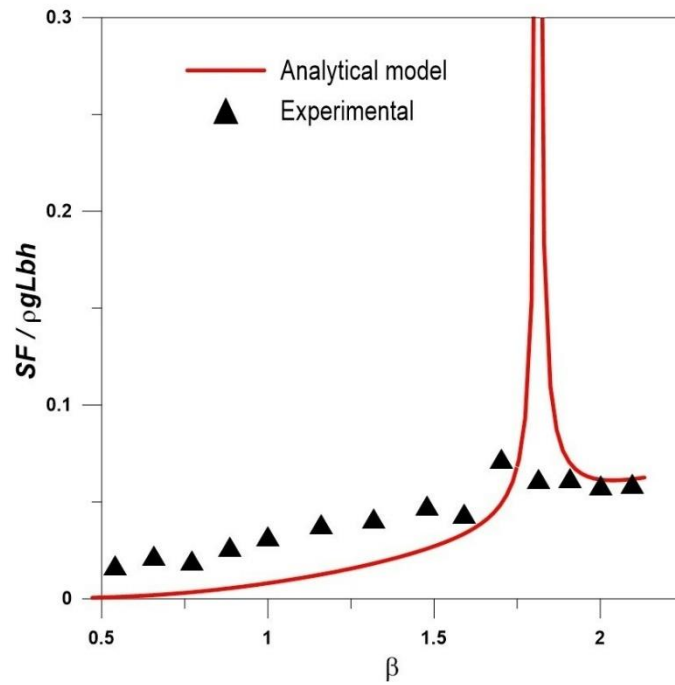


Figure 4.54 Tank with single porous baffle of 4.4% porosity

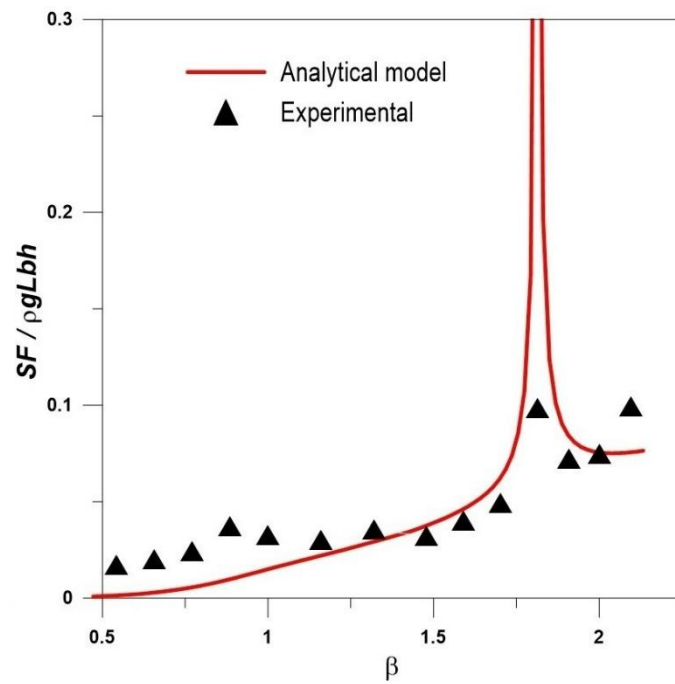


Figure 4.55 Tank with single porous baffle of 6.8% porosity

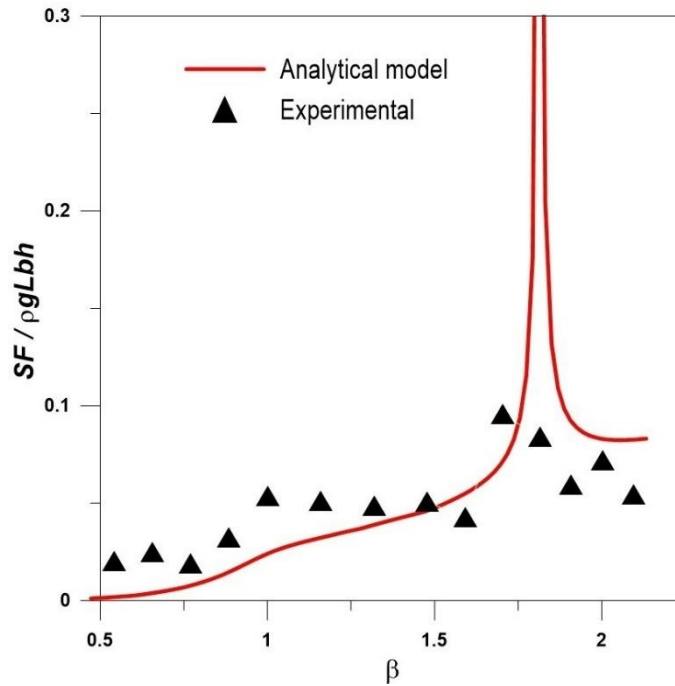


Figure 4.56 Tank with single porous baffle of 9.2% porosity

peak at second sloshing mode increase with small magnitude as porosity increases and its observed that 0.05, 0.06, and 0.07 respectively. The analytical model results at this condition agreed with test results with some quantitative differences and again fail show energy dissipation variations in a 25% FL tank with single porous baffles the primary peaks at second resonant mode. in the tank with 9.2% porous baffles case, a small secondary peak observed near the first resonant mode by analytical model results. This indicates that model is not properly behaving with single porous baffle condition at tank centres. This behaviour may due to the time step and total simulation time span during the analysis. The similar behaviours are observed in the case of tank 75% fil level for all porous baffle condition (Figure 4.45, 4.46, and 4.47). Overall the force repose decreases by porous of baffle in all filled level condition in comparing to the clean tank conditions.

#### 4.4.7 Energy dissipation variations in a 25% FL tank with single porous baffles

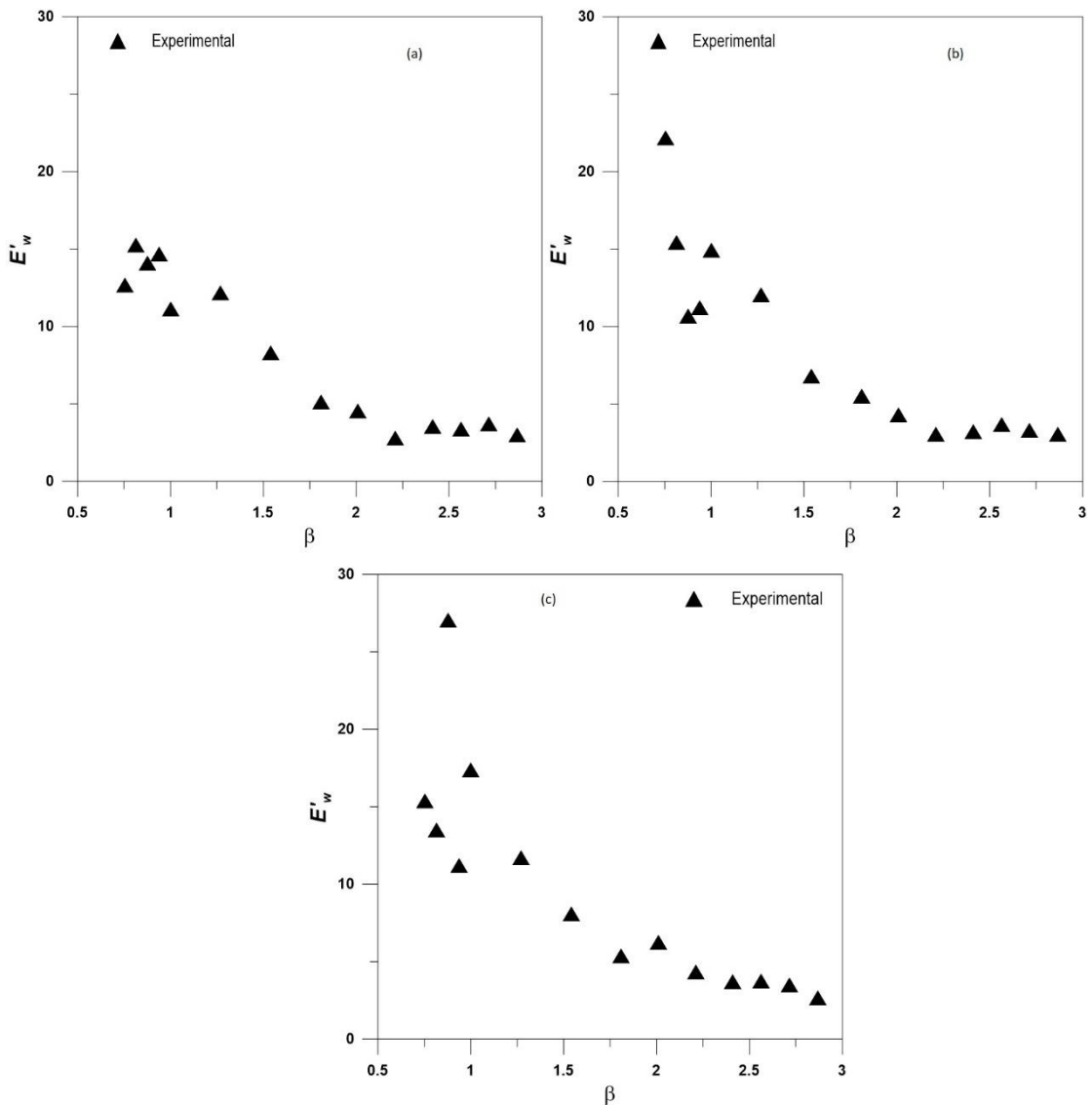


Figure 4.57 Tank with single porous baffles of (a) 4.4%, (b) 6.8%, and (c) 9.2% porosity

The energy dissipation variation in the single porous baffled tank are shown in figure 4.57, Figure 4.58, and Figure 4.59 for 25%, 50%, and 75% liquid fill level respectively. The dissipation of energy response in the baffled tank decreases as fill level increases. This due to higher fill levels in the tank results lesser free surface motion and yield less force. Further it is observed that a similar variation with increasing porosity of baffles in all liquid fill levels. This effect is attributable to the smaller variance in porosity value between porous baffles. In comparing to the clean tank condition, the energy dissipation

variation in the baffled tank to show similar except initial excitation frequencies. This conclude the higher excitation frequencies not more influenced the energy dissipation characteristics in both baffled and clean tanks.

#### 4.4.8 Energy dissipation variations in a 50% FL tank with single porous baffles

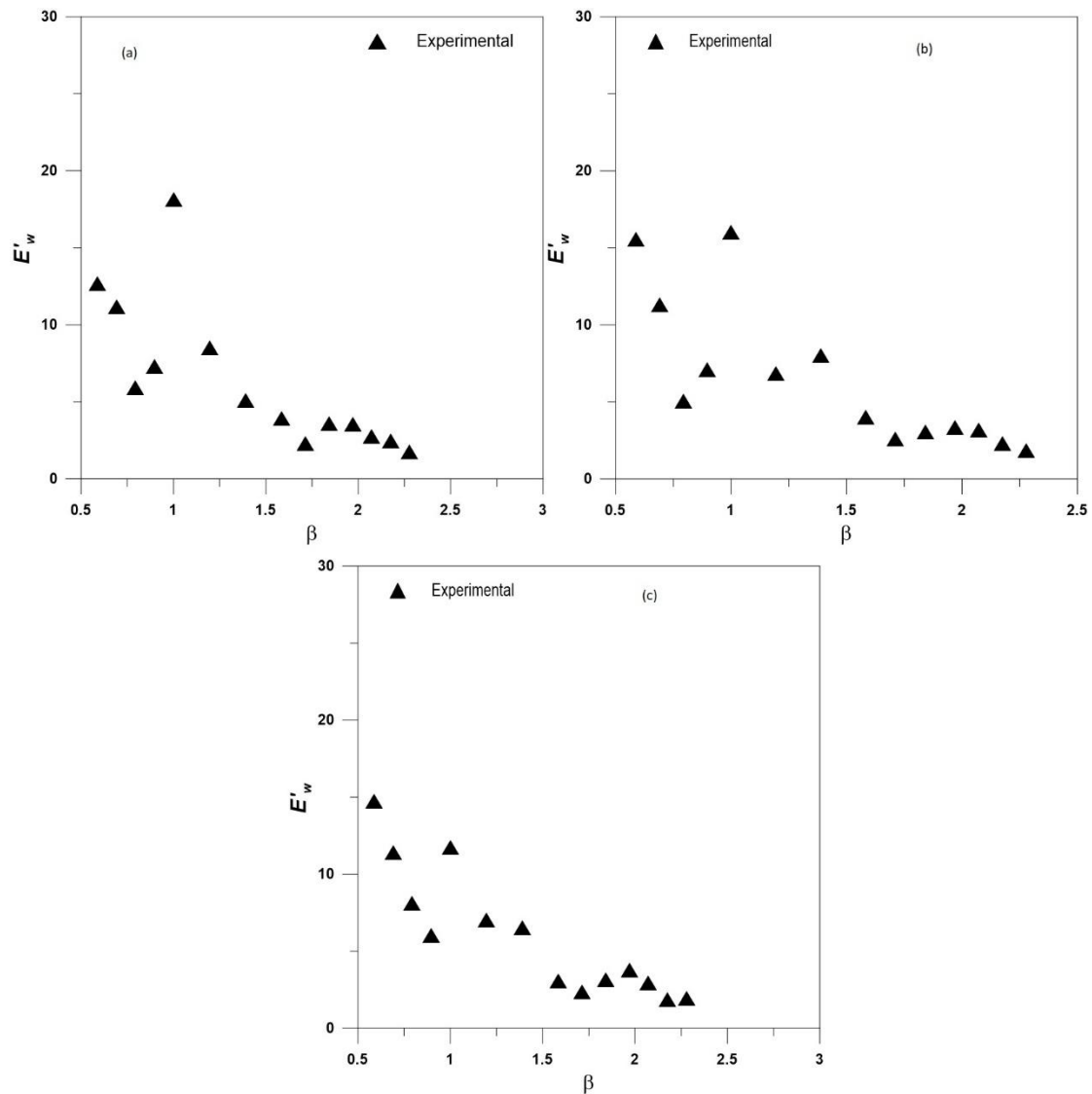


Figure 4.58 Tank with single porous baffles of (a) 4.4%, (b) 6.8%, and (c) 9.2% porosity

#### 4.4.9 Energy dissipation variations in a 75% FL tank with single porous baffles

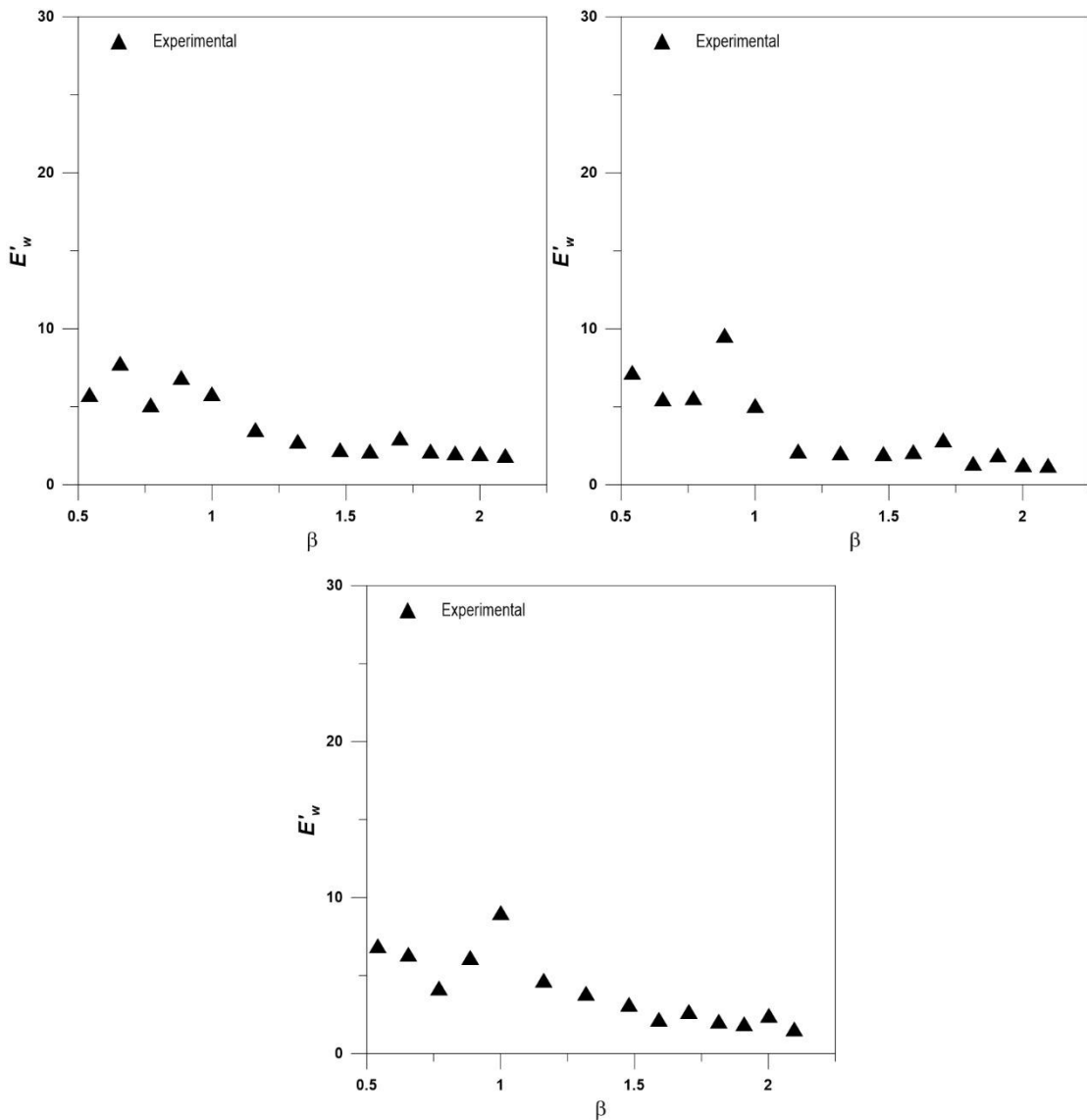


Figure 4.59 Tank with single porous baffles of (a) 4.4%, (b) 6.8%, and (c) 9.2% porosity

## 4.5 POROUS BAFFLES PERFORMANCE IN A SLOSHING FOR STRUCTURE-TLD INTERACTION

### 4.5.1 Model validation

The dynamic analysis of structures, both with and without TLD is considered in the present work. The dynamic equation for structure and structure-TLD solved using

Newmark's method. The present analytical model of without TLD is verified by considering the solution of equilibrium equations in the dynamic analysis (Bathe 2014). The initial displacement of the system is considered as zero. The time step was taken as 0.28.

$$\begin{pmatrix} 2 & 0 \\ 0 & 1 \end{pmatrix} \begin{Bmatrix} \ddot{x}_1 \\ \ddot{x}_2 \end{Bmatrix} + \begin{pmatrix} 6 & -2 \\ -2 & 4 \end{pmatrix} \begin{Bmatrix} x_1 \\ x_2 \end{Bmatrix} = \begin{Bmatrix} 0 \\ 10 \end{Bmatrix}$$

Figure 4.60 shows the displacement response of the first mass of the system with time. It is understood that the displacement responses of the 2-DOF system have the same trend as observed by Bathe 2014.

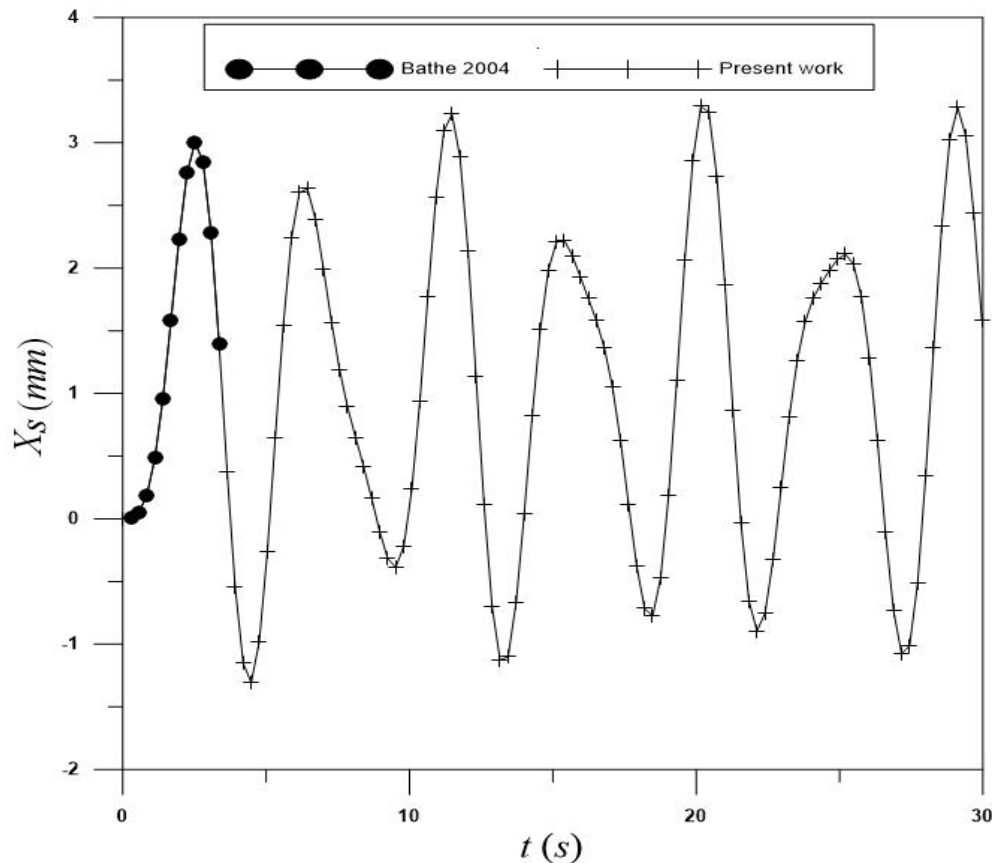


Figure 4.60 Displacement time history of the first mass

To understand the coupled behavior of structure and TLD, further complexity is added into the mathematical model. For the present structure-TLD with porous screens, mathematical model is analyzed and validated with Tait (2008) and Soliman et al. (2015) work. A TLD is attached to the center of the floor slab of building and is excited

by steady-state sinusoidal excitation over a range of frequencies. The properties of structure and TLD are presented in Tables 5 and 6. Figure 4.61 show the equivalent damping ratio values corresponding to harmonic excitation. The variation of relative response amplitude ( $x_r/L$ ) with a normalized damping ratio for a depth ratio ( $h/L$ ) of 0.1 is agreed with the results of Tait (2008).

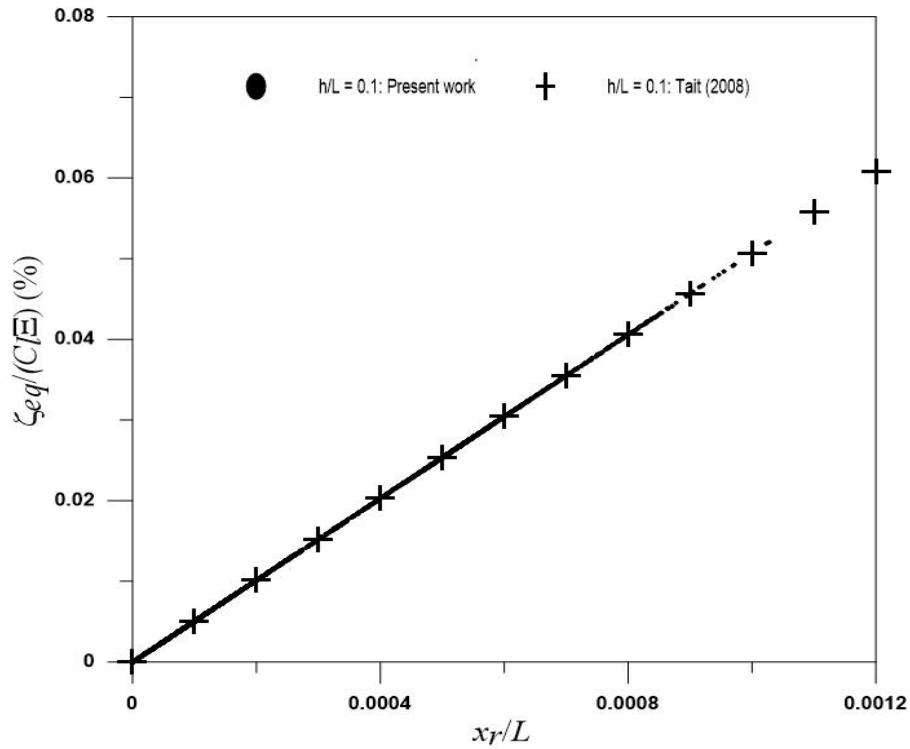


Figure 4.61 Normalized linearized equivalent damping ratio

Table 5 Building Properties

Model	Excitation type	Excitation Amplitude (N)	Structural frequency (Hz)	Mass ratio (%)	Structure mass (kg)	Structure stiffness (N/m)	Structure damping (kg/sec)
Soliman et al. (2015)	Harmonic	23	0.558	2.5	4040	49,656	28.33

Table 6 TLD Properties (Soliman et al. (2015))

Excitation type	$f_{TLD}$ (Hz)	$h$ (m)	$L$ (m)	$b$ (m)	$m_w$ (kg)	$m_{TLD}$ (kg)	$S$
Harmonic	0.546	0.119	0.966	0.874	100.5	77.6	0.42



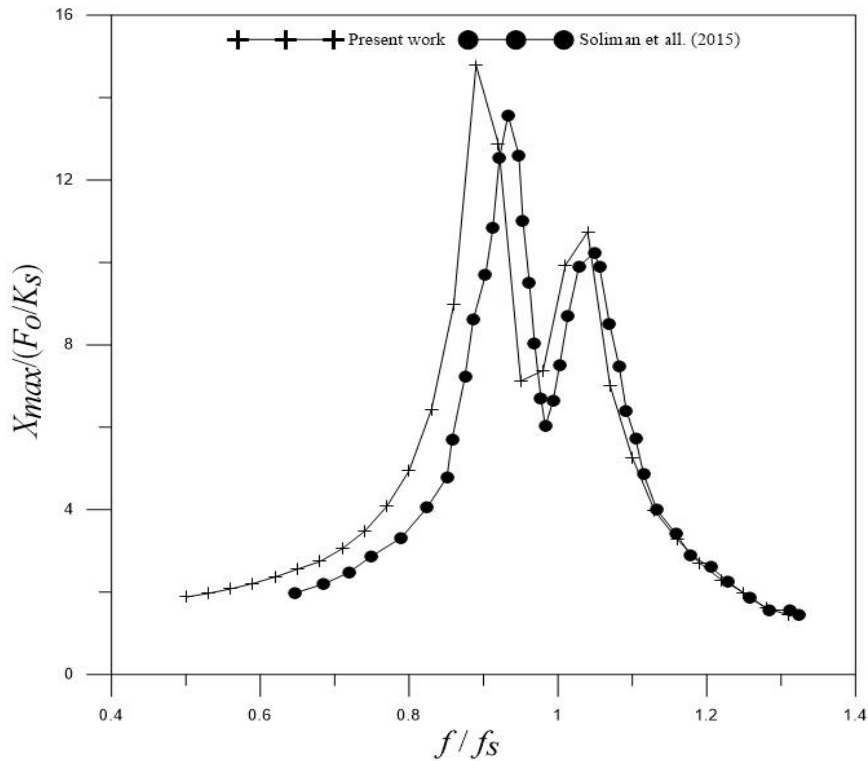


Figure 4.62 Frequency response curve for the structure-TLD system model

The frequency response curve for the structure-TLD model is plotted (Figure 4.62) for validating the present mathematical model. The structural displacement with TLD was found to be in good agreement with the results of Soliman et al. (2015). The effectiveness of TLD with porous screens is evident as shown in Figure 18 in comparison with displacement response of the structure, structure-TLD with and without porous screen under resonance conditions. And, it is understood that the amplitude of structure under dynamic load can be reduced by the use of TLD with slotted screens.

#### 4.5.2 Performance of porous baffles in the TLD

The performance of porous baffles of three varying porosities of 4.4%, 6.8%, and 9.2% in a tuned liquid damper system to reduce the structural vibration is discussed. For structure-TLD interaction model, the structure (building) model and its properties are considered based experimental test investigation conducted by Tait (2008) on structure-TLD with damping screens. In the test series, the authors consider a structure of mass

( $M_s$ ) is 4040 kg, stiffness ( $K_s$ ) of 49656 N/m, and inherent damping of structure ( $C_s$ ) is 14 N s /m. The tank dimension for TLD in the present study is considered similar to the tank dimension of TLD in the study of Soliman et al. (2015).

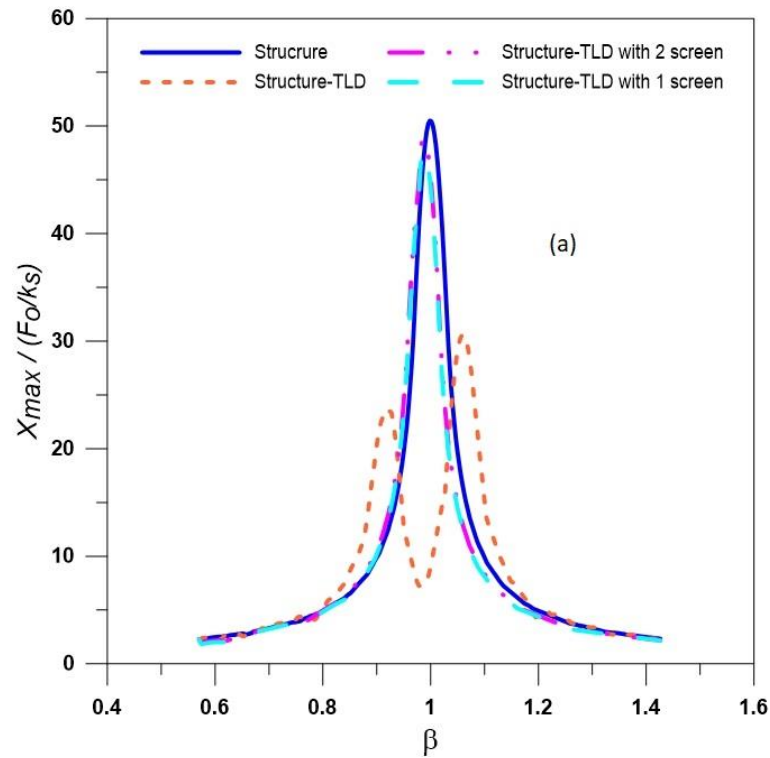


Figure 4.63 TLD with 4.4% porosity baffle

In the analytical simulation, firstly the structure alone is subjected to a range of sinusoidal excitation with an amplitude of 11.7 N. in the test series in the structure-TLD interaction, TLD with liquid alone is considered. The maximum displacement of the structure under each excitation is calculated. Further, structural response amplitude is normalized for a range of frequency ratios ( $\beta$ ). Figure 4.8a, Figure 4.8b, Figure 4.8c, and Figure 4.8d shows the response of structures with TLD attached with damping screens of porosity 4.4%, 6.8%, 9.2%, and 52% respectively.

From Figure 4.63, Figure 4.64, and Figure 4.65 it is observed that the porous screens of 4.4%, 6.8%, and 9.2% porosities are less effective to reduce the structure response near the resonant mode ( $\beta = 1$ ). TLD with a single baffle at the tank center is somewhat effective in comparison with the tank with two porous baffles. In the tank with two screens of 4.4% porosity, the structure response is reduced by 4%, whereas in the tank

with a single screen, it is reduced by 8%. It also observed that a liquid alone in the tank reduces the structure response by 88%. As the porosity of the baffle in the TLD increases, the response of the structure reduces.

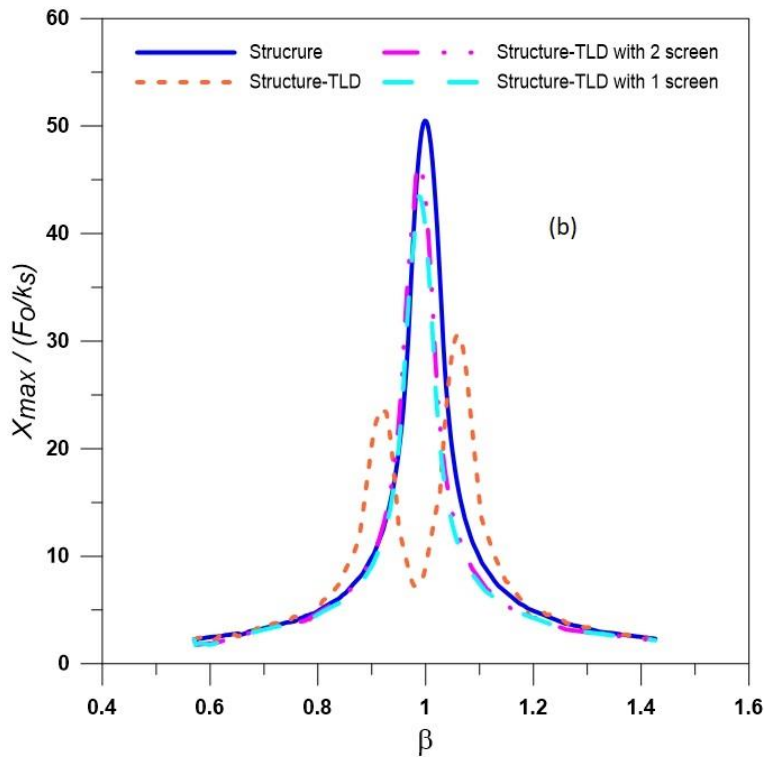


Figure 4.64 TLD with 6.8% porosity baffle

For the porous baffles of 6.8% porosity, structure response is reduced by 10% and 14% with baffled TLD of two screens and single screen respectively. Where in the case of the tank with 9.2% porosity, structure response is reduced by 15% and 30% with baffled TLD of two screens and single screen respectively. Similarly, as porosity increases in the baffle, the response goes on decreasing. For the case of TLD with 52% porosity Baffle (Figure 4.66), the response of structure reduced as similar to TLD without baffle. Along with small amplification at frequency ratio one, there are two peaks observed near the resonant mode of structure. At those two peaks, the TLD with two screen conditions is found to be more effective than other conditions.

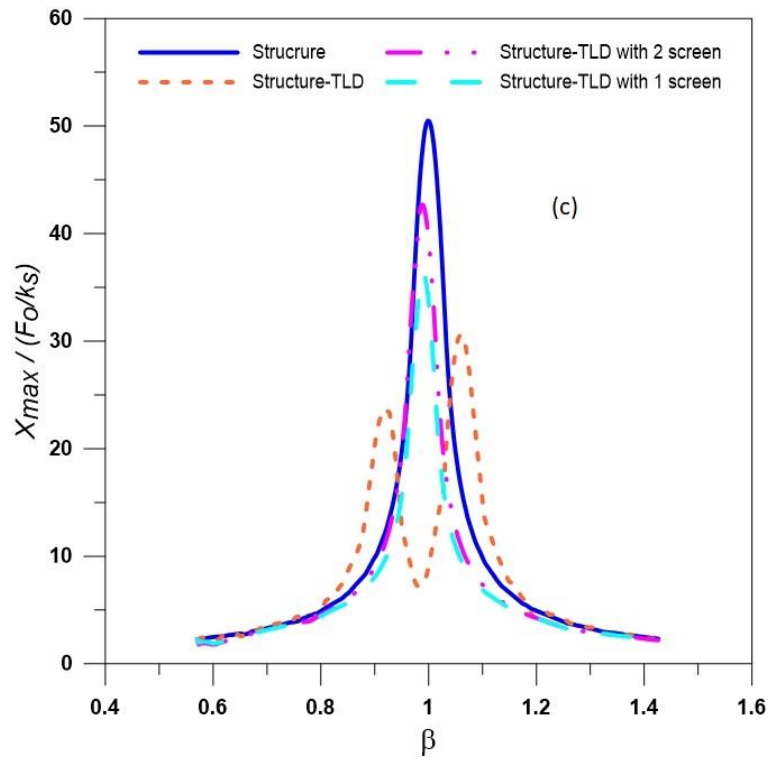


Figure 4.65 TLD with 9.2% porosity baffle

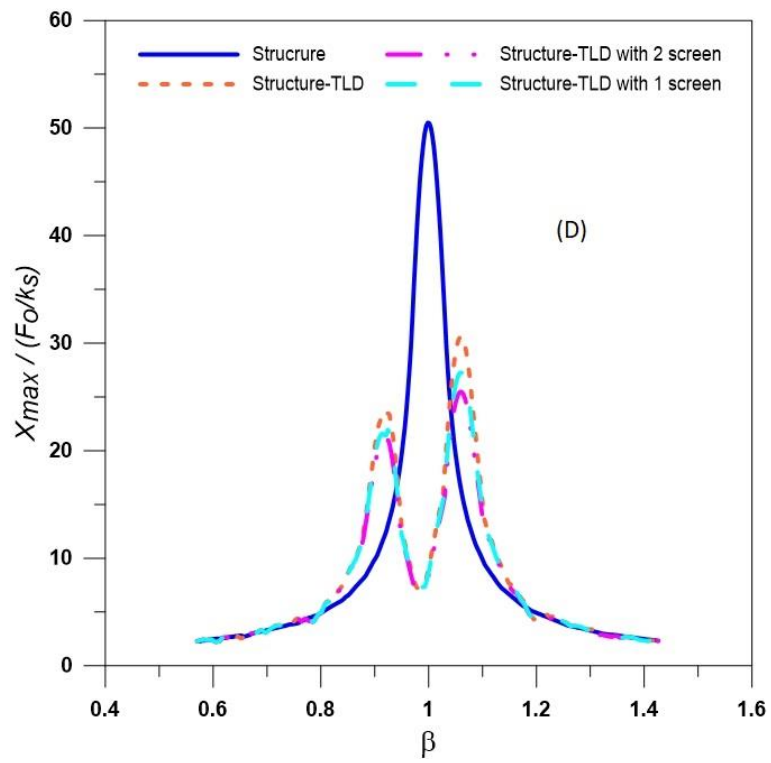


Figure 4.66 TLD with 58% porosity baffle



### SUMMARY AND CONCLUSIONS

---

Here is presented a study on liquid sloshing dynamics and its applicability to structural response control. An analytical and experimental investigation of sloshing dynamics in rectangular with and without porous baffle is conducted. To estimate the drag coefficient for porous baffles, a gravity flow test between the two tanks is conducted. The drag coefficient is accounted in the analytical simulation for porous baffles. The model's output is compared to experimental shake table tests. Furthermore, the performance of the porous baffle in the TLD to control the response of the main (single degree of freedom) system is investigated. The following findings are drawn from this study:

#### 5.1 GENERAL CONCLUSIONS

The analytical and experimental investigation carried out herein on rectangular sloshing tank with and without porous baffles conditions, the study findings lead to the following broad conclusions:

1. The resonant response in the clean rectangular tank dependent on the depth liquid fill level in the tank.
2. Response due the liquid sloshing in the tank is a summation of all sloshing modes present in the tank.
3. Screen placement in the tank is based on the maximum velocity that can occur due to the tank's sloshing modes.
4. The low-level porosity of the tank's baffles acts as an impermeable barrier, causing sloshing in the compartment tank.

#### 5.2 SCREEN DRAG COEFFICIENT

A hydraulic flow test between two reservoirs is performed to evaluate the drag coefficient of porous screens as a function of flow velocity for a wide range of Reynolds numbers, the study findings lead to the following conclusions:

1. The relation between the drag coefficient and the Reynolds number shows that as the flow velocity through the screen increases, the steepness of the goodness of fit increases. This indicates that the drag coefficient is susceptible to lower Reynolds numbers.
2. The empirical constants for different porosities indicate the limiting value of Reynolds number in the lower range.
3. The empirical constants used to estimate the drag coefficient for different porosities at the limiting value of Reynolds number in the lower range increases as the porosity increases from 4.4% to 25%.
4. The Reynolds number, which measures flow, rises as porosity increases. The highest limit of the Reynolds number value in the higher range remains unchanged above 20% porosity.
5. As the porosity increases from 4.4% to 25%, the drag coefficient tends to decrease in the higher range of Reynolds numbers and shows the best fit for all screen porosities.

### **5.3 TANK WITHOUT BAFFLES (CLEAN TANK) AND WITH POROUS BAFFLE.**

1. In a clean tank with three different fill levels resembles the resonant phenomenon at first two odd natural frequencies by analytical model. The test results well correlate with experimental results except some quantitate difference.
2. The tank with relatively low porous baffles of porosities 4.4%, 6.8%, and 9.2% exhibits resonant frequency shift phenomenon with respect to the tank liquid depth level.
3. The shift in natural frequency is helpful for some engineering applications, such as structural –TLDs interaction problems for effective mitigation of vibration, where the natural frequency of the tank should match the resonant frequency of the building.

4. In the tank with two baffles condition due to resonant frequency shift, the maximum peak is observed in the third resonant mode of the tank with three varying fill levels. The analytical model response is confirmed by experimental findings.
5. In the experimental results for a tank with a single porous baffle, peaks are observed near the tank's second and third resonant modes at all fill levels. whereas it is observed only one peak similar to the tank with two baffle condition by analytical approach.
6. As the baffles porosity increases in the tank, a secondary peak start appearing near first resonant mode of tank. The same behaviour is observed in the two baffled tank with 9.2% porosity screen.
7. Analytical model results show that, tank with two baffles of porosities 4.4%, 6.8%, and 9.2% can reduce the maximum elevation of sloshing motion and sloshing force near fundamental sloshing mode ( $n=1$ ) of the tank with all three fill levels. The reduction in amplification is observed to be between 94% - 97% compared to no screen tank.
8. The higher amplification is observed at  $n = 3$  due to sloshing behaviour shifts from the screened tank to that of a compartment tank for all fill levels. The tank with porous screens of porosities 6.8% and 9.2% is more effective for frequencies close to the third resonant mode ( $n=3$ ) as compared to 4.4% porosity of screen.
9. The performance of two porous screens in the sloshing tank with Reynold number dependent loss coefficient is found be more effective compare to independent one. The model results show the reduction in amplification of sloshing motion and force is nearly 100% compared to the no screen tank.
10. The experimental test results for the tank with two baffles condition support the model results of sloshing motion and force response in the tank with Reynold number independent drag coefficient ( $C_d$ ) porous baffles performance. However, experimental results proved the performance of Reynold number dependent porous baffles in tank at around the third resonant mode alone.



11. In the tank with single screen condition, the sloshing motion amplification near first resonant mode is reduced by 72% to 78% through experimental investigation. But it is observed higher (90% to 95%) by analytical model.
12. The analytical model results for single baffle condition are well matched with experimental findings except resonant conditions.
13. The energy dissipation characteristics in the baffled tank resembles the exact phenomenon with varying baffles porosities and tank fill levels. It is observed that as fill level increases the dissipation of energy decreases.
14. The three varying porous baffles in the TLD not shown exhibit the effective performance in mitigating structural vibration for fixed excitation amplitude and liquid fill level in the tank.
15. The TLD found to be more effective to reduce structural vibration for porous baffles of porosity 58%. The two baffles in a TLD with this porosity shows the better performance compared to the single porous baffle in the TLD.

#### **5.4 SCOPE FOR FURTHER RESEARCH**

Possible avenues for further research could include examinations into

- New baffles of varying scattered position and arrangements of holes with varying diameters.
- Liquid sloshing dynamic in the clean and porous baffles tank under range excitation amplitudes.
- Baffles drag coefficient in an oscillating flow condition.
- Nonlinear dynamics in the baffled tank with porous baffles under both regular and random excitations.

## REFERENCES

- Akyildiz, H., and Ünal, E. (2005). "Experimental investigation of pressure distribution on a rectangular tank due to the liquid sloshing." *Ocean Engineering*, 32(11-12), 1503-1516.
- Akyildiz, H., and Ünal, E. (2006). "Sloshing in a three-dimensional rectangular tank: numerical simulation and experimental validation." *Ocean Eng*, 33(16), 2135-2149.
- Baines, W. D., and Peterson, E. G. (1951). "An investigation of flow through screens." *Transactions of the American Society of Mechanical Engineers*, 73(5), 467-477.
- Bauer, H. F. (1984). "Oscillations of immiscible liquids in a rectangular container: a new damper for excited structures." *Journal of Sound and Vibration*, 93(1), 117-133.
- Bellezi, C. A., Cheng, L. Y., Okada, T., and Arai, M. (2019). "Optimized perforated bulkhead for sloshing mitigation and control." *Ocean Engineering*, 187, 106171.
- Cassolato, M. R., Love, J. S., and Tait, M. J. (2011). "Modelling of a tuned liquid damper with inclined damping screens." *Structural Control and Health Monitoring*, 18(6), 674-681.
- Cavalagli, N., Biscarini, C., Facci, A. L., Ubertini, F., and Ubertini, S. (2017). "Experimental and numerical analysis of energy dissipation in a sloshing absorber." *Journal of Fluids and Structures*, 68, 466-481.
- Chen, B. F., and Nokes, R. (2005). "Time-independent finite difference analysis of fully non-linear and viscous fluid sloshing in a rectangular tank." *Journal of Computational Physics*, 209(1), 47-81.
- Cheng, L. Y., Bellezi, C. A., Amaro, R. A., Arai, M., and Okada, T. (2016). "A numerical study on the effects of the perforated swash bulkheads on sloshing behaviors of liquid cargo tanks." In *The 26th International Ocean and Polar Engineering Conference*. One Petro.
- Cho, I. H., and Kim, M. H. (2016). "Effect of dual vertical porous baffles on sloshing reduction in a swaying rectangular tank." *Ocean Engineering*, 126, 364-373.

- Crowley, S., and Porter, R. (2012a). "The effect of slatted screens on waves." *Journal of Engineering Mathematics*, 76, 33-57.
- Crowley, S., and Porter, R. (2012b). "An analysis of screen arrangements for a tuned liquid damper." *Journal of Fluids and Structures*, 34, 291-309.
- Deng, X., and Tait, M. J. (2009). "Theoretical modeling of TLD with different tank geometries using linear long wave theory." *Journal of Vibration and Acoustics*, 131(4), 041014.
- Faltinsen, O. M., and Timokha, A. N. (2009). "Sloshing." *Cambridge University Press*, ISBN 0521881110, 9780521881111.
- Faltinsen, O. M., Firoozkoobi, R., and Timokha, A. N. (2011). "Analytical modeling of liquid sloshing in a two-dimensional rectangular tank with a slat screen." *Journal of Engineering Mathematics*, 70, 93-109.
- Faltinsen, O. M., Firoozkoobi, R., and Timokha, A. N. (2011). Effect of central slotted screen with a high solidity ratio on the secondary resonance phenomenon for liquid sloshing in a rectangular tank. *Physics of Fluids*, 23(6), 062106.
- Fediw, A. A., Isyumov, N., and Vickery, B. J. (1995). "Performance of a tuned sloshing water damper." *Journal of Wind Engineering and Industrial Aerodynamics*, 57(2-3), 237-247.
- Frandsen, J. B. (2004). "Sloshing motions in excited tanks." *Journal of computational physics*, 196(1), 53-87.
- Gardarsson, S., Yeh, H., and Reed, D. (2001). "Behavior of sloped-bottom tuned liquid dampers." *Journal of Engineering Mechanics*, 127(3), 266-271.
- George, A., and Cho, I. H. (2020). "Anti-sloshing effects of a vertical porous baffle in a rolling rectangular tank." *Ocean Engineering*, 214, 107871.
- Goudarzi, M. A., and Sabbagh-Yazdi, S. R. (2012). "Analytical and experimental evaluation on the effectiveness of upper mounted baffles with respect to commonly used baffles." *Ocean Engineering*, 42, 205-217.
- Hamelin, J. (2007). "The effect of screen geometry on the performance of a tuned liquid damper" (Doctoral dissertation).

- Hamelin, J. A., Love, J. S., Tait, M. J., and Wilson, J. C. (2013). "Tuned liquid dampers with a Keulegan–Carpenter number-dependent screen drag coefficient." *Journal of Fluids and Structures*, 43, 271-286.
- Ibrahim, R. A. (2005). "Liquid sloshing dynamics: theory and applications." Cambridge University Press.
- Ikeda, T. (2010). "Non-linear dynamic responses of elastic two-story structures with partially filled liquid tanks." *International Journal of Non-Linear Mechanics*, 45(3), 263-278.
- Isaacson, M., and Premasiri, S. (2001). "Hydrodynamic damping due to baffles in a rectangular tank." *Canadian Journal of Civil Engineering*, 28(4), 608-616.
- Jin, H., Liu, Y., and Li, H. J. (2014). "Experimental study on sloshing in a tank with an inner horizontal perforated plate." *Ocean Engineering*, 82, 75-84.
- Ju, Y. K., Yoon, S. W., and Kim, S. D. (2004). "Experimental evaluation of a tuned liquid damper system." *Proceedings of the Institution of Civil Engineers-Structures and Buildings*, 157(4), 251-262.
- Kaneko, S., and Ishikawa, M. (1999). "Modeling of tuned liquid damper with submerged nets." *Journal of Pressure Vessel Technology*, 121(3), 334-343.
- Kaneko, S., and Yoshida, O. (1999). "Modeling of deepwater-type rectangular tuned liquid damper with submerged nets." *Journal of Pressure Vessel Technology*, 121(4), 413-422.
- Keulegan, G. H. (1968). "Wave Damping Effects of Screens: Hydraulic Model Investigation (No. 2-12)." *US Army Engineer Waterways Experiment Station, Corps of Engineers*.
- Keulegan, G. H., & Carpenter, L. H. (1958). "Forces on cylinders and plates in an oscillating fluid." *Journal of research of the National Bureau of Standards*, 60(5), 423-440.
- Kim, H., Dey, M. K., Oshima, N., and Lee, Y. W. (2018). "Numerical study on sloshing characteristics with Reynolds number variation in a rectangular tank." *Computation*, 6(4), 53.

- Koh, C. G., Mahatma, S., and Wang, C. M. (1995). "Reduction of structural vibrations by multiple-mode liquid dampers." *Engineering Structures*, 17(2), 122-128.
- Kumar, A., and Sinhamahapatra, K. P. (2016). "Dynamics of rectangular tank with perforated vertical baffle." *Ocean Engineering*, 126, 384-401.
- Lee, S. C., and Reddy, D. V. (1982). "Frequency tuning of offshore platforms by liquid sloshing." *Applied Ocean Research*, 4(4), 226-231.
- Li, S. J., Li, G. Q., Tang, J., and Li, Q. S. (2002). "Shallow rectangular TLD for structural control implementation." *Applied Acoustics*, 63(10), 1125-1135.
- Li, H. N., Jia, Y., and Wang, S. Y. (2004). "Theoretical and experimental studies on reduction for multi-modal seismic responses of high-rise structures by tuned liquid dampers." *Modal Analysis*, 10(7), 1041-1056.
- Maleki, A., and Ziyaeifar, M. (2008). "Sloshing damping in cylindrical liquid storage tanks with baffles." *Journal of Sound and Vibration*, 311(1-2), 372-385.
- Miles, J. W. (1958). "Ring damping of free surface oscillations in a circular tank." *J. Appl. Mech*, 25(2), 274-276.
- Miles, J. W. (1967). "Surface-wave damping in closed basins." *Proceedings of the Royal Society of London. Series A. Mathematical and Physical Sciences*, 297(1451), 459-475.
- Modi, V. J., and Seto, M. L. (1997). "Suppression of flow-induced oscillations using sloshing liquid dampers: analysis and experiments." *Journal of Wind Engineering and Industrial Aerodynamics*, 67, 611-625.
- Molin, B. (2011). "Hydrodynamic modeling of perforated structures." *Applied Ocean Research*, 33(1), 1-11.
- Molin, B., and Remy, F. (2013). "Experimental and numerical study of the sloshing motion in a rectangular tank with a perforated screen." *Journal of Fluids and Structures*, 43, 463-480.
- Molin, B., and Remy, F. (2015). "Inertia effects in TLD sloshing with perforated screens." *Journal of Fluids and Structures*, 59, 165-177.

- Morison, J. R., Johnson, J. W., and Schaaf, S. A. (1950). "The force exerted by surface waves on piles." *Journal of Petroleum Technology*, 2(05), 149-154.
- Nguyen, T. P., Pham, D. T., and Ngo, K. T. (2018). "Effectiveness of multi tuned liquid dampers with slat screens for reducing dynamic responses of structures." In *IOP Conference Series: Earth and Environmental Science* (Vol. 143, No. 1, p. 012023). IOP Publishing.
- Panigrahy, P. K., Saha, U. K., and Maity, D. (2009). "Experimental studies on sloshing behavior due to horizontal movement of liquids in baffled tanks." *Ocean engineering*, 36(3-4), 213-222.
- Poguluri, S. K., and Cho, I. H. (2020). "Mitigation of liquid sloshing in a rectangular tank due to slotted porous screen." *Proceedings of the Institution of Mechanical Engineers, Part M: Journal of Engineering for the Maritime Environment*, 234(3), 686-698.
- Reed, D., Yu, J., Yeh, H., and Gardarsson, S. (1998). "Investigation of tuned liquid dampers under large amplitude excitation." *Journal of Engineering Mechanics*, 124(4), 405-413.
- Samanta, A., and Banerji, P. (2010). "Structural vibration control using modified tuned liquid dampers." *The IES Journal Part A: Civil & Structural Engineering*, 3(1), 14-27.
- Sarpkaya, T., and O'Keefe, J. L. (1996). "Oscillating flow about two and three-dimensional bilge keels." *Journal of Offshore Mechanics and Arctic Engineering*, 118(1), 1-6.
- Shih, C. C., and Buchanan, H. J. (1971). "The drag on oscillating flat plates in liquids at low Reynolds numbers." *Journal of Fluid Mechanics*, 48(2), 229-239.
- Soliman, I. M., Tait, M. J., and El Damatty, A. A. (2015). "Development and validation of finite element structure-tuned liquid damper system models." *Journal of Dynamic Systems, Measurement, and Control*, 137(11), 111001.
- Sun, L. M., Fujino, Y., Pacheco, B. M., and Chaiser, P. (1992). "Modelling of tuned liquid damper (TLD)." *Journal of Wind Engineering and Industrial Aerodynamics*, 43(1-3), 1883-1894.

- Sun, L. M., Fujino, Y., Chaiseri, P., and Pacheco, B. M. (1995). "The properties of tuned liquid dampers using a TMD analogy." *Earthquake Engineering & Structural Dynamics*, 24(7), 967-976.
- Tait, M. J. (2008). "Modelling and preliminary design of a structure-TLD system." *Engineering Structures*, 30(10), 2644-2655.
- Tait, M. J., El Damatty, A. A., and Isyumov, N. (2005). "An investigation of tuned liquid dampers equipped with damping screens under 2D excitation." *Earthquake Engineering & Structural Dynamics*, 34(7), 719-735.
- Tait, M. J., El Damatty, A. A., Isyumov, N., and Siddique, M. R. (2005). "Numerical flow models to simulate tuned liquid dampers (TLD) with slat screens." *Journal of Fluids and Structures*, 20(8), 1007-1023.
- Tait, M. J., Isyumov, N., and El Damatty, A. A. (2007). "Effectiveness of a 2D TLD and its numerical modeling." *Journal of Structural Engineering*, 133(2), 251-263.
- Tait, M. J., Isyumov, N., and El Damatty, A. A. (2008). "Performance of tuned liquid dampers." *Journal of Engineering Mechanics*, 134(5), 417-427.
- Tamura, Y., Fujii, K., Ohtsuki, T., Wakahara, T., and Kohsaka, R. (1995). "Effectiveness of tuned liquid dampers under wind excitation." *Engineering Structures*, 17(9), 609-621.
- Tsao, W. H., and Hwang, W. S. (2018). "Tuned liquid dampers with porous media." *Ocean Engineering*, 167, 55-64.
- Tuong, B. P. D., and Huynh, P. D. (2020). "Experimental test and numerical analysis of a structure equipped with a multi-tuned liquid damper subjected to dynamic loading." *International Journal of Structural Stability and Dynamics*, 20(07), 2050075.
- Victor L. Streeter et al. (2010). "Textbook of Fluid Mechanics." *Ninth edition, Tata McGraw-Hill Edition*.
- Wakahara, T., Ohya, T., and Fujii, K. (1992). "Suppression of wind-induced vibration of a tall building using tuned liquid damper." *Journal of Wind Engineering and Industrial Aerodynamics*, 43(1-3), 1895-1906.

Warnitchai, P., and Pinkaew, T. (1998). "Modelling of liquid sloshing in rectangular tanks with flow-dampening devices." *Engineering structures*, 20(7), 593-600.

Yamamoto, K., and Kawahara, M. (1999). "Structural oscillation control using tuned liquid damper." *Computers & Structures*, 71(4), 435-446.

Yu, J. K., Wakahara, T., and Reed, D. A. (1999). "A non-linear numerical model of the tuned liquid damper." *Earthquake Engineering & Structural Dynamics*, 28(6), 671-686.

Yu, L., Xue, M. A., & Zheng, J. (2019). "Experimental study of vertical slat screens effects on reducing shallow water sloshing in a tank under horizontal excitation with a wide frequency range." *Ocean engineering*, 173, 131-141.

Yu, L., Xue, M. A., and Jiang, Z. (2020). "Experimental investigation of parametric sloshing in a tank with vertical baffles." *Ocean Engineering*, 213, 107783.





### JOURNAL PAPERS

Bhandiwad, M. S., & Dodamani, B. M., (2022). “Porous Baffle Performance in a Sloshing Tank.” *SSRG International Journal of Civil Engineering, Volume 9 Issue 12, 1-6*. <https://doi.org/10.14445/23488352/IJCE-V9I12P101>

Bhandiwad, M. S., Dodamani, B. M., & Deepak M.D, (2023). “Effect of the loss coefficient on the performance of vertical porous baffles in a sloshing tank.” – *Journal of Engineering, Design and Technology (Accepted)*.

Bhandiwad, M. S., & Dodamani, B. M., (2023). “Analytical investigation on vertical porous screen performance in a sway-excited sloshing tank.” - *Journal of Marine Science and Application (under review)*

Bhandiwad, M. S., & Nasar, T. (2023). “An analytical investigation of porous baffle in a horizontally excited sloshing tank.” *Journal of Naval Architecture and Marine Engineering (under review)*.

### CONFERENCE PAPERS

Bhandiwad, M. S., & Nasar, T. (2021, June). Drag Coefficient for Porous Screen in a Non-Oscillating Perpendicular to Plane-in Flow. In *International Conference on Offshore Mechanics and Arctic Engineering* (Vol. 85161, p. V006T06A011). American Society of Mechanical Engineers. <https://doi.org/10.1115/OMAE2021-62799>



## RESUME

---

**Name** : Mallikarjun S Bhandiwad

**Date of Birth** : 30-06-1987

**Mobile** : 9591207109

**Email** : [msbhandiwad@gmail.com](mailto:msbhandiwad@gmail.com)

**Permanent Address** : S/O Shivappa SK Bhandiwad.  
At: Harlapur, Tq: Kundgol,  
Dist; Dharwad, Karnataka -581107

**Qualifications** : B. Tech (Civil Engineering)  
M. Tech (CAD Structure)

**Publications** : International journals – 2  
International conferences - 1



